BEHAVIOUR OF ELLIPTICAL TUBE COLUMNS FILLED WITH SELF-COMPACTING CONCRETE

Munir MAHGUB

A dissertation submitted for the award of Doctor of Philosophy
PhD

Faculty of Engineering and Informatics

University of Bradford

2016

PAPERS PRODUCED FROM THIS THESIS

1. J. Abdalhmid1 , M. Mahgub, A.F. Ashour, D. Lam and T. Sheehan, “Prediction of drying shrinkage of self-compacting concrete using artificial neural networks“,34th Cement and Concrete Science Conference, 14-17 September 2014, University of Sheffield, Sheffield.

2. Mahgub, M, A. Ashour, Lam, D. and Dai, X, “Tests of self-compacting concrete filled elliptical steel tube columns”. Published in Thin-walled structures: Elsevier.

Behaviour of elliptical tube columns filled with self-compacting concrete

Munir Mahgub

Abstract

Keywords: Self-compacting concrete, elliptical columns filled with concrete, experimental study, axial compressive capacity, prediction, comparison.

The present research is conducted to investigate the behaviour of elliptical tube columns filled with self-compacting concrete (SCC). In total, ten specimens, including two empty columns, were tested to failure. The main parameters investigated were the length and the sections of the columns, and the concrete compressive strength. Artificial Neural Network (ANN) model was developed to predict the compressive strength of SCC using a comprehensive database collected from different previous studies. The database was used to train and test the developed ANN. Moreover, parallel to the experimental works, a three dimensional nonlinear finite element (FE) model using ABAQUS software was developed to predict the behaviour of SCC elliptical tube columns. The proposed ABAQUS model was verified against the current experimental results.

The experimental results indicated that the failure modes of the SCC filled elliptical steel tube columns having large slenderness ratios were dominated by global buckling. Moreover, the composite columns possessed higher critical axial compressive capacities compared with their hollow section companions due to the composite interaction. However, due to the large

slenderness ratio of the test specimens, the change of compressive strength of concrete core did not show significant effect on the critical axial compressive capacity of concrete filled columns although the axial compressive capacity increased with the concrete grade increase. The comparisons between the axial compressive load capacities obtained from experimental study and those predicted using simple methods provided in Eurocode 4 for concrete-filled steel rectangular tube columns showed a reasonable agreement. The proposed three dimensional FE model accurately predicted the failure modes, the load capacity and the load-deflection response of the columns tested. The experimental results, analysis and comparisons presented in this thesis clearly support the application of self-compacting concrete filled elliptical steel tube columns in construction engineering practice.

ACKNOWLEDGEMENTS

First of all, I express my deepest thanks to almighty **Allah** for blessing me with the health, wisdom, perseverance, patience, understanding and motivation needed to successfully complete this work.

I would like to express my sincere gratitude to my supervisors **Prof. Ashraf Ashour, Prof. Dennis Lam** and **Dr. X Dai** for their invaluable guidance and advice, encouragement and support throughout this work.

Also, I wish to express my sincere thanks to **my mother,** who died on 06 Aguste 2016. She and **my father** have given all my academic endeavours unwavering encouragement and in the pursuit of my study this support substantially contributed to its completion. I would like to thank my **brothers** and **sisters** who support me for this long journey.

My great gratitude and my sincere thanks are to be dedicated towards **my wife and kids, Iftima and Mohammed** for their invaluable encouragement and patience during my study. Without them, none of this would have been possible.

I would also like to thank my sponsors, The Ministry of Libya Higher Education, for awarding me with the PhD scholarship. These supports have been greatly appreciated.

I am grateful to **all members and friends** of civil engineering for their great advice and encouragement during this research.

I am deeply grateful to **laboratory staff** in the Heavy Structural Laboratory for their technical support throughout the experimental investigation of this research.

Contents

List of Figures

List of Tables

NOTATIONS

The following symbols are used in this thesis:

σ	Stress
ε	Strain
E_{cm}	Average elastic modulus
F_{cm}	Average strength
SI	The segregation index
N_{ed}	The compressive resistance of concrete filled steel tubes
$N_{Pl,Rd}$	The plastic resistance of the composite section
χ	The reduction factor for the relevant buckling mode
λ	Slenderness
α	The imperfection factor
A_c	Cross-sectional area of concrete
A_s	The cross-sectional area of steel tube
f_c	The compressive concrete cubes strength
f_s	The yield strength of steel
N_{cr}	Critical elastic normal force for the relevant buckling mode
$(EI)_{eff}$	the effective flexural stiffness
L	The actual effective height
I_a	The second moments of inertia of the structural steel section
I_s	The second moments of inertia of the un-cracked concrete Section
E_a	The elastic modulus of steel section
E_s	The elastic modulus of un-cracked concrete section
P_{EC4}	The predicted load-carrying capacities by EC4
P_U	Experimental load capacity
COV	Coefficient of variation
fy	The steel yield strength
fu	The ultimate strength

εy	The yield steel strain
ψ	Dilation angle
f'_{cc}	The uniaxial compressive strength
ε'_{cc}	The corresponding strain
f'_c	Mean value of concrete cylinder compressive strength
ε_{c1}	The strain at peak stress
ε_{cu1}	The ultimate nominal strain

ABBREVIATION

The following symbols are used in this thesis:

ANN	Artificial neural network
CFT	Concrete-filled tube columns
FA	Fly ash
ggbs	Ground-granulated blast-furnace slag
HSS	Hollow structure steel
MC	Moisture content
NC	Normal concrete
SCC	Self-compacting concrete
SP	Superplasticiser
VMAs	Viscosity modifying agents
w/b	Water to binder ratio
FE	Finite elements model
EC4	European code
EC3	Eurocode for steel columns

CHAPTER ONE

INTRODUCTION

1.1 Background

Self-compacting concrete (SCC) was originated in Japan and then spread to Europe and South America. A good SCC mixture should have the capability to flow through dense reinforcement under its own weight, and completely fill all voids without segregation or excessive bleeding, and without the need for vibration or other mechanical consolidation. This type of concrete is able to maintain its stability and homogeneity whilst still achieving good compaction. For these reasons, SCC has been successfully used in numerous applications where normal concrete would be difficult to install, or in places with limited accessibility due to reinforcement congestion (Siddique et al. 2011).

SCC was initially used for concrete slabs and beams, however since the beginning of this century it was increasingly employed in concrete-steel composite members due to its self-compaction performance, higher load capacity, inherent ductility and toughness when they are used as columns in buildings. Composite members can also lead to significant savings in materials and increases in the net floor space. In the past, the most commonly used composite column section shapes were square, rectangular and circular. However, elliptical hollow sections have been recently introduced to the construction market and its application is becoming popular in contemporary building design due to its pleasing appearance.

The behaviour of hollow steel section tube filled with normal concrete has been the main focus of high number of research investigations. It was found that the strength of concrete is increased by the confining effect obtained from the steel tube and the local and global buckling of steel wall was delayed by the restraining effect of concrete (Yu et al. 2008 & Giakoumelis and Lam, 2004).

The orientation of the steel and concrete member in the composite column cross section has a significant role in terms of enhancing the strength and stiffness of the structure. The steel section is located at the outer perimeter, where it performs most effectively in tension and bending moment. Moreover, the stiffness of the composite column is enhanced as the steel section has a greater modulus of elasticity compared with concrete members and a greater moment of inertia owing to the fact that the steel section is situated farthest from the centroid of the cross-section (Gourley et al., 2001). Circular and rectangular tube columns made with SCC have been studied and compared with those using normal concrete, and the results were close. However, very few researchers have investigated SCC-filled elliptical steel tube columns. Elliptical hollow sections (EHS) can offer greater efficiency than circular ones, particularly when subject to eccentric loading (generating a bending moment about a particular axis) or when differing end restraints or bracings exist about the two principal axes (Zhao and Packer, 2009). Unfilled elliptical columns have been used recently in a number of structures including a coach station at Heathrow terminal three in the UK, Sword Airside project in Ireland and the main railway station at Bern in Switzerland.

However, the elliptical hollow section is not currently covered by any structural design code.

At this moment, there is limited understanding of structural performance on the elliptical tube section. The results on elliptical hollow sections are currently insufficient, and very limited experimental information can be found concerning elliptical tube columns filled with concrete (CFT). Most of the researches on elliptical columns focused on short columns and limited number were focused on long columns. The confinement effect is an issue which needs to be addressed, particularly in consideration of how it affects to the steel section. The interaction between local and global buckling also needs to be investigated, especially for slender columns. The work presented in this thesis highlights the mechanical behaviour of elliptical CFT columns. In order to comprehend the behaviour of elliptical CFT columns, it is first necessary to understand the response of elliptical tubes in the composite structure and the interactions between individual materials in structure. Furthermore, the potential and advantages associated with the use of hollow section columns in the composite column have been established. Thus, the knowledge gained from the experiments and FE analysis and the failure process in the columns are vital in order to add information which fundamentally benefits both the researcher and engineers.

1.2 Aims and Objectives of the research

The main goal of this PhD project is to study the behaviour of elliptical tube columns filled with SCC. The principal objectives of this research are categorised below:

- To develop an artificial neural network (ANN) model to design appropriate self-compacting concrete mixture and predict the compressive strength because all the available mix design methods for SCC are not clear to follow.
- To experimentally investigate the behaviour of elliptical tube columns filled with SCC in order to extend the limitations for the slenderness ratio investigated previously and provide more experimental data.
- To develop a three dimensional nonlinear finite element model to analyse the behaviour of elliptical tube columns filled with SCC. The proposed model will be evaluated against the present and previous experimental results.
- To carry out a parametric study using the proposed finite element model to extend the range of parameters which were not fully covered by experimental study.
- To assess the applicability of using the current design rules, provided in Eurocode 4 for circular and rectangular columns, for predicting the load capacity of elliptical CFT columns.

1.3 Research methodology

As shown in Figure 1.1, the following approaches have been employed to achieve the research aims and objectives mentioned above:

- Artificial neural network program has been developed using MATLAB (R2009a) to predict the compressive strength of SCC.
- Eight elliptical tube columns filled with SCC were tested to failure in the laboratory. Two hollow section columns with the same section sizes of filled one were also tested for comparison purposes.
- Numerical modelling (ABAQUS) was carried out in parallel with experimental programme.
- The design guidelines (EC4) has been evaluated against the experimental results.
- Comparisons between the computational results obtained from the current program and those obtained from the experimental results have been carried out.

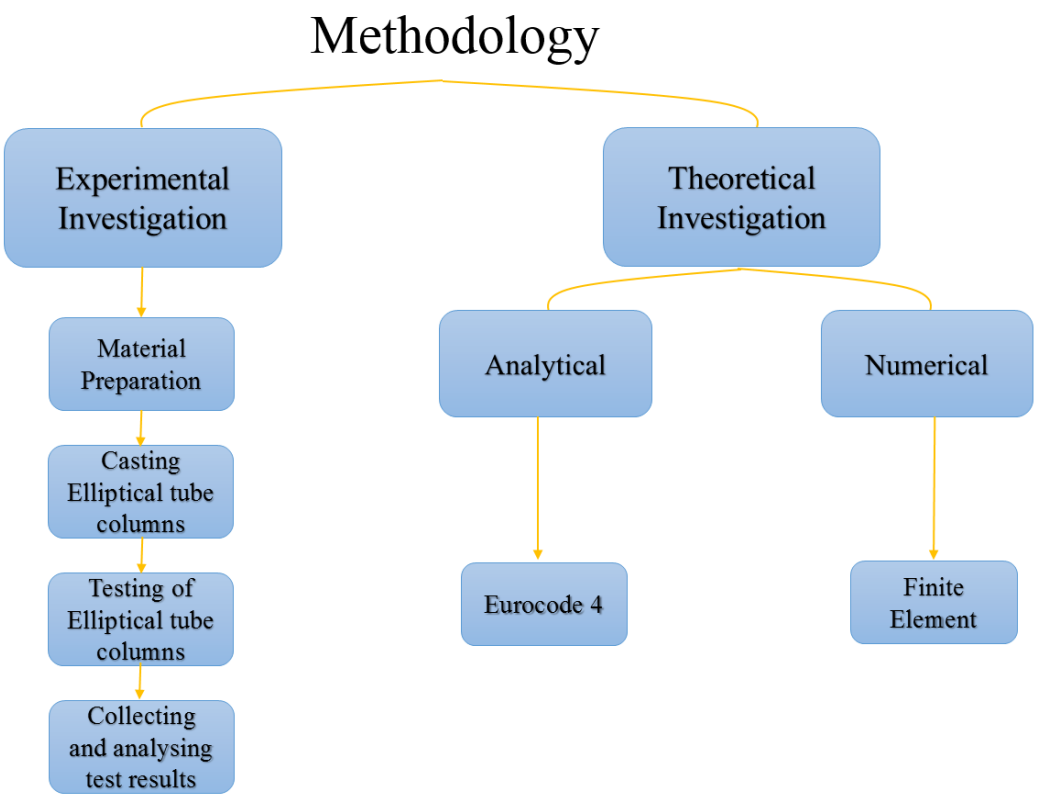

Figure 1. 1 Thesis's Methodology

1.4 Research significance

Several researchers have introduced SCC to the construction industry as a new type of concrete materials. The overall success of use in construction practise paved a way for others to investigate the possibility of using SCC for composite columns, including elliptical columns.

In comparison with the investigations carried out in this field, the current research has attributed the following significance:

- The outcome of this investigation will increase the limited number of previous researches in the field of using SCC with elliptical tube columns.

- Phase one of the project develops ANNs to predict the compressive strength of SCC. Engineers can use ANNs to predict the compressive strength of SCC as a replacement to other complicated mix design methods.
- Engineers and researchers will have a better understanding of the performance of SCC filled elliptical tube columns.
- The developed numerical technique can be used for further parametric studies to provide more insight into the behaviour of elliptical tube columns filled with SCC.

1.5 Thesis outlines

- This chapter presents general background of SCC, filled elliptical tube columns. Then the scope, aim and objectives of the research are presented.
- Chapter two reviews self-compacting concrete properties and its mix design methods. Then, it presents a review of different tube sections columns filled with concrete. Finally, previous experimental and computational investigations of elliptical tube columns filled with concrete are presented in this chapter.
- Chapter three presents a review of the ANN as a design method for predicting compressive strength of SCC. It covers the procedure of modelling and verification of the results obtained throughout the Matlab analysis phase. A series of parametric study was also conducted to study the effect of parameters on the compressive

strength and validate the ANN model. Moreover, comparison between the ANN prediction and experimental results of cube compressive strength are also presented.

- Chapter four presents the experiments in detail including material property tests of the concrete mix and explained in detail the procedure of columns preparation, the rig-frame setting-up and the tests involved in this study.
- Chapter five reports the results of columns tests, which include load capacity, lateral displacement and shortening. Moreover, experimental results have been assessing the adaptability of current design rules provided in Eurocode 4 for circular and rectangular columns.
- Chapter six presents the details of the finite element modelling. The commercial package ABAQUS, was used to establish and validate finite element models against the experimental results. Parametric study were using finite elements to investigate the behaviour of elliptical tube columns filled with SCC under axial load for variation in geometric arrangements and material properties were presented as well.
- Chapter seven summarizes the main conclusions from the work undertaken for this thesis and gives recommendations for future research.

CHAPTER TWO

LITERATURE REVIEW

2.1 Introduction

Concrete-filled steel tubular (CFT) columns are being used widely in all types of constructions, owing to their many advantages such as high strength/stiffness, attractive appearance, high fire resistance and large energy absorption capacity (Hu et al., 2003; Han et al., 2007; Giakoumelis and Lam, 2004; Ding and Wang et al, 2004). Moreover, confinement of the concrete core by the steel tube enhances the strength of the concrete core. Furthermore, the steel tube also prevents the concrete core from spalling under fire exposure (Hu et al., 2005; Hu et al., 2003).

CFT columns have been studied for many decades (Giakoumelis and Lam, 2004; Zeghiche and Chaoui, 2005). The first research investigation on CFT column was presented by Sewell in 1901 (Johansson, 2002), and the earliest complete test on CFT columns was conducted in 1957 by Kloppel and Goder (Han, 2002). The purpose of filling the tube column with concrete in the study conducted by Sewell was to protect the internal hollow tube from rusting. The enhancement of the structure stiffness was noticeable after some of the columns were accidentally overloaded. The first column was tested by Kloppel and Goder in the late 1970s, since then, the development in studying the axial load capacity of the CFT columns has risen significantly. (Han, 2002).

A new elliptical shape of steel tube column has been used in few places, but is not yet popular. The elliptical hollow section can provide greater efficiency than a circular hollow section, particularly when subjected to eccentric loading (Chan and Gardner, 2009). Only few studies had been undertaken on this new section shape. Therefore, it is considered that further investigations and experimental data are needed in order to obtain a better understanding of the elliptical CFT columns, particularly on slender columns behaviour.

Most of the CFT columns in the last century were filled by normal concrete, but since Self-compacting Concrete was presented to construction materials, it takes part of filling the tube columns.

The interaction between the steel tube and the concrete core plays the most important role in increasing the load capacity of the composite columns.

Although furthermore, the concrete core in the CFT column is confined by the steel tube and shows different behaviour to the normal unconfined concrete. In order to accurately simulate CFT columns, an appropriate material model for the confined concrete should be employed.

The aim of this review is to summarise the leading studies that have been conducted on self-compacting concrete (SCC). A brief introduction to the materials used with SCC is followed by a description of a fresh, mix design method and discussion of the hardened properties of SCC. Then a detailed review of columns filled by normal and SCC is given, as this project focuses on elliptical tube columns filled with SCC.

2.2 Constituent materials used for SCC

There are no specific materials used to produce SCC. Its composition is largely the same as normal concrete, but with admixtures, which are key to improving workability. The constituent materials, which will occupy a brief part in this literature review, are as follows:

2.2.1 Cement

In Japan, some types of cement are popular for use in SCC, such as Portland blasé-furnace slag, and modified cement, where Fly ash (FA) or slag will reduce the shrinkage and delay the initial setting time (Su et al., 2001). Indeed, other types of cement are also used, and the cement selection has an effect on the SCC.

SCC behaviour is affected by cement composition, because C3A and C4AF absorb the superplasticiser (SP) after mixing (Nawa et al., 1998). The C3A

and C4AF content has an effect on the initial set time of cement (Collepardi, 1998). It was shown that those types of cement containing low levels of C3A and C4AF, such as low and heat content Portland cement, were perfect in the early development of SCC in Japan (Ouchi et al., 2003).

2.2.2 Aggregates

It has been noted that SCC has different properties when using different grades of aggregates. Geiker (2008) found that SCC can be created with significant grading of aggregates. The size of the dividing sieve between fine and coarse aggregates depends on the region. For instance, 4mm is used in Europe (The European Guidelines for Self-Compacting Concrete, 2005), 5mm in Japan (Nawa et al., 1999) and 8mm in Sweden (Billberg, 1999).

In general, natural gravel provides better filling ability due to smaller inter-particle friction (Billberg, 1999). Crushed aggregates also have an effect on the strength of concrete. By using crushed aggregate, the mix needs an increased volume of paste and less aggregate in order to avoid blockages. It also requires a higher quantity of dosage (Petrsson, 1999). Therefore, the fineness, shape, gradient, packing density, flakiness and ratio of fine to coarse aggregate, all have an effect on the fresh properties of SCC (Khayat et al., 1999).

2.2.2.1 Coarse aggregate

All previous research has shown that the choice of crushed or gravel aggregate depends on local availability. In some countries, lightweight and recycled concrete aggregate has been used in SCC (Domone, 2007). The

high viscosity of lightweight aggregate leads to a decreased risk of segregation, while recycled concrete aggregate has a high level of water absorption, which affects the filling ability because of the quick loss of consistency (Shi and Yang, 2005).

Since SCC was first invented, researchers have used coarse aggregate with a maximum size between 16 - 20 mm in order to avoid blocking. However, as SCC was developed, larger size aggregate was used, resulting in good properties. One example of this is the use of 40 mm aggregate in a bridge connecting two Japanese islands (Liu, 2009).

Assaad and Khayat (2005) studied the effect of coarse aggregate characteristics on lateral pressure exerted by SCC. They found that lateral pressure is significantly affected by coarse aggregate, and that by increasing the percentage of coarse aggregate, the lateral pressure was reduced. This could be a result of the increasing volume of coarse aggregate, which reduces mixture mobility, leading to a reduction in lateral pressure.

Topcu and Bilir (2009) tried to replace aggregate with rubber to improve the properties of SCC and find an acceptable alternative to aggregate. They found that the fresh properties were improved by adding 180 kg/m^3 of rubber to the mix. However, the hard properties showed no improvement, where strength decreased due to aggregate replacement with rubber. Bignozzi and Sandrolini (2006) had previously reported a similar finding.

2.2.2.2 Fine aggregates

- **Sand**

The ideal sand for SCC has good grading, spherical shape and low absorption (Skarendahl, 2000). However, poor grading and irregular shaped sand has been used, but by increasing the paste volume or the viscosity (Westerholm et al., 2008). The quality of the sand used is often dependent on availability in the region (Skarendahl, 2000).

Billberg (1999) reported that different kinds of sand have an effect on the performance of SCC by proving the influence of aggregate fineness on the slump flow and the fill height of a U-shaped box, which varied with different aggregate moisture content (MC). Moreover, sand'MC affects the SCC properties. Any slight mistake in MC will lead to huge changes in the SCC fresh properties (Bartos, 2005).

Fine particles in sand have a greater effect on SCC than on normal concrete (Skarendahl, 2000). This is due to the fact that fine particles like clay, i.e. increasing w/b, delaying cement hydration, and affecting volume stability (Topcu and Ugurlu, 2003). Moreover, fine particles reduce the compressive strength, and cause an increase in superplasticiser (SP) dosage (Felekoglu and Sarikahya, 2008).

Kou and Poon (2009) replaced the fine aggregate with fine recycled aggregate. They found that resistance to chloride ion penetration increased with increasing amount of fine recycled aggregate. However, this resulted in lower strength and greater shrinkage.

- **Powder**

Powders constitute the smallest solid particles in concrete, including cement and additives. Powder size differs from one country to another. For example, powder particles may be as large as 90μm in Japan (Liu, 2009) and up to 125μm in Europe (the European guide code of SCC, 2005). The powder must be chosen carefully, because it has an effect on the fresh and hardened properties due to infiltration in a large proportion of the concrete mix. For instance, limestone and chalk can be used with SCC to obtain a good mixture, but the mix needs more SP (Zhu and Gibbs, 2005). The main purpose of using powder is to fill the voids between aggregate particles.

The quantity of particles sized less than 100μm is a significant factor in improved filling ability and segregation resistance (Noumowe et al., 2006). Ozawa et al. (1990) tested concrete mixed with different powder particle sizes. They concluded that paste with fine powder has a higher segregation resistance than that with coarse powder. Khayat et al. (1999) found that the segregation resistance was due to the increased water retention of fine powders. Moreover, they established that increased levels of powder with particle sizes below 80μm leads to higher resistance to surface settlement. However, coagulation occurs when powder size is smaller than 20μm, and as a result, a larger SP quantity is required in order to disperse them (Felekoglu, and Sarikahya, 2008). Boukendakdji et al. (2009) studied the effect of slag on the SCC, and agreed with the previous result. However, they found that the increased slag in the mix led to a reduction in the compressive strength.

2.2.3 Admixtures

Admixtures are materials that are added in small quantity to improve the SCC mix properties. The desirable properties of SCC are heavily dependent on the presence of admixtures. Some admixtures have been used since the development of SCC, such as SP and viscosity modifying agents (VMAs). The European guidelines (2005) presented the dosage rang of SP and VMAs admixture in concrete mix. The admixture development stages will be described in subsequent sections.

2.2.3.1 Superplasticiser (SP)

Flocculation of cement occurs when it is mixed with water. It happens due to an electrostatic attractive force produced by the electric charge on the surface of the particles. This flocculation creates large portions of free water, which reduces the consistency of the concrete (Uchikawa et al., 1995). Therefore, SP is a solution to the flocculation. It breaks up the flocculation, agglomeration and trapped water by entering between the cement particles and imparting a negative surface charge that causes electrostatic repulsion, as shown in Figure (2.1).

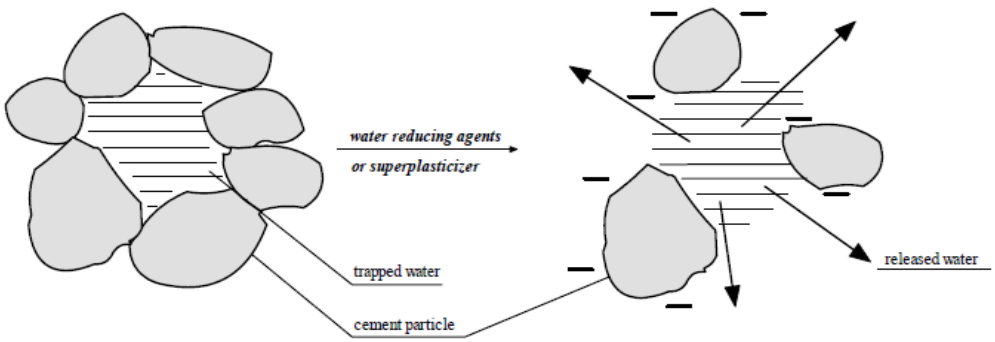

Figure 2.1 Effect of SP on the cement particles (Unhikawa et al., 1995)

SPs are mainly based on steric repulsive forces, and include polycarboxylate-based agents. They have a molecular structure composed of a backbone of a long straight chain of carbon atoms with ethylene oxide side chains that absorb water, and produce a thick layer on the cement surface, resulting in the generation of effective steric repulsion (Yamada et al., 2000). Cement particles also get a negative charge from the carboxyl group in the molecule, thus providing some electrostatic particle repulsion. However, this is weaker than that of the sulfonic group (Uchikawa et al., 1995).

New research has resulted in new polycarboxylic acid-based SPs, which presents high consistency, proper viscosity, and long consistency retention even for a small water cement ratio. For this reason, it is suitable for SCC, and is commonly used nowadays. SPs have some properties that affect SCC, such as absorption and consistency. The ability of absorption depends on the electrostatic repulsion, which is a function of the cement fineness, C3A content and grade of polymerisation (Bonen and Sarkar, 1995). Yamada et al. (2000) found out that the lower the specific surface and C3A in the cement, the lower the SP absorption that can be obtained.

SP absorption is also affected by temperature and time. When the temperature is high the absorption rate increases, while consistency decreases with time (Liu, 2009). Moreover, the effect of SPs depend on the powder and the mix method. These therefore form the main disadvantages of SPs, which affect the SCC properties.

Yamada et al. (2000) studied the behaviour of cement paste affected by SPs and water ratio. They found that with a water to cement ratio less than 0.25, consistency has a significant effect. Otherwise, for water cement ratios higher than 0.35, the spread paste was more sensitive to SP dosage causing the SCC to be weaker. Low water content or SP dosage could have a strong effect on the consistency of SCC.

Collepardi et al. (2005) mentioned that polycarboxylic acid-based SPs have been more commonly used in SCC in the past ten years, due to their higher dispersing effect, longer consistency retention, and greater robustness. However, it reduces yield stress significantly, keeping plastic viscosity while not affecting setting time and air content (Yamada et al., 2000; Felekoglu and Sarikahya, 2008).

2.2.3.2 Viscosity modifying agents

Viscosity modifying agents (VMAs) fall into two groups, depending on whether they employ an adsorbing or non-adsorbing mechanism ((Yammamuro and Mizunuma, 1997; Nawa et al., 1998). The first type of VMA acts on cement. After addition, it is adsorbed onto the surface of cement particles and produces a structure, which imparts viscosity to the concrete. When the quantity of VMAs absorbed by cement particles is increased, it leads to a reduction in consistency. This type of VMA includes cellulose-based polymers and acrylic-based water-soluble polymers (Nawa et al., 1998).

Non-adsorbing VMAs act on water; because they are non-adsorbing, the plastic viscosity is increased. This results in water-soluble polymer chains imbibing some free water (Khayat, 1999). Nawa et al. (1998) found that the amount of SPs does not have to change with an increase in the non-adsorptive VMA added. Therefore, the plastic viscosity increases, but the spread value may not change.

The first types of non-adsorbing materials were used in Japan, Welan and Dituan, and are now being used in South America. They are all anionic, long-chain biopolymers with sugar side chains, produced by a controlled aerobic fermentation process (Khayat, 1999). Welan and Dituan can be used at low concentration to improve the stability and robustness of SCC without any effect on the consistency, therefore making quality control easier. However, this type is very expensive (Khayat et al., 2003).

Starch, precipitated silica and new polysaccharide-based VMAs have been developed to reduce the cost of SCC (RoIs et al., 1999). Lechemi et al. (2004) found that SCCs made with these new VMAs have better fresh and hardened properties than those made with Welan and Dituan. Moreover, new VMAs, can give the same consistency SCC as Welan and Dituan, but with lower dosage.

VMAs improve the yield stress, plastic viscosity, appearance, and the thixotropic behaviour of the mix (Khayat et al., 1999). Some years later, Khayat worked on the latter result and found that SCCs with VMAs can exhibit high viscosity at low shear rate. However, viscosity decreased with an

increase in shear rate. This helps at placement of SCC, as the viscosity is improved due to association and entanglement of the polymer chains of VMA at the low shear rate. Moreover, adding VMA to SCC will improve the robustness and decrease the occurrence of segregation. It can also reduce the sensitivity of SCC to water content (Okamura and Ouchi, 1998).

As previously mentioned, SCC needs a high powder content in order to exhibit good workability. If cement only is used, SCC will cost too much and cracks will occur due to the large amounts of cement. Some cement must therefore be replaced with additions such as fly ash (FA), Ground-granulated blast-furnace slag (ggbs) or limestone filler. Admixtures must not be expensive, because one purpose of using SCC is to reduce the cost.

2.2.4 Water

The water in the fresh concrete includes both free water and any water retained by powder, cement, sand and VMA. Free water controls the performance of SCC and determines the filling ability and segregation resistance (Oh et al., 2002). Coarse aggregates do not hold water, but water content in the aggregate has little effect on the free water. Kasemchisir and Tangermsirikul (2008) pointed out that slump flow T500 may be predicted by free water content.

2.3 SCC Mix design

There are no standard specifications or methods for SCC mix design, as for normal concrete, such as British, ACI method, etc. Mix design methods of SCC have passed through stages of development before reaching their final

form. Each method has been developed for its purpose and environment, and has its own specifications and limitations. Thus, it becomes difficult to compare one method to another. The following sections will briefly describe some SCC mix design methods.

Mix design methods for SCC usually start with the required fresh properties. The goal is to add SPs with or without VMA, to reduce the amount of coarse aggregate and to ensure a sufficient water powder ratio to obtain the fresh properties required (Ozawa et al., 1990).

The mix design methods of SCC have been developed individually, with different methods used in different countries. Six methods have been presented since the development of SCC. Some of them are not clear to follow, such as the general-purpose method, (LCPC)'s method and Hon's method, while others could be follow. The general-purpose method presented the percentage of coarse aggregate and fine aggregate (particles sized more than 0.09 mm), which is 50% and 40% respectively and 10% air content, water to binder ratio (w/b) and SPs dosage (Okamura and Ozawa, 1994; Ozawa et al., 1990). On the other hand, the LCPC method cannot be used without software that must be purchased (Sedran et al., 1996), and Hon's method presented the volume of paste in the mix, but it is not clear to follow. Easily followed methods are the CBI method (Petersson and Billberg, 1999), Hwang's method (Hwang et al., 1996), and a simple mix method (Su et al., 2001). In general, different methods of SCC design have their own basis, and usually the details of the methods are not published. Moreover,

SCC design is not simple, but needs much work, where experience is important in order to solve the problems effectively. Computing software has become more interesting, with Matlab tools giving good results, saving time and reducing the loss of materials. In chapter three, an artificial neural network model is developed to predict the SCC compressive strength and also used for SCC mix design for the group of the columns in this thesis.

2.4 Fresh properties of SCC

SCC has special properties, which must be available in order to be considered a good mix. These properties are filling ability, passing ability, segregation resistance, robustness and consistency retention. All of these will be explained in the following sections.

2.4.1 Filling ability

Filling ability is the ability of the fresh concrete to distort and flow under its own weight without vibration or extra assistance into the formwork (Okamura et al., 2000). Distortion has two defining properties: the distortion capacity, which is the ability to flow; and the distortion velocity, which is the time the concrete takes to stop flowing. Filling ability is related to distortion capacity and distortion velocity and encourages a balance between them. For instance, concrete with low distortion velocity and high distortion capacity is very viscous, and so takes time to fill the formwork (Skarendahl and Petersson, 2000).

SCC must flow through the formwork and attended area without segregation. To achieve the filling ability, the friction between the aggregate pieces must

be reduced by adding SP and by decreasing the amount of coarse aggregate (Khayat et al., 1999; Sonebi and Bartos, 2002). The common method to measure the filling ability is the slump test. This test uses a standard slump cone to give an indication of the filling ability and, to some extent, the cohesion.

2.4.2 Passing ability

Passing ability is exclusive to SCC, and is the ability of concrete to flow through restricted, confined spaces and narrow openings, guaranteeing that its particles can be applied within tightly reinforced structures (Domone, 2007). It is suitable to evaluate this using the L- box test, which is affected by aggregate volume, dosage of water and high range water reducer quantity (Sonebi and Bartos, 2002). The L-box test measures the passing ability by observing any tendency to block the flow when a reservoir of concrete passes an obstruction (three closely spaced reinforcing bars) under gravity into an open channel. Another test is called the J-ring test, which is similar to the slump test except that arrangement of the bars surrounds the slump cone.

SCC must pass through formwork and between bars of steel without blocking. Blocking results from an interaction between aggregate particles and reinforcement structures (Noguchi et al., 1999; Okamura and Ouchi, 2003). To prevent blockages, adequate mixture viscosity is needed. If SCC is highly deformable, but has enough cohesiveness, the concrete could not spread itself homogeneously through the formwork. Otherwise, mixtures with

low deformability may result in segregation that can lead to blocking (Emborg and Hedin, 1999).

2.4.3 Segregation resistance

Segregation resistance occurs between water and solids, paste and aggregate, or mortar and coarse aggregate due to the mix of SCC having different materials with different specific gravities (Skarendahl and Petersson, 2000). Free water in concrete is the main reason for segregation (Ozawa et al., 1990). Felekoglu et al. (2007) found that the optimum water/cement ratio for production SCC is 0.84 to 1.07 by volume, where ratios above or below these limits causes blocking or segregation. There are two types of segregation, where the first is referred to as dynamic, and occurs during placing. The second type is known as static or bleeding, which happens after placing (Kim et al., 2003). For enhanced segregation resistance, binding of free water is encouraged by the use of a lower water to binder ratio (w/b), VMA or high volumes of powder, and a reduction in the content of coarse aggregate. This will give good flow as a result of good viscosity (Sonebi and Bartos, 2002). There are three tests to measure segregation; settlement column, penetration and sieve stability test. The popular one is the penetration test, which measures the segregation potential as the depth of penetration of a standard mass (54g) into the concrete. If segregation is high, then the top part of the concrete would be mainly mortar, and the resultant depth of penetration would be high. For good SCC, penetration should not be more than 8 mm (Skarendahl and Petersson, 2000).

2.4.4 Robustness

Robustness is the ability of concrete to protect its properties under different situations. Due to SCC being more sensitive to variations in condition than normal concrete, robustness is affected by changes in water content and SP dosage (Embrorg and Hedin, 1999). However, by using powder and VMA to increase the viscosity, the robustness will improve (Domone, 2007).

2.4.5 Consistency retention

Consistency retention means SCC properties must be close to the initial mix after transporting and placing. The fresh properties are usually retained for 60 to 90 minutes (Kasemchaisiri and Tangermsirikul, 2008; Skarendahl and Petersson, 2000; Sonebi and Bartos, 2002).

Due to the interaction between SP and powder, loss of consistency occurs for different effects of powder on the water absorption and admixture (Khayat et al., 1999). Moreover, the effect of the lower absorption of SP on the hydration of cement results in loss of consistency (Uchikawa et al., 1995). However, polycarboxylate-based SPs give high consistency (Hanehara and Yamada, 1999), and the composition of additions, minimisation of coagulation of cement, and adequate hydration provide a high consistency (Bonen and Sarkar, 1995).

From previous sections, the factors, which affect the passing ability and segregation of SCC, are clearly understood. Blocking or poor pass ability could occur due to too small gaps in the reinforcement, high aggregate content, poor flow ability and segregation. However, segregation can be

treated by controlling the reinforcement spacing, limiting the coarse aggregate, increasing the concrete flow ability, and increasing the viscosity.

2.5 Hardening Properties

The hardening properties of SCC are similar to normal concrete with regard to strength (Petersson, 1999, Persson, 2001). However, the main difference between SCC and NC is that the SCC has a high powder content and less coarse aggregate. This results in a difference in properties, such as the elastic modulus, shrinkage and creep (Pentti, 1999; Van Khanh and Montgomery, 1999). Due to the blends of powder reducing the amount of voids in the cement paste, the durability of SCC is better than that of normal concrete. This durability includes air and water impermeability, and freeze-thaw resistance (Billberg, 1999). The following sections give a brief explanation of the hardening properties of SCC.

2.5.1 Compressive strength

There is no great difference in strength between SCC and normal concrete when the water powder ratio is similar (Dehn et al., 2000; Domone, 2007; Gibbs and Zhu, 1999; Skarendahl and Petersson, 2000; Sonebi and Bartos, 2002). Moreover, the gain of SCC strength development from the time of first placing until design strength obtained is similar to that of normal concrete (Dehn et al., 2000; Domone, 2007; Gibbs and Zhu, 1999; Skarendahl and Petersson, 2000; Sonebi and Bartos, 2002). Domone (2007) found that the compressive strength of SCC at 28 days may reach up to 100 MPa, depending on the water powder ratio. Moreover, it was found that 4 MPa is

the difference in strength of SCC when mixed with crushed and uncrushed aggregate, which is half the typical value, 8MPa, for normal concrete (Domone, 2007). Ahmadi et al. (2007) presented that compressive and flexure strength of SCC is higher than NC when using rice husk ash. Moreover, Assie et al. (2007) and Holschemacher (2004) have agreed in their findings, when the water cement ratio and raw materials was similar, except for a greater quantity of SP in SCC.

2.5.2 Elastic modulus

The elastic modulus is defined as the ratio between stress and strain. The elastic modulus of the concrete depends on the proportion of Young's Modulus of the individual components and their percentages by volume (Holschemacher, 2004). With regard to concrete, a stress-strain curve is non-linear, which is obtained from different elastic modulus. A static modulus is the slope of the tangent to the curve at the particular point S, whereas the slope of the tangent to the curve at origin is called initial modulus, as shown in Figure (2.2) (Domone and Illston, 2010).

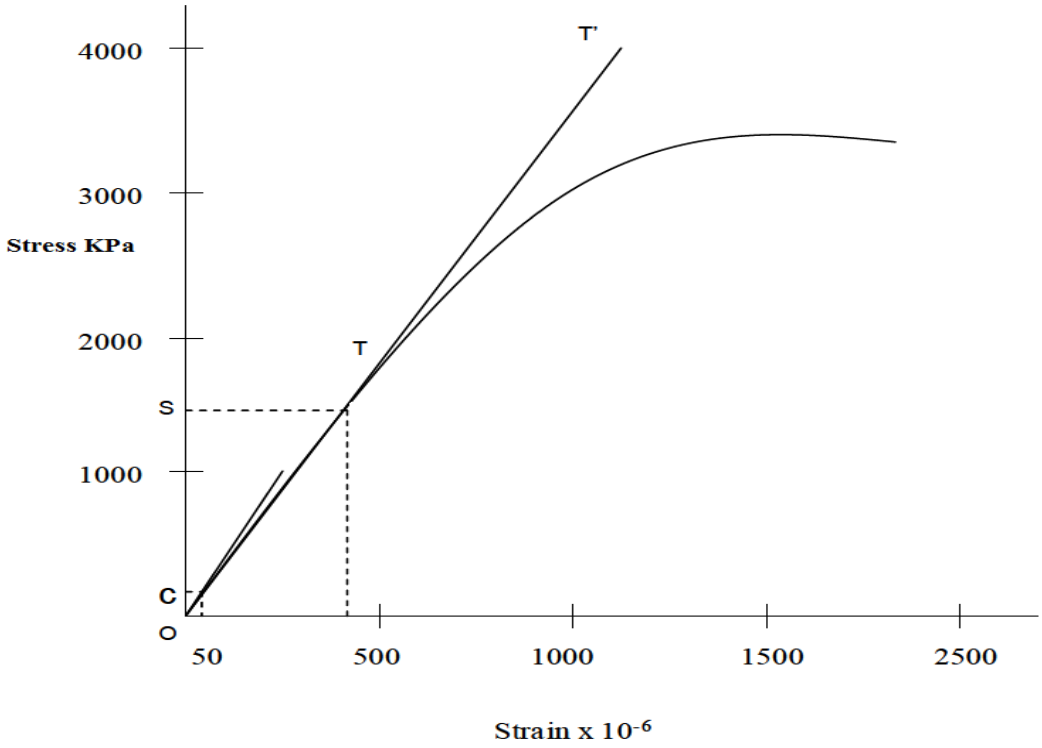

Figure 2.2 Types of elastic modulus (Mata, 2004)

The ratios of elastic modulus to initial modulus do not exceed one (Boneu and Shah, 2005). The elastic modulus can be estimated from the following equation:

$$E = \frac{\sigma}{\varepsilon} \qquad (2.1)$$

where E is elastic modules, σ is stress and ε is strain

The elastic modulus of SCC is affected by the elastic modulus of the aggregate, the cement paste, porosity and by Young's Modulus. It increases with high content of aggregate and decreases with high content of cement paste and increased porosity. Therefore, elastic modulus for SCC are lower than for normal concrete, because of the higher content of paste and lower

content of coarse aggregate (Dehn et al., 2000; Collepardi et al., 2005; Domone, 2007).

Persson (2001) presented that the elastic modulus of SCC coincided well with the same properties of NC when strength was held constant. However, Dehn et al. (2000) and Jacops and Hunkeler (1999) disagreed with him, and concluded that elastic modulus for SCC is lower than that of NC.

Turatsinze and Garros (2008) used rubber aggregate with SCC then studied the behaviour of elastic modulus. The result shows that the elastic modulus is affected by rubber, and its variation cannot follow the classical relationship with compressive strength, which is presented by European standard EN1992-1-1 between average elastic modulus and average strength by the following relation:

$$E_{cm} = 22\left(\frac{F_{cm}}{10}\right) \qquad (2.2)$$

Where: E_{cm} is an average elastic modulus by Gpa and F_{cm} is average strength by MPa.

Initial modulus (Eit) has different equations, as presented by ACI, BIS or researchers. Kumar et al. (2011) have worked on initial elastic modulus of SCC and NC using different equations. They found that the equation of elastic modulus presented by ACI 2008 can be used for SCC and gives accurate results.

2.5.3 Creep and Shrinkage

Shrinkage occurs due to increasing paste volume (Roziere et al., 2007). There are two types of shrinkage; the first is plastic shrinkage caused by the drying surface, and as such, is affected by humidity, wind temperature and bleeding, which creates a dry surface due to evaporation. Leemann et al. (2011) found that the plastic shrinkage of SCC is four times higher than for normal concrete.

Drying shrinkage is the second type. It occurs over a long period of time and is associated with the properties of the paste, including water cement ratio, water content, graduations and the volume of paste (Persson, 2001). Mata (2004) showed that the drying shrinkage of SCC is 25% higher than that of normal concrete.

Creep and drying shrinkage are usually studied together, because they occur for approximately the same reason (Mehta, 1986). They are associated with the movement of moisture, but the most important factor, which affects creep shrinkage, is the external load rather than different humidity. The deformation by creep is governed by the age of the load, the time of applying the load, concrete properties, method of curing and environment condition. The creep of SCC is 50% higher than that of normal concrete due to the high content of cement paste (Holschemacher, 2004). However, the shrinkage and creep of SCC coincided well with corresponding properties of NC when the strength was held constant (Persson, 2001).

2.5.4 Permeability

Permeability is defined as the transport of water under a hydrostatic pressure differential. The main influences on permeation include the paste volume, pore structure and interface between aggregate and mortar. SCC made with high water cement ratios gives a higher permeability for the same curing time and curing temperature (Schonlin and Hilsdorf, 1988). The porosity of SCC was lower than that of normal concrete of the same strength, because of the higher content of powder and lower water content (Tragardh, 1999; Zhu et al., 2004; Zhu and Bartos, 2003).

2.6 Behaviour of tube columns filled with concrete

A column is a structural element that primarily loads in compression along its height. It can be either subjected to compression forces, or combined with eccentric load or bending moment. The failure of short compression columns is the result of compression axial force, whereas in the case of longer columns, compression members are affected by the strength and stiffness of the material, as well as the geometry of the members.

The steel hollow section is known to be a very efficient structure in terms of resisting compression loads, and has been widely used in the case of framed structures in industrial buildings. However, it is nevertheless recognised that the material is vulnerable to heat, and the potential of exposed steel section to be used in design might therefore be compromised.

There are several factors that may have a considerable effect on the ultimate strength of CFT columns, such as slenderness ratio, thickness, cross-section shape, and the mechanical properties of steel and concrete (Alatshan and

Mashiri, 2013). Generally, the compression axially loaded CFT members can fail in two principal ways: in terms of slenderness, and material properties.

2.6.1 Confinement of concrete

Concrete core has been confined by different elements such as carbon fibre reinforced wrap, fibre reinforced polymer tube, glass fibre reinforced wraps and spiral steel hoops. The result showed that the concrete confined by fibre reinforced polymer tube FRP experienced the highest enhancement in compressive strength (Khairallah, 2013). The concrete confined by steel tubes is popular these days because of its advantage and the cost (Han, 2001, Morino and Tsuda, 2002; Lam and Gardner, 2008)

The confining effect depends on a variety of factors, such as the dimension of the steel tube, tube thickness, the yield stress of the steel tube and the overall shape of the column cross-section (Ellobody and Young, 2006, Ellobody et al., 2006). In a CFT column, particularly when using a circular steel tube, the concrete is confined by the steel tube and is subjected to triaxial compressive stresses (Hu et al., 2003). This happens as a result of the Poisson's ratio of the concrete core being greater than that of the steel when the concrete approaches failure.

Different sections shapes effect on confinement was investigated by many researchers such as (Hajjar and Gourley, 1996; Fujimoto et al., 2004; De Nardin and El Debs; 2007). The studies concluded that the confinement is found to be superior in circular and octagonal CFT columns, but not in CFT columns with a square steel section. This is owing to the uniformed lateral

pressure in the circular tube, which confines the concrete core. In the case of the square section, however, higher confining pressure only occurs at the centre and corner of the section compared to the other side. Further investigation also demonstrates that the thickness of the tube influences the ductility behaviour of the square section.

Moreover, rectangular tubes were studied by (Shanmugam and Lakshmi, 2001; Hu et al., 2003). They concluded that the tension hoop developed along the side of the tube was not constant, and therefore could be the reason why a confinement effect was not present, except in the corner of the steel tube.

Comparisons have been made between different sections of tube columns by some researchers. Fujimoto et al. (2004) showed that the improvement in the load capacity of circular tube columns was higher than that of square columns when they filled with similar grade of concrete strength. However, the confinement effect on the load capacity of square sections was higher than that of rectangular sections, which was represented by greater ductility in the post-peak behaviour (De Nardin and El Debs, 2007).

2.6.2 Buckling

There are two types of buckling, the first one is local buckling, which occurs in short columns, and other type is global or overall buckling that takes place in slender columns. Global buckling is more important in this study because all the columns are slender. The failure is illustrated by sideways bending where, for the particularly columns, the global stability is more vulnerable, as

the columns tend to fail owing to flexural buckling (Oehlers and Bradford, 1995). This failure occurs when the condition of a stable equilibrium between the internal and external forces in the structure is no longer possible (Shanmugam and Lakshmi, 2001). The type of buckling depends on the ratio of the effective length of columns to the radius of gyration (L/r) is known. If the column is long ($L/r \geq 45$), global buckling is prominent. Otherwise ($L/r \leq 45$), failure will be due to local buckling.

2.6.3 Failure Modes

The common failure mode of slender columns is global buckling. The slender columns failed after reaching its steel yield strain with small lateral mid height deflection. Moreover, the removal of the steel envelope for some specimens revealed no sign of concrete-crushing at the mid-length of the sections (Zeghiche and Chaoui, 2005, Jamaluddin et al., 2013).

2.7 Composite columns materials

The main materials of composite columns are concrete and steel, and most important properties of both of them are their strength and stiffness. The strength of materials controls the determination of the collapse load of a structure, while stiffness does not let the structure fail rapidly under the load (Seward, 2014). The following paragraphs will briefly show the concrete strength grade that has been used before and yield strength of steel as well.

Most researchers used concrete with strengths grade 30, 60 and 100 MPa of cubes and some others use high and low concrete strength. The main difference between a low concrete strength and a higher concrete strength,

in terms of stress-strain curves, indicates that the concrete, which possesses a higher strength, has large elastic rigidity, as the initial elastic modulus of concrete increases parallel with the increase in the concrete strength (Jamaluddin et al., 2013).

The bond strength and confinement effect has been examined of different concrete compressive strengths: 30, 60 and 90 MPa, and it has been concluded that for high-strength CFT columns, peak load was achieved for small shortening, whereas for normal concrete, the ultimate load was gained with corresponding large displacement. This clearly illustrates that the use of high strength concrete possibly made the structure stiffer. Moreover, with regard to confinement effect, the effect of the bond between concrete and steel was more critical for high-strength concrete in terms of enhancing axial capacity (Giakoumelis and Lam, 2004).

Zhang and Shahrooz, (1999) divided the steel in two groups: normal strength steel tube with yield strength of less than 400 MPa; and high-strength tubes with yield strength of above 400 MPa. The properties of steel are assessed from the stress-strain curves of coupon tests in tension.

2.8 Columns filled with SCC

SCC very quickly became popular in Japan due to its benefits, and then its use spread to Europe and South America. In the beginning, slabs and beams were the first members placed with SCC, because it is easy to notice any variation in the mix. However, columns have received more attention from the beginning of this century. A large number of previous studies have concentrated on different-shaped Hollow steel section (HSS) filled with NC

and SCC. Columns filled with SCC were found to be similar to those of the CFT columns with traditional concrete in terms of the load capacity (Zhu et al., 2010; Yu et al., 2008). This might be attributed to the low slenderness ratio of the HSS considered in these studies. However, Han and Yao (2004) found that the load capacity of tube columns filled with NC is higher than those filled with SCC when it has a good compaction and no segregation appears. In contrast, it is impossible to achieve perfect compaction in the columns due to their small sections comparability to its height, making it difficult for NC to be properly placed and vibrated.

Aoude et al. (2009) and Ahmed (2013) studied the effect of steel fibres on the column made using SCC. They noted that adding a high amount of fibre reduced the workability of concrete mix. However, additional steel fibres to reinforce concrete columns caused an increase in peak load-carrying capacity, and significant improvement in the post-peak response of the column. Moreover, steel fibres of more than 1.5% of volume can be partially substituted for the transverse reinforcement in reinforced concrete columns, and hence could result in improved constructability.

In order to benefit from the many advantages of CFT column construction, it is important that the steel tube and the concrete core work compositely to resist the applied load. If a CFT column is loaded at the top directly on both the steel tube and the concrete core, composite action is guaranteed. The natural bond between the steel tube and the concrete core plays the most important role in transferring the load from the steel tube to the concrete

core. Previous investigations of tube columns filled with concrete are presented in the next sections.

2.8.1 Rectangular and circular tube columns

Han and Yao (2004), Han et al. (2005) and Lachemi et al. (2006a) studied the behaviour of columns and beam-columns of HSS filled with SCC. The concrete cubic strength of their studies ranged from 50 to 90MPa. It was found that, the behaviour of SCC filled steel tubular columns is generally similar to those of the composite columns filled with NC. It seems that the conclusions regarding strength predictions using existing design codes developed for normal concrete-filled HSS columns remain valid for SCC filled HSS columns within the scope of tested concrete strength. However, there is still a lack of information on SCC filled steel tubular columns when the concrete strength is higher than 90MPa.

Yu et al. (2008) studied the possibility of using square and circular SCC-filled HSS columns, and tested the properties after 28 days. The results showed that the failure mode of the square column was mainly occurred due to a local failure mechanism, while that of the circular column was via shear failure. The overall failure mode was buckling failure. With regard to NC, the local wall bucking of square and rectangular tubes columns occurred before the local wall buckling of circular columns (Schneider, 1998). However, these studies covered only short columns which failed under local buckling failure mode. Therefore, slender columns filled with SCC should be studied to investigate its properties.

Yu et al. (2007) carried out a study to investigate the behaviour of circular SCC-filled short tube columns under concentric loads by using different deformation measurement methods. They concluded that tube columns filled with high strength concrete, experienced a significant rise in the ultimate capacity with regard to the samples with entire section loading. However, their residual capacity after peak point was constant, then the compressive axial loads of specimens were reduced. In some situations, the ultimate capacity was reduced as well, and the steel tube acted more as a transverse confinement than an axial compression component. Mandal (2010) presented circular columns filled with NC tested under axial load. For high strength concrete, the ultimate load was achieved for a small displacement, while for normal concrete, the peak load was obtained with large displacement. However, in the literature there is disagreement among researchers about the axial compressive stiffness of the stub columns. This may be attributed to the fact that different deformation measurement methods were employed for the stub columns under axial compressive loading. Therefore, comparisons between these methods should be made to obtain the most accurate one.

Khairallah (2013) tested a number of short columns made with SCC and NC using different techniques of confinement to examine their mechanical behaviours under concentric axial loading. SCC and NC with the same confinement technique have similar failure modes, as well as stress and strain responses. Moreover, confinement has more effect in columns designed with lower nominal concrete strength. However, Lin et al. (2008)

found that compacting concrete resulted in slightly higher compressive strength than SCC. Moreover, many studies still have the argument about the difference in the load capacity between NC and SCC. For stub columns, close results could be obtained but for slender one, higher load may be obtained from NC.

Paultre et al. (2005) and Khayat et al. (2001) compared the findings between confining steel columns filled with SCC and NC. They reported that regarding the distribution of in place properties along the column, SCC was more homogenous than NC. However, columns made with SCC offered slightly lower axial load-carrying capacities, but were more ductile than confined columns made with NC. Reduction is due to the lower elasticity of SCC, which results in larger lateral expansion under compressive loads. Galano and Vignoli (2008) and Lin et al. (2008) agreed with the previous results.

Lacheni et al. (2006) compared results between NC and SCC with regard to columns at different properties. Their results showed that the ease of placement and time of casting were considerably improved for columns with SCC compared to those with NC, and the ductility of short columns for both NC and SCC were similar at some values. Ductility also decreased with the increase of slenderness ratio (L/D) of columns. No significant differences in strain development were found due to the presence of concrete core, or due to the presence of longitudinal and hoop reinforcement. The confined strength of SCC was found lower than that of NC. Moreover, confined

strength decreased with the increase of slenderness of the columns (Lacheni et al. 2006).

Zhu et al. (2010) presented the behaviour of square tube columns filled with steel reinforced SCC. The failure mode for composite columns with or without inner steel sections was quite different, because steel sections can effectively delay or restrain the generation of shear sliding crack in the high-strength concrete. Moreover, the square steel tube can enhance the strength and the ductility of the core concrete; the inserted steel section mainly influences the post peak behaviour of the core concrete, and its effect on the enhancement of concrete strength can be neglected.

Eramma and Niranjan (2012) studied the behaviour of long fluted columns with and without reinforcement. They found that the ultimate load of column without reinforcement reduced by increasing the L/D. However, the reinforcement of columns with four bars improved the ultimate strength of the columns with similar reduction percentage compared with non-reinforced columns.

Tao et al. (2005) presented the behaviour of stiffened concrete-filled square tube columns. They concluded that the sectional capacity of the composite column can be increased when stiffeners were provided. Moreover, longitudinal stiffeners delay the local buckling and improve the lateral confinement of the concrete core.

2.8.2 Elliptical tube columns

Elliptical columns are new type of columns, whose properties have not all been investigated yet. Researchers found that elliptical hollow section columns offered greater load carrying capacity in comparison to their circular counterparts (Chan and Gardner, 2009). Due to the increasing use of the elliptical hollow section shape, broad studies have been conducted to provide an insight into the behaviour of this form of structure (Yang et al., 2008, Zhao and Packer2009, Jamaluddin et al., 2013). The compressive behaviour of concrete filled elliptical hollow section stub columns have recently been well established through experimental research, and numerical modelling has also been carried out. Elliptical tube columns filled with normal concrete have received more attention than those filled with SCC. Therefore, most studies in this review refer to NC. Moreover, numerical modelling on elliptical hollow section (EHS) has been reported in several studies and will be discussed in this review.

2.8.2.1 Experimental works of elliptical tube columns

The structural behaviour of elliptical tube columns has been studied deeply since last decade by Gardner (Gardner &Chan 2006, Gardner et al. 2008, Chan & Gardener 2008 a, b, and McCann et al., 2015), covering cross-section classification and evaluation of compressive, shear and bending resistance. Moreover, the elastic buckling response of elliptical hollow section in compression has been studied by Ruizteran & Gardner (2008) and Silvestre (2008). Their results were that Class 3 slenderness limit from EN 1993-1-1 for the circular hollow section can be safely adopted for

compression members. The studies also proposed a system for cross-section classification limits for elliptical hollow sections in bending, and a combination of compression and bending.

A review article was published by Gardner et al. (2010) on the structural design of elliptical hollow section, which compiles the previous developments. The structural behaviour of elliptical hollow section under combined compression and uniaxial bending has been studied by Gardner et al (2011). Law & Gardner (2012) have also studied the lateral instability of elliptical hollow section members in bending.

A number of elliptical tubes specimens filled with three different concrete grades have been studied by Yang et al. (2008). The results were that higher tube thickness improved the load-bearing capacity and ductility of the columns, while higher concrete strength resulted in higher load-bearing capacity but reduced ductility. Moreover, the strength and ductility of the concrete core was greatly improved by steel confinements. Furthermore, comparison between experimental results and existing code provisions for concrete filled hollow section were made. They confirmed that the behaviour of concrete filled elliptical hollow section columns lies between that of concrete filled circular and rectangular hollow section, which was approved earlier by Gardner &Chan (2006). Few years later, Chan and Gardner (2009) presented that, elliptical hollow section columns offered greater load carrying capacity in comparison to their circular counterparts. However, these results

need more validation due to the lack in the experimental results that compare the load capacity of different tube sections.

Zhao and Packer (2009) have tested elliptical hollow section tube columns filled with SCC with different loads with maximum length 600mm. The results showed an increase in the strength, stiffness, energy-absorption and fire resistance. Campione and Fossetti (2007) used single hoops to study the behaviour of elliptical columns. Due to the effective distribution of stresses along the hoops, the non-uniform confinement pressure around the perimeter of the sections developed. These studies investigated the stub tube columns with limited specimens. Therefore, these results may not be applied to long columns due to the fact that the behaviour of slender columns is not well represented by stub columns. In this case, more tests on slender columns filled with concrete are required for further check.

Testo (2007) investigated the behaviour of elliptical tube columns filled with concrete; it was found that there are various differences in column response for different tube thicknesses. The concrete infill in the thinner tube experienced inclined shear failure, which is believed to be due to the tube offering less confinement compared with thicker tubes. The relationship between the slenderness and concrete contribution ratio shows thicker tubes have a greater capacity as the strength of concrete increases which has been approved later by Yang *et al.* (2008)

Jamaluddin et al. (2013) studied the behaviour of elliptical tube columns filled with concrete under axial load. The results were that, axial load capacity and

ductility were sensitive to steel hollow section dimension, concrete infill and slenderness ratio. Moreover, the experimental study results were assess the adaptability of current design rules provided in Eurocode 4 for circular and rectangular columns, and the agreement was reliable, which was been approved later by McCann et al., (2015). However, previous studies were mainly concentrated on the stub columns. As for long columns, only few slenderness ratios were studied. Therefore, variety of slenderness ratios for slender columns should be investigated to enrich the literature in terms of the behaviour of elliptical tube columns filled with concrete.

2.8.2.2 Analytical Model

The finite element method (FE) is popular for civil engineering applications worldwide. With the power of computer hardware improving dramatically over the last 30 years, the simulation speed has increased dramatically and the use of new elements and finer meshes, plus experience and feedback from experiments has improved the accuracy of the results, saving engineers both time and money. The use of numerical simulations is commonly accepted as a replacement owing to expensive experimental programmes. Many researchers have adopted the finite element analysis programme to model the CFT columns in order to predict the structural response and simulations with ABAQUS software package, as it was found to be the most preferred programme to model the structural.

Experimental study and numerical modelling of elliptical tube columns have been attempted by some researchers; the main areas investigated geometric features, non-linear material properties and initial geometric imperfections.

Several amplitudes of initial geometric imperfection were considered and it was found that the structural behaviour of hollow sections was very sensitive to the level of imperfection. However, the ultimate load capacity was relatively less sensitive to the amplitude of the imperfection (Gardner and Ministro, 2004, Dai et al., 2014).

Jamaluddin et al. (2013) compared and analysed the results against available experimental data to propose a modified stress–strain model. This modified model has been successfully used in the prediction of axial compressive load and failure modes of stub elliptical CFT columns. Moreover, Dai et al (2014) carried out a numerical investigation on elliptical CFT columns and developed a new confined concrete model. They showed that for columns with high concrete compressive strength, the confined concrete properties have little effect on the behaviour.

Parametric studies on the compressive response of elliptical hollow sections with different aspect ratios and varying slenderness were reported in a study by Chan and Gardner (2008b). This study follows the satisfactory agreement achieved between the experiment on compression resistance of EHS and numerical results. From the results, the authors have established a relationship between cross-section slenderness and cross-section compressive resistance. The results further demonstrate that the Class-3 for circular in Eurocode 3 was safely adopted for elliptical tube.

Sheehan et al. (2012) tested the response of concrete-filled elliptical steel hollow sections under eccentric compression; it was sensitive to tube thickness, loading eccentricity and axis of bending. The behaviour of these

sections was successfully captured by finite elements using ABAQUS. The shell elements used in this study was successful in predicting the behaviour of stub columns. However, in term of slender columns, Dai et al. (2014) found that the solid elements are more successful in simulating the failure mode than shell elements.

Dai and Lam (2010) used ABAQUS to investigate the axial compressive behaviour of concrete-filled elliptical steel tube columns. The ultimate load capacity, load versus end-shortening relationship and failure modes, were obtained from the numerical models and predicted results were compared against the experimental results, and good agreement was obtained. Moreover, the difference in concrete confinement between circular and elliptical hollow section studied, finding that the circular hollow sections provided higher confinement than elliptical ones. Unlike the uniform contact stress distribution around the perimeter of circular sections, the contact forces along the perimeter of elliptical sections were non-uniform, with higher stress at sharper corners (Dai and Lam, 2010).

2.9 Concluding Remarks

Most of the studies on using SCC in civil engineering applications have focused on the use of chemical and mineral admixtures to obtain high flow concrete, with high strength and durability and less water demand, and have compared them with normal concrete. The most important factor in studying the properties of SCC is to obtain high segregation resistance, which represents one of the major issues concerning scientists in the field of

concrete structures. Moreover, most of available mix design of SCC are complicated and not easy to follow. Computing software has become more interesting, with Matlab tools giving good results, saving time and reducing the loss of materials.

The influence of using different types of raw material on the properties of SCC was also investigated. As mentioned before, different types of secondary raw materials, such as limestone powder and FA, and different types of cement and different grades of aggregate, were intensively tested to produce SCC with the best possible properties. In contrast, most of these studies have been conducted on small concrete specimens under laboratory conditions, which do not sufficiently represent the properties of SCC when casting at the construction site.

In addition, research on beams and slabs made with SCC is very rare. Columns made using SCC in field conditions were totally ignored in the beginning, and then some researchers began to show interest in this. CFT columns are a new area, which is still being investigated, and many researchers are interested with it because of its advantages compared to steel or reinforced concrete systems. Circular and rectangular columns made with SCC have been studied and compared with those using normal concrete, but not to a large extent, and SCC-filled elliptical columns have been neglected. It is worth noting that few studies on slender elliptical tube columns filled with SCC has been done yet. Although a high number of previous studies have been conducted on elliptical tube columns filled with

concrete, most of these studies focused on the behaviour of stub columns. Only few studies were carried out to study the behaviour of slender columns with few slenderness ratios. Therefore, there is a need for more experimental results on the structural performance of slender columns with extended range of slenderness ratios.

CHAPTER THREE

SCC COMPRESSIVE STRENGTH MODELLING USING ANN

3.1 Introduction

SCC is widely used throughout the world as a key construction material in civil engineering projects. It is a complex compound comprised of cement, sand, coarse aggregate, admixture and water, as mentioned in the previous chapter. The compressive strength of SCC is a highly nonlinear function of its constituents, thereby making its modelling and prediction a difficult task.

Nature inspired computational techniques provide an efficient and uncomplicated approach for modelling complex, nonlinear functions, for which it is otherwise difficult to establish relationships between the independent and dependent variables. Artificial Neural Networks (ANN), inspired by the learning ability of the human brain, are regarded as the engineering counterpart of a biological neuron. Their highly interconnected

and parallel nature gives ANNs immense ability to learn from past examples, capturing unknown relationships and making them a versatile tool for modelling real world problems (Chandwani et al., 2014).

ANN methods were introduced to civil engineering during the late eighties. Their use now covers a range of civil engineering fields, such as environmental studies, wide resource engineering, traffic engineering, highway engineering and geotechnics (Adeli, 2001).

3.2 Previous investigations on predication of compressive strength using ANN

In recent years, ANNs have been applied to many civil engineering applications with varying degrees of success. Several researchers have used ANN in structural engineering problems. Some have recently proposed a new method of mix design and prediction of concrete strength using neural networks. Many studies have investigated the use of a neural network based modelling approach for predicting concrete strength. ANNs have been used in a range of other applications relating to concrete, such as predicting drying shrinkage (Bal and Bodin, 2013), durability (Jepsen, 2002), the compressive strength and slump (Oztas et al., 2006; Ni and Wang, 2000), workability of concrete incorporating metkaolin and fly ash (Bai et al., 2003), tensile capacity of single adhesive anchors (Sakla and Ashour, 2005), and cement hydration (Basma et al., 1999).

ANN has also been used with SCC to predict various properties. Aggarwal and Aggarwal (2011) used back-propagation neural networks to develop two

neural network models (ANN-I and ANN-II) based on (a) data taken from the literature, and (b) experimental data for SCC containing bottom ash as a partial replacement of fine aggregates, respectively. ANN-I showed a reasonable prediction of the compressive strength of SCC after 28 days, with a correlation coefficient above 0.9. ANN-II was used for predicting the compressive strength at various ages, and the results in the form of correlation coefficient and mean absolute error values were found to be better at all ages for the data obtained experimentally.

Suryadi et al. (2011) used an artificial neural network to evaluate the compressive strength of SCC for data collected from the ready-mix factory and the concrete laboratory. The data were randomised and divided into training, validation, and testing data sets. The neural network inputs were formed by the proportions of cement, coarse aggregate, fine aggregate, fly ash, and chemical admixture, and the water-cement ratio. The compressive strength after 28 days was treated as the neural network output. The error between the predicted and observed compressive strength was found to be less than 10%, thereby proving the effectiveness of ANN modelling.

Uysal and Tanyildizi (2011) predicted the compressive strength of SCC mixtures with mineral admixtures (limestone, marble powder and fly ash) using ANN. Compared to conventional concrete, the SCC showed effective consolidation under its own weight in the case of narrow reinforcement construction elements. An ANN model with ten inputs was developed with one hidden layer containing fourteen and fifteen neurons. The inputs were: amount of cement; amount of fly ash; amount of limestone; amount of marble

powder; amount of natural aggregates I and II; amount of super-plasticizer; unit weight; and water absorption. The single output variable was the compressive strength of the concrete.

Raheman and Modani (2013) used an ANN to predict the properties of SCC. The results showed that the SCC properties predicted from neural network are very close to the actual properties of SCC measured experimentally. However, the amount of input data was too low, such that a sufficient range of properties was not covered, and the accuracy was therefore compromised. Moreover, the number of outputs was high compared to the number of inputs data used in ANN.

All previous research in this field has obtained suitable values when they used predicted data at lab. Thus, ANN is very suitable for use in the prediction of fresh or hardened properties. In this project, the number of ANN inputs used to predict the compressive strength is higher than that used by previous authors (Prasad et al., 2009; Raheman and Modani, 2013; Uysal and Tanyildizi, 2011 and Aggarwal and Aggarwal, 2011). Increasing the number of inputs leads to a high number of training, which in turn increases the accuracy of ANN. This chapter will identify ANN functions, then explain the process of using ANNs to predict the compressive strength of SCC, and compare the predicted results with the actual data collected by different studies, as well as the present study.

3.3 Artificial Neural Network (ANN)

Artificial neural network exhibit analogies to the way arrays of neuron function in biological learning and memory. The fundamental building blocks are units (‘nodes’) comparable to neurons, weighted connections that can be linked to synapses in biological systems. Nodes are simple information processing elements. The number of nodes in ANNs and the connection patterns of the nodes can vary. The total number of nodes in the input and output layers coincide with the number of input and output variables in the data set. The ideal number of nodes in the hidden layer has to be found through trial and error. It is known that more neurons give the ability to memorize and reduce the reasoning capability of the ANN. As a general rule, an ANN should contain the minimum number of neurons that are capable of simulating the training data. Each connection between nodes carries a weight representing some previous learning process. By varying these weights, the input-output relation can be simulated. The network has to be trained to reproduce this input-output relation, which is to find the optimal weights (Aggarwal and Aggarwal 2011a)

An ANN works similarly to a biological nervous system (Flood and Kartam, 1994). In simple terms, it does not need a specific equation form. It is available as a toolbox in Matlab, which requires sufficient inputs and outputs to function properly, and can retrain many times with new data. Briefly, for a given input pattern, a flow of activation is forwarded from the input layer to the output layer via the hidden layers. Then the errors in the output are

initiated. The neural network based modelling process includes five main aspects: (a) data acquisition, analysis and problem representation;(b) architecture determination; (c) learning process determination; (d) training of the networks; and (e) testing and validating of the trained network for generalization evaluation (Pala et al. 2007). After carrying out these processes, ANN can supply meaningful answers including errors and can process information extremely rapidly when applied to solve engineering problems (Topcu and Sarıdemir 2007).

It can usefully adapt to new data, and deal with problems involving incomplete or imprecise information (Hakim et al., 2011).

The ANN consists of a high number of simple processing elements called neurons, as shown in Figure 3.1. The ANN technique offers an advantage since it can use an unlimited number of characteristic parameters of the phenomenon, compared to statistical methods. The ANN model must include some consideration to design, such as suitable structure, a suitable activation function, and an appropriate number of hidden layers.

An artificial neuron is composed of five main parts: inputs, weights, sum function, activation function and outputs. Inputs are information that enter the neural network cell from other cells of external world. Weights are values that express the effect of an input set or another process element in the previous layer on this process element. Sum function is a function that calculates the effect of inputs and weights totally on this process element. This function

calculates the net input that comes to a cell. Activation function is a function that processes the net input obtained from sum function and determines the cell output. (Topçu and Sarıdemir 2008). There are many kinds of activation functions. Usually nonlinear activation functions are used, such as sigmoid and step functions. ANNs are trained by experience; therefore, when an unknown input is applied to the network, they can generalise from past experience to produce a new result (Uysal and Tanyildizi, 2011).

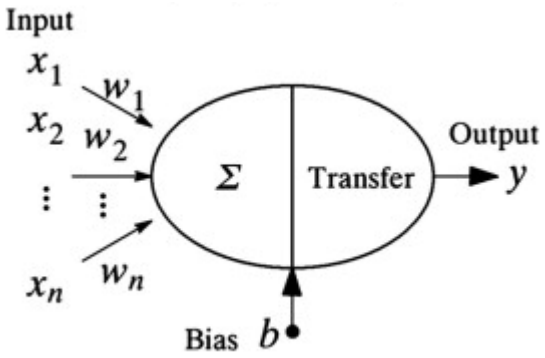

Figure 3.1 Artificial neuron model

The output of a neuron is given by Equation (3.1):

$$y = \sum_j^n Xj\, Wj - b \qquad (3.1)$$

where Xj= ($x1, x2, x3$,…) represents the n inputs applied to the neuron, Wj represents the weight of the output Xj, and b is the bias (Uysal and Tanyildizi, 2012).

In an ANN, neurons work together to solve specific or complicated problems. Similar to the human brain, ANNs are fed by examples in order to identify the main variables and the main problem to be solved. ANNs are designed for

specific applications, such as pattern recognition, through a learning process. Learning in biological systems involves adjustments to the synaptic connections that exist between the neurons; the same process happens in ANNs (Naderpour et al., 2010).

It is important to note that when training a neural network, three non-overlapping sets of data must be used. Typically, a researcher would start with a compendium of data from different sources. These data are then divided into three subsets: the training set, the validation set and the testing set. The training set is used for the adjustment of weights during training. The validation set is used to decide when to stop training. The testing set is used to provide an independent measure of network performance during and after training (Dayhoff and DeLeo, 2001).

Different numbers of hidden layers were used to try to determine the best number of hidden layers. As mentioned before, the ideal number of nodes in the hidden layer has to be found through trial and error which can be controlled by the accuracy between the target and the output (Momeni et al, 2015). It was found that a number of hidden neurons can affect the prediction of the ANN by increasing connection weight and therefore reducing the error. However, increasing the connection weight requires longer computational time or more computational resources. Moreover, the percentage of good patterns achieved by a network with one hidden layer is lower than that of a network with two hidden layers (Hakim et al., 2011).

Optimal performance of ANN models can be achieved if their parameters are selected properly. Therefore, in this study, sensitivity analyses were performed to determine the optimum ANN parameters. The performance of ANN in minimising the mean square error was evaluated during the sensitivity analyses. It should be noted that ANN can only adjust the weights and biases to minimise the learning error, whereas, the network architecture (the number of hidden layers and the number of nodes in each hidden layer) needs to be determined using a trial-and-error method (Momeni et al, 2015).

In this study, the ANN toolbox in Matlab 2009 was used. This was fed with both inputs and target outputs, and then the model was running to obtain a prediction value. After trial and error process, the most accurate predictions were achieved when using two hidden layers. Figure 3.2 shows the input layers, which can include cement content (C), fly ash content (FA), slag (ggbs), water to binder ratio (w/b), superplasticiser dosage (SP), sand (S), coarse aggregate (CA) and rubber, and the output layers that have compressive strength. The input variables have been chosen depending on their effect on the compressive strength. The main variables that has a significant effect on the compressive strength are the binder material (cement and fly ash) and the water to binder ratio (Domone, 2007). The fineness, shape, gradient, packing density, flakiness and ratio of fine to coarse aggregate also have an effect on compressive strength (Khayat et al., 1999). Moreover, superplasticiser has a significant effect on the compressive strength when the water to binder ratio is higher than 0.35 (Yamada et al., 2000). Another factor that has an effect on the compressive strength is the

amount of the rubber phase in the mix. It was mentioned that a noticeable reduction in the compressive strength was observed when the amount of rubber exceeded 180 kg/m^3 (Topcu and Bilir ,2009).

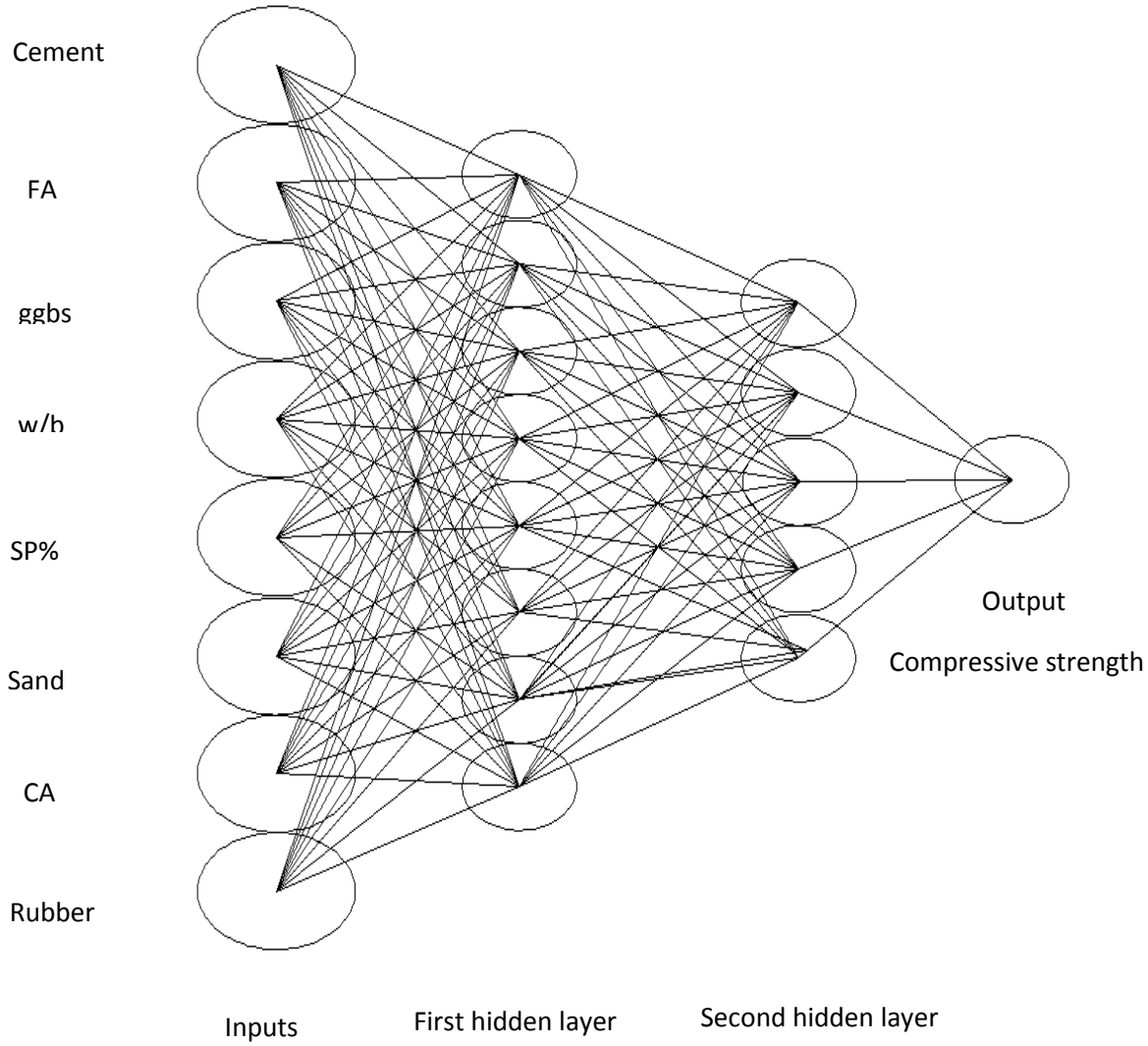

Figure 3.2 Selected architecture for prediction of compressive strength

3.4 Data sets

The data used in the present study consisted of 239 sets of experimental results that was collected from a number of previous research investigations (Sonebi and Bartos, 2003; Siddique 2011; Bouzoubaa and Lachemi 2001; Siddique et al. 2011; Khayat et al .2003 ; Almeida Filho et al. 2010 ; Su et al. 2001; Prasad et al. 2009; Felekoğlu et al. 2007 ; Topcu et al. 2009; Sonebi 2004; Boukendakdji et al. 2009 ; Kou and Poon 2009 ; Lin and Chen 2012; Hassan et al. 2010; Ding et al. 2011; Zhu et al. 2001; Zhu and Gibbs, 2005). A total of 239 SCC compressive strength design mix were collected from eighteen different previous investigations as shown in Table 3.1. The full details of the database are shown in Appendix A.

Table 3.1 Database of SCC compressive strength

Reference	No. of cubes	Range of compressive strength N/mm^2
Sonebi and Bartos (2003)	20	10.2- 54.3
Siddique (2011)	21	31.0- 52.0
Bouzoubaa and Lachemi (2001)	13	26.2- 48.3
Siddique et al. (2011)	14	46.5- 73.5
Khayat et al . (2003)	18	13.3- 41.2
Almeida Filho et al. (2010)	25	38.08- 50.7
Su et al. (2001)	8	25.6- 48.0
Prasad et al. (2009)	7	24.0- 48.0
Felekoğlu et al. (2007)	5	28.8- 42.4
Topcu et al. (2009)	21	13.3- 41.92
Sonebi (2004)	29	11.0- 54.3
Boukendakdji et al. (2009)	11	30.9- 68.0
Kou and Poon (2009)	12	30.9- 51.4

Lin and Chen (2012)	14	30.4- 49.1
Hassan et al. (2010)	5	38.5- 53.0
Ding et al. (2011)	3	31.4- 38.8
Zhu et al. (2001)	2	37.6- 57.5
Zhu and Gibbs (2005)	11	32.0- 57.6

Test data were assembled for concrete containing cement, fly ash, blast furnace slag, coarse aggregate, sand, rubber and superplasticizer. A determination was made to ensure that these mixtures were a fairly representative group governing all of the major parameters that influence the compressive strength and present the complete information required for such evaluation. In all about 280 concrete samples from the above investigations were evaluated. During the evaluation, some of the concrete samples were deleted from the data due to larger size aggregates (larger than 20 mm), special curing conditions, etc. About 239 concrete samples made with ordinary Portland cement and cured under normal conditions were selected. Different studies used specimens of different sizes and shapes. All the specimens were converted into 10-cm cubes through accepted guidelines. Table 3.2 shows the range of input parameters in the database, as obtained from the literature. The database often contain unexpected inaccuracies, for instance, the class of fly ash is sometimes not reported. The greatest difficulty seems to be related to the application of superplasticizers. They are from different manufacturers, of different chemical compositions, and without details concerning the solid contents in the suspension.

The ANN was feeding by this data, and the predicted results were compared with the experimental data (see Appendix A). Input elements consisted of a mixture of variables and an output vector of 28-day compressive strength of cubes (F_{cu}).

Table 3.2 Range of input parameters in database

Limitation	Cement Kg/m³	FA kg/m³	ggbs kg/m³	w/b	SP%	Sand kg/m³	CA kg/m³	Rubber kg/m³	F_{cu} MPa
Min	160	0	0	0.22	0	478	480	0	10.2
Max	465	295	135	0.61	2	1172	1105	180	73.5
Mean	312.5	147.5	67.5	0.42	1	825	792.5	90	41.85

It is important to mention that in ANNs, learning is better achieved if the data is collected over different ranges. The scattering of input information for the training phase will affect the accuracy of a neural network. Therefore, classification of the input information is very important in the training phase.

The percentages of training, validation and testing data are fundamentally important to obtaining output data close to the target. 75 %, 5 % and 20 % were used in this study for the training, validation and testing respectively. The data was collected through the process for each group. Figures 3.3 to 3.11 show the percentage of each variable used for training, validation and testing.

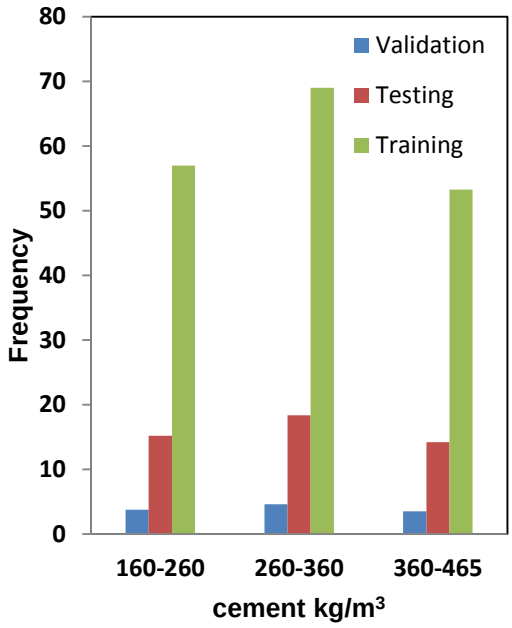

Figure 3.3 Frequency of cement content

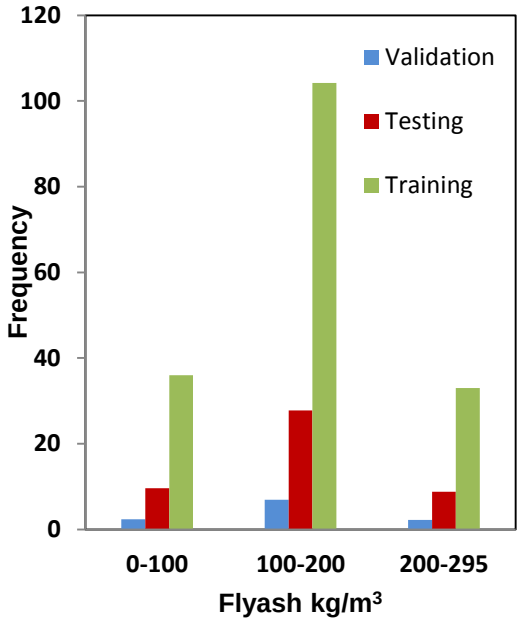

Figure 3.4 Frequency of FA

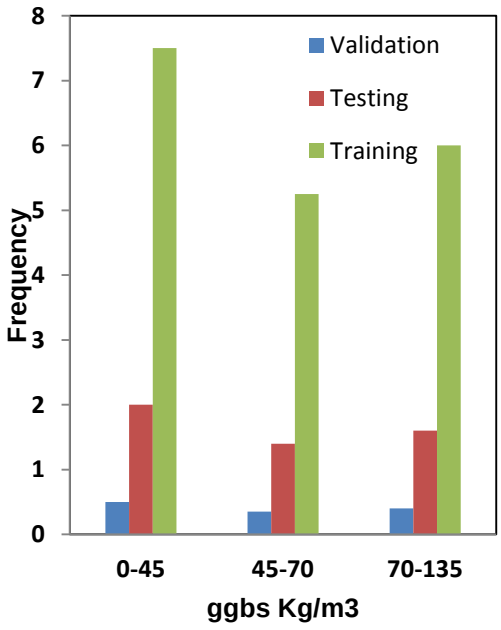

Figure 3.5 Frequency of ggbs

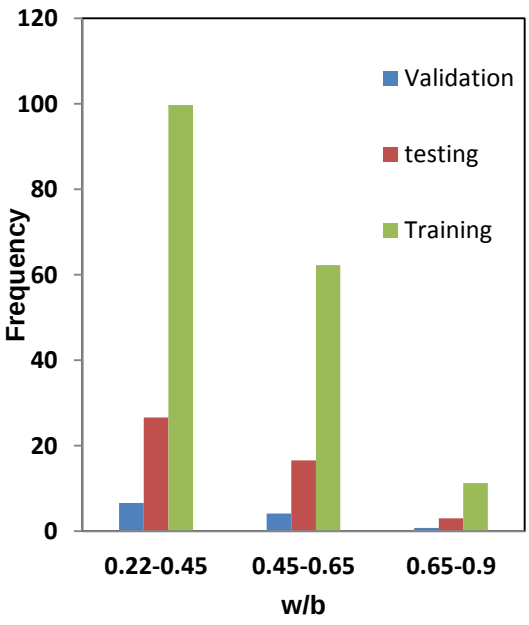

Figure 3.6 Frequency of w/b

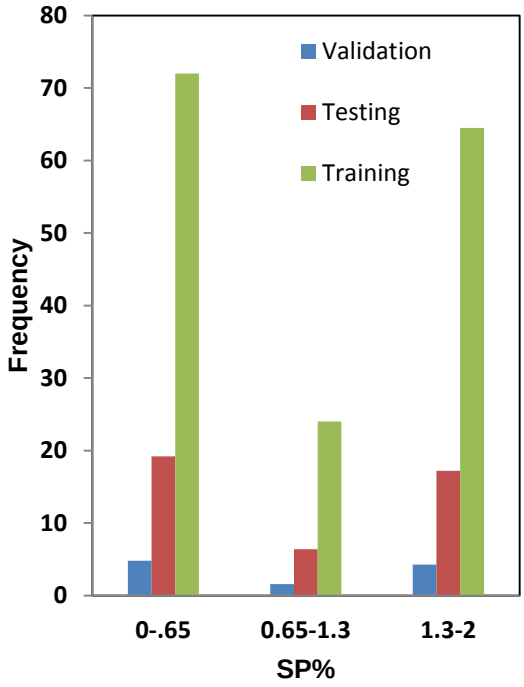

Figure 3.7 Frequency of SP%

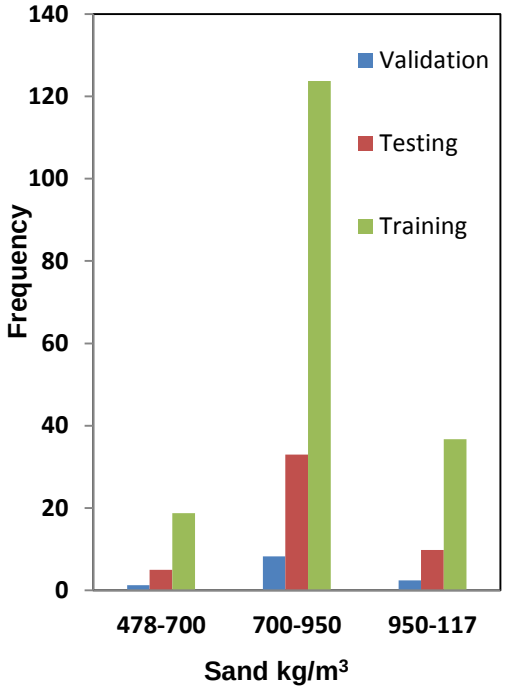

Figure 3.8 Frequency of sand

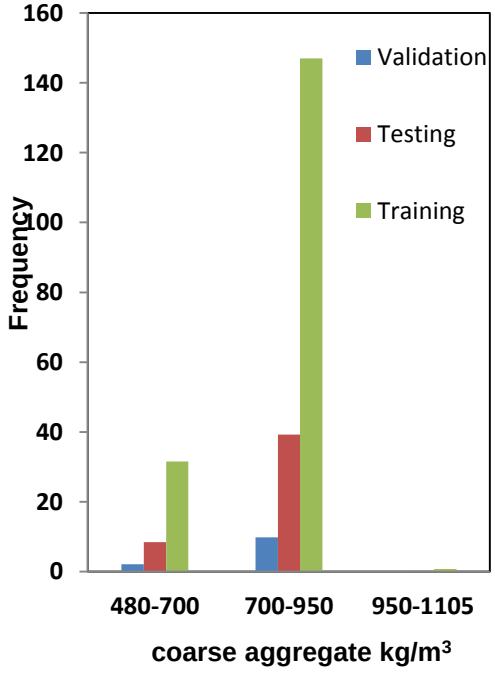

Figure 3.9 Frequency of CA

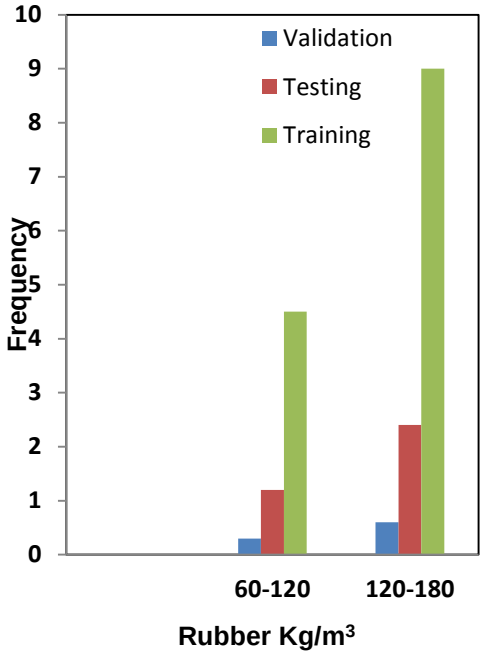

Figure 3.10 Frequency of Rubber

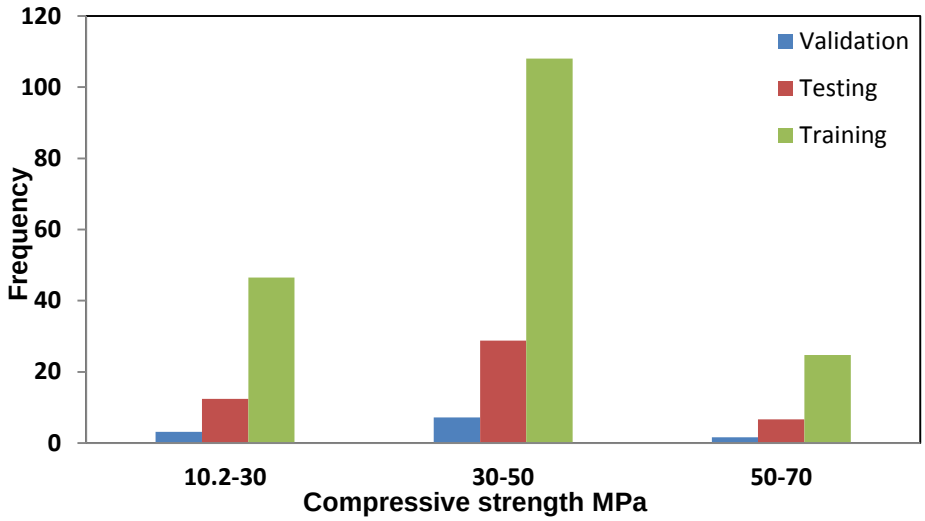

Figure 3.11 Frequency of actual strength

3.5 Analysis and discussion

The ANN model developed in this chapter was used to predict the concrete compressive strength of SCC mix designs. Around 179 samples were used for training the network, 48 for testing and 12 for validation. These samples were chosen from collected data, and the chosen data of training, testing and validation were converted to excel files using matlab. ANNs gave an accurate prediction for all data where large datasets were used in training. In contrast, the ANN gave an inaccurate prediction where small datasets were input, because the ANNs were poorly trained in these cases (see Appendix A). However, the target of this study was among the highest of the collection data. The predicted data were checked using different variable values, and their effects on the compressive strength were examined. Figures 3.3 to 3.11 show the zone of higher training numbers, which gives values close to the collected data.

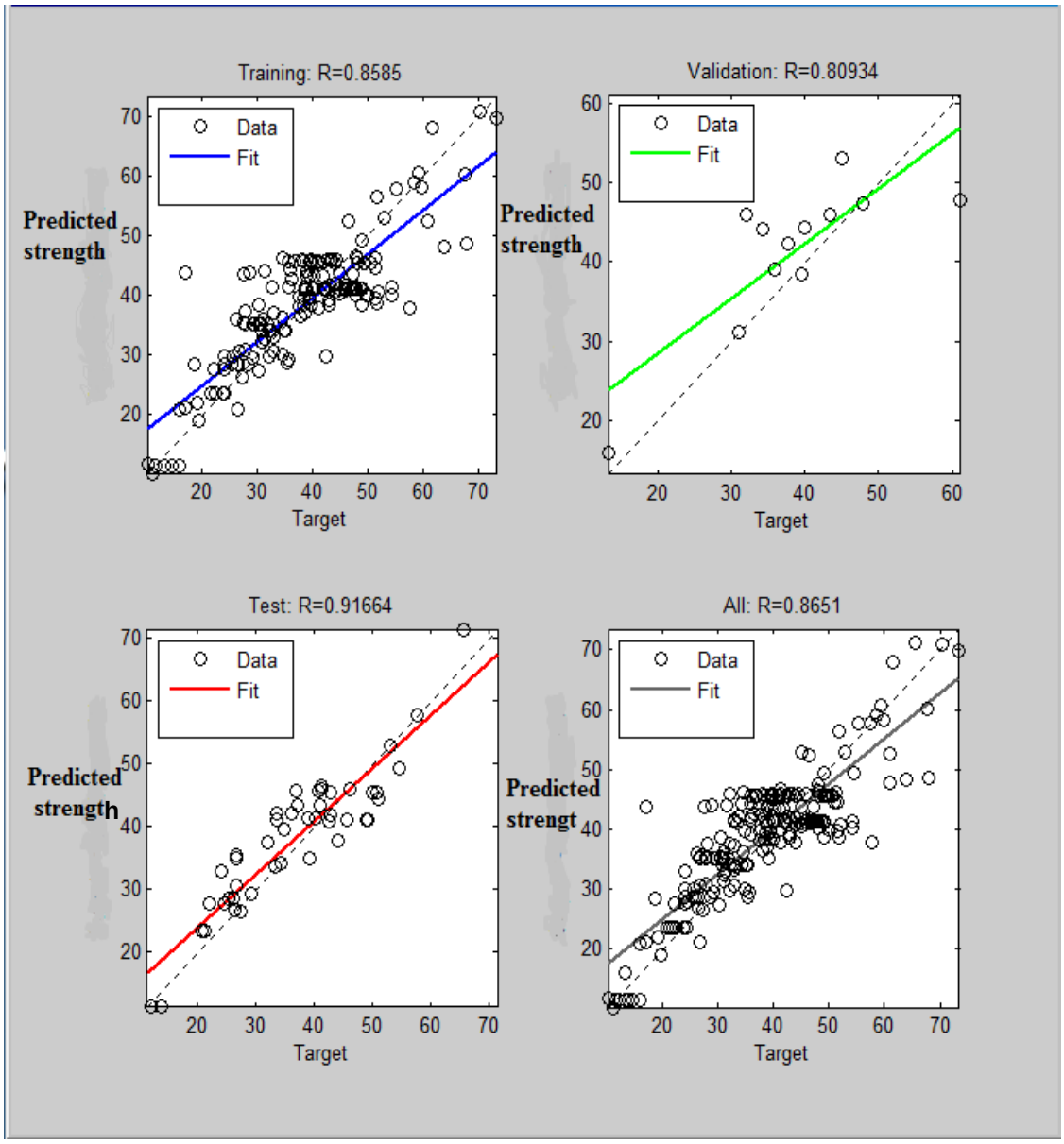

Figure 3.12 Data training, validation and testing results

Figure 3.12 shows the results from the training, validation, and testing of the data. The data used for training are presented to the network during the training phase, and the network is adjusted according to its error. Validation data are used to measure the network generalisation, and to halt training when the generalisation stops improving as additional data does not have

any effect on the training. In this manner the validation data provides an independent measure of network performance during and after training. R is a regression value for each plot, which measures the correlation between the output and the targets. An R value of 1 means a perfect relationship, while 0 means a completely random relation (no relationship). From Figure 3.12, it can be clearly seen that the relation between the predicted compressive strength and the targets (experimental data) is highly acceptable. Some data does not fit with vast majority of the other literature so it has been omitted from the outset. The results of the testing phase show that the ANN was able to generalise between the input and output, and to give reasonably good predictions.

From the results obtained, the ANN developed seems to be acceptable for the prediction of SCC compressive strength. Appendix A shows the predicted compressive strengths of SCC. The average ratio of predicated values to experimental measurements is 1.05. Next section will show the results of mix design of SCC in the lab which has been used to filled tube columns of project study.

3.6 Design of concrete mix for elliptical tube columns

The acceptance or rejection of the developed model is determined by its ability to predict the compressive strength of SCC. A successfully trained model is characterised by its ability to predict property values for the data it was trained on. Two targets (measured values) of concrete compressive strength were predicted in this study by ANN to use for elliptical columns.

The first was 38 MPa and the second was 76 MPa, each after 28days. The average values of compressive strength of six cubes for each target are presented in the table below.

Table 3.3 Experimental and prediction compressive strength of concrete

No of mix	Cement Kg/m³	FA kg/m³	w/b	SP%	Sand kg/m³	CA kg/m³	ANN MPa	F_{cu} MPa	$\frac{F_{cu}}{ANN}$
1	250	160	0.55	0.5	745	830	36.4	38	1.04
2	340	200	0.35	1.96	662	850	72.8	76	1.04

Table 3.2 summarises the average concrete compressive strengths measured for all the specimens cubes used in the experiments (F_{cu}) and those predicted by the ANN models (ANN). Overall, the strength estimations of the proposed models showed a good agreement for all mixes. The average ratio of the concrete compressive strength predicted by ANN models to the experimental results was found to be 1.04. Moreover, all fresh properties were acceptable and presented in chapter five. Figure 3.13 shows a cross-sectional view of tube columns filled with SCC. It is clear that the concrete composition was homogeneous inside the columns.

Figure 3.13 Concrete core inside the steel tube column

The following sections will show elements of an important parametric study, which compares the compressive strength of SCC with varying w/b, fly ash, SP, coarse aggregate and cement content.

3.7 Parametric study

The quality of a predictive model of compressive strength is dependent on the weight of each parameter governing the phenomena at play. A parametric study was thus conducted in order to investigate the factors that influence the concrete compressive strength.

3.7.1 w/b Effect on compressive strength

w/b was varied from 0.25 to 0.7 while all other mix ingredient quantities were held constant, as shown in Table 3.3. The effect of w/b was clear: compressive strength decreased as w/b increased, as shown in Figure 3.14.

Table 3.4 The value of materials with varying w/b

Cement Kg/m³	FA kg/m³	ggbs kg/m³	w/b	SP %	Sand kg/m³	CA kg/m³	Rubber kg/m³	Strength MPa
300	0	0	0.25 To 0.7	0	900	800	70	50 To 10

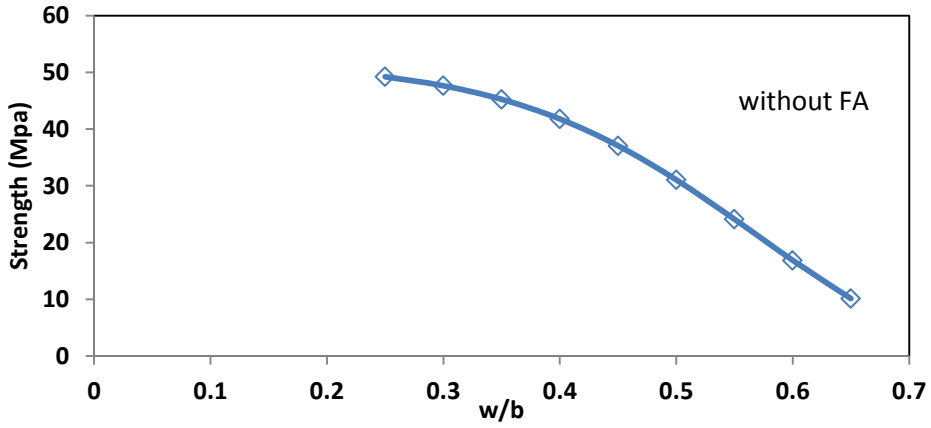

Figure 3.14 Effect of w/b ratio on the compressive strength

Then, cement was replaced with 30 % FA and 20 % slag, for a w/b range from 0.25 to 0.7. With these new values, the strength exhibited a different relationship with w/b. This occurred due to the few instances when the ANN was supplied with training data based on slag, which led to inaccurate predictions. Neglecting slag, the ANN gives the expected relation between strength and w/b, as shown in Figure 3.15.

Table 3.5 Effect of w/b ratio on the compressive strength with variable materials

Cement Kg/m³	FA kg/m³	ggbs kg/m³	w/b	SP %	Sand kg/m³	CA kg/m³	Rubber kg/m³	Strength MPa
150	90	60	0.25 To 0.7	0.5	900	800	0	55 To 15

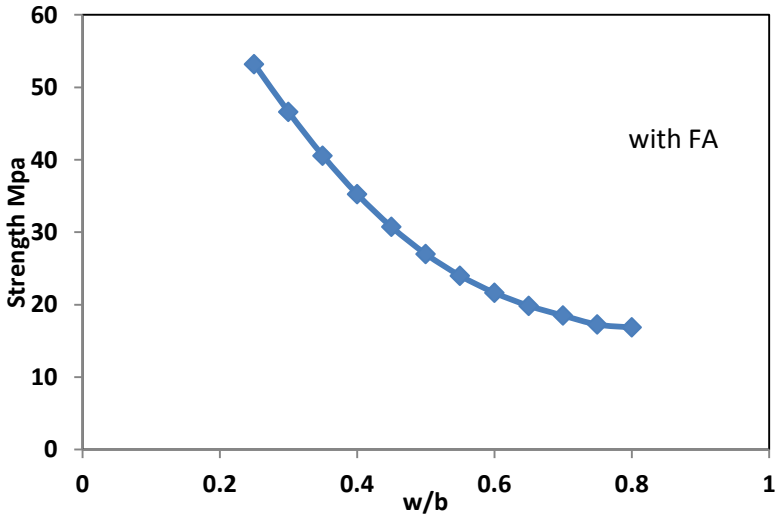

Figure 3.15 Effect of w/b ratio on the compressive strength with variable materials

3.7.2 Effects of Superplasticiser on compressive strength

Superplasticiser (SP) content was varied from 0.1% to 0.6%, while other material values were held constant, as shown in Table 3.5. This range was repeated three times for different w/b vales of 0.35, 0.45 and 0.55 respectively. As shown in Figure 3.16, the SP does not have a significant effect on the concrete compressive strength, even with changing w/b.

Table 3.6 The material parameters with changing SP% and w/b

Cement Kg/m³	FA kg/m³	ggbs kg/m³	w/b	SP%	Sand kg/m³	CA kg/m³	Rubber kg/m³	Strength MPa
210	90	0	0.35 0.45 0.55	0.1 To 0.6	900	800	0	

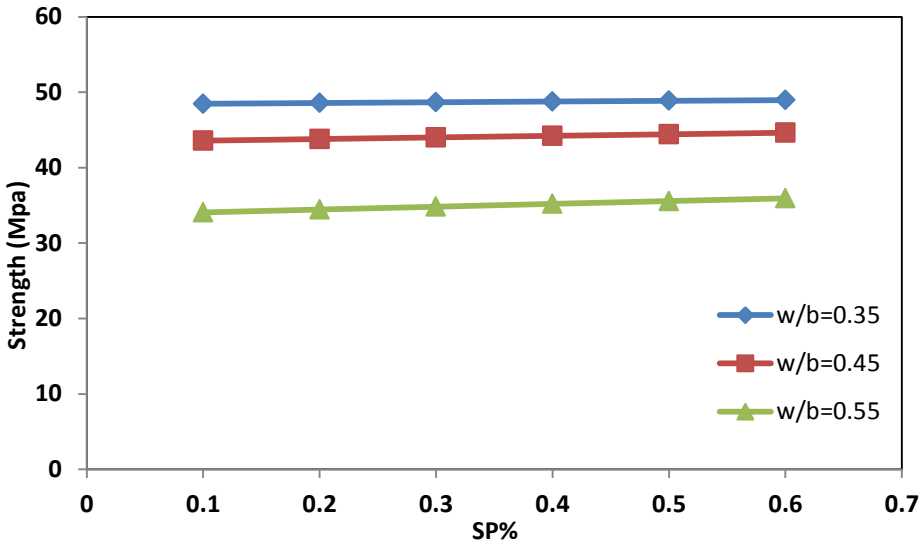

Figure 3.16 Effect of SP% on the compressive strength

3.7.3 Effect of coarse aggregate on compressive strength

The amount of coarse aggregate was varied from 700 to 950 kg/m³, while quantities of other materials were held constant, as shown in Table 3.6. This change was repeated three times for different w/b values of 0.35, 0.45 and 0.55 respectively. As shown in Figure 3.17, increasing the coarse aggregate does not result in much change, but with increasing w/b, the compressive strength decreases for the same volume of coarse aggregate.

Table 3.7 The value of material parameters with changing coarse aggregate content and w/b ratio

Cement Kg/m³	FA kg/m³	ggbs kg/m³	w/b	SP%	Sand kg/m³	CA kg/m³	Rubber kg/m³	Strength MPa
210	90	0	0.35 0.45 0.55	0.5	900	700 To 950	0	

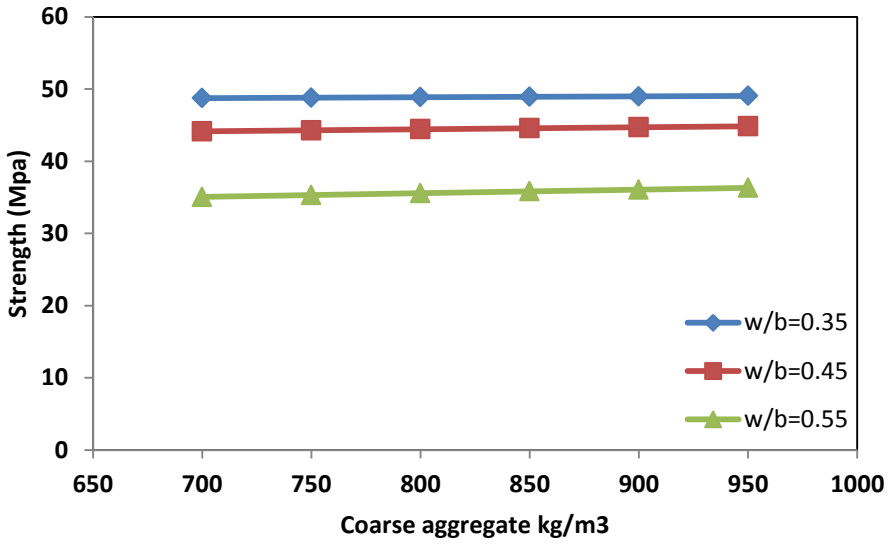

Figure 3.17 Effect of coarse aggregate content on the compressive strength

3.7.4 Effect of cement content on compressive strength

The cement content was increased from 160 to 460 kg/m³, with a constant quantity of water (155 kg/m³) as shown in Table 3.7. The results are presented in Figure 3.18. The results give a predictable graph, i.e. increasing compressive strength with higher cement content. However, the change is small. This could be due to the properties of other materials in the mix.

Table 3.8 The values of material parameters with changing cement content

Cement Kg/m³	FA kg/m³	ggbs kg/m³	w/b	SP%	Sand kg/m³	CA kg/m³	Rubber kg/m³	Strength MPa
160 To 460	150	0	0.25 To 0.5	0.4	800	750	0	

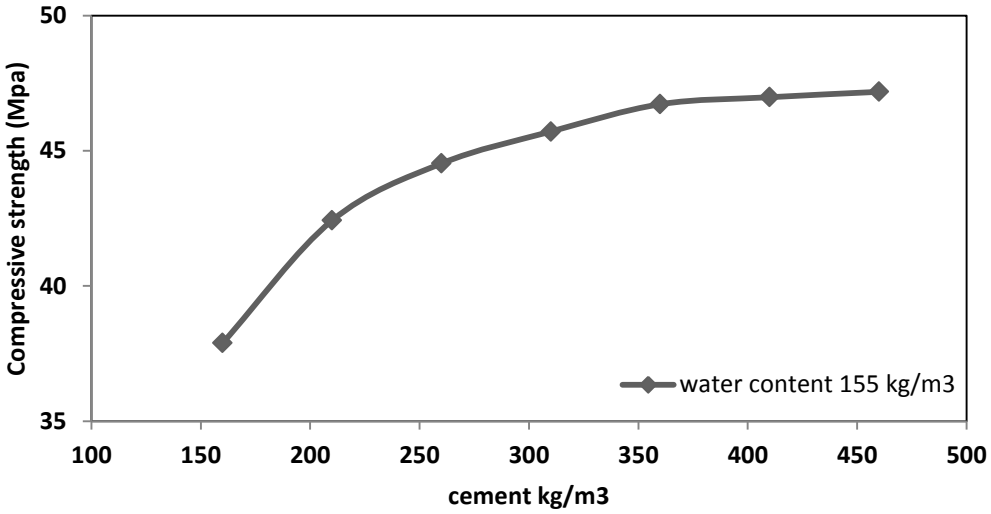

Figure 3.18 Effect of cement content on the compressive strength

From the parametric study it can be concluded that the most important factor was w/b and cement content. It has a much stronger influence on the compressive strength compared with other parameters, as is indicated by Figures 3.14 to 3.18.

3.8 Conclusions

This study has shown that the ANN approach can be used as a new modelling technique to predict the mechanical performance of SCC mixtures. Compressive strength was predicted by the ANN based on several parameters with reasonable accuracy when compared to the experimental results. From this chapter some key conclusions can be drawn:

- ANNs are data intensive computational models and do not require any prior knowledge about the underlying relationships between input and output variables.
- The Multilayer Feed Forward neural network, with an error back-propagation learning algorithm, is the most efficient and widely used neural network for function approximation. The applications of ANN reviewed in this chapter are a testimony to the extensive use of this type of neural network in modelling the composite material behaviour of concrete.
- Using ANN modelling, one can gain insight into the composite nature of concrete. The factors that govern the compressive strength can be easily determined through sensitivity analysis. Moreover, the effect of variability in the quantity of each constituent on the compressive strength of the concrete can be easily evaluated using the ANN modelling methodology.
- The developed ANN could be used as a predicting tool, based on historical data, to estimate the compressive strength of concrete

based on mix proportions before the placement of concrete takes place.

- The comparison between the ANN results and the experimental results showed good agreement in terms of the compressive concrete strength.
- The ANN produced the expected relationships for all the parameters used in this study. The water to binder ratio had the strongest effect on the behaviour of the compressive strength, which is also true for normal concrete. This means that the ANN was very well trained, and is ready for use in the design of SCC mixes.
- The ANN became more accurate when fed with more input data during the training phase, which is shown in the Appendix A. Moreover, the use of a larger volume of training data results in a more reliable prediction network.

CHAPTER FOUR

EXPERIMENTAL WORK

4.1 Introduction

This chapter describes the main experimental programme that was developed to investigate the behaviour of elliptical tube columns filled with self-compacting concrete. The experimental programme is divided into two parts: column preparation; and material properties. A series of eight SCC-filled columns were tested. Additionally, two elliptical hollow tube section columns were also tested for comparison purposes. The main parameters investigated via the column testing were (i) section shape, (ii) column length, and (iii) concrete compressive strength. The properties of Self-compacting concrete were predicted by artificial neural network (as presented in Chapter 3). Tests were then conducted on fresh and hardened concrete to evaluate the characteristics and the quality control process until an acceptable mix specification was found. The resulting concrete properties for all columns are presented in Chapter 5. Then, the experimental results (including buckling and ultimate load) are used in Chapter 6 for validation purposes.

4.2 Experimental Investigation

4.2.1 Properties of elliptical shapes

Elliptical hollow sections (EHS) have two defining dimensions known as the major and minor axes, as shown in Figure 4.1. The X-X axis is the major axis, with length 2a; while the Y-Y axis is the minor axis, with length 2b. The area of ellipse may be obtained by the general formula $A = \pi ab$. All the elliptical sections are predicted with major to minor axis dimension 2:1, as hot finished hollow structures.

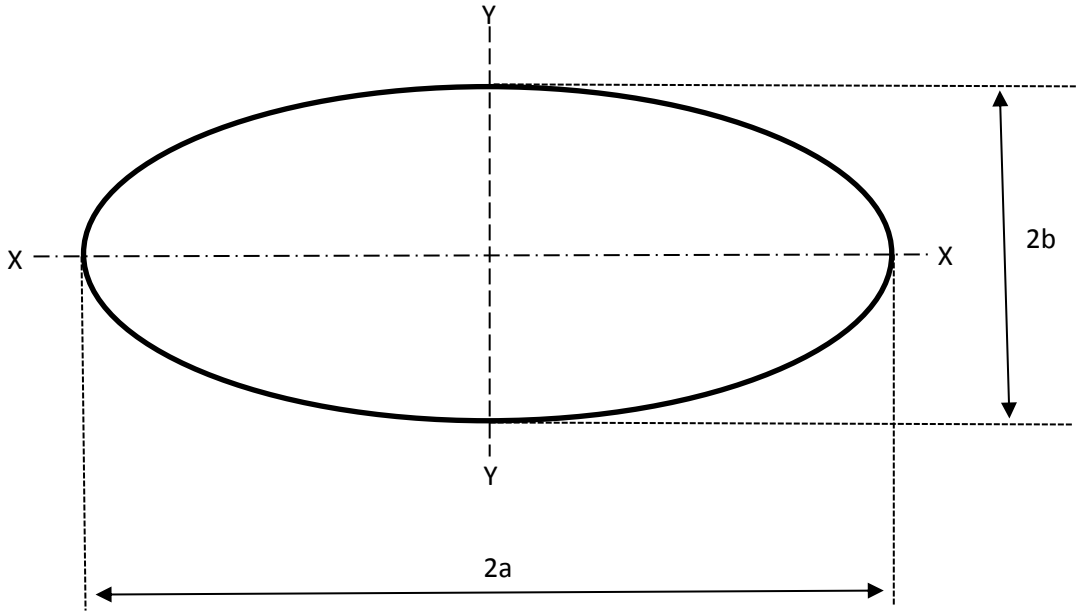

Figure 4.1 Definition of ellipse

4.2.2 Instrumentation

Two types of instruments were used to record data during the experimental tests; linear vertical displacement transducers (LVDTs) and strain gauges. LVDTS were used to measure out of plane deflection, while the strain gauges were located on the outer surfaces of the steel columns to ascertain

the local effect on the cross section. The axial shortening was measured by LVDTs, which were attached to the top plates of the columns as shown in Figure 4.2. The lateral displacements and strain measurements were predominantly taken at the centre and at one third from each end. Figure 4.3 shows the locations of the LVDTs and strain gauges. Eight strain gauges were attached to each column. Vertical gauges were affixed at the top, and at the middle of the major and minor axes. Horizontal gauges were attached at the bottom, and at the middle of the major and minor axes. The LVDTs and strain gauges were connected to a data logging system that was controlled by an automatic data acquisition system and operated by a personal computer.

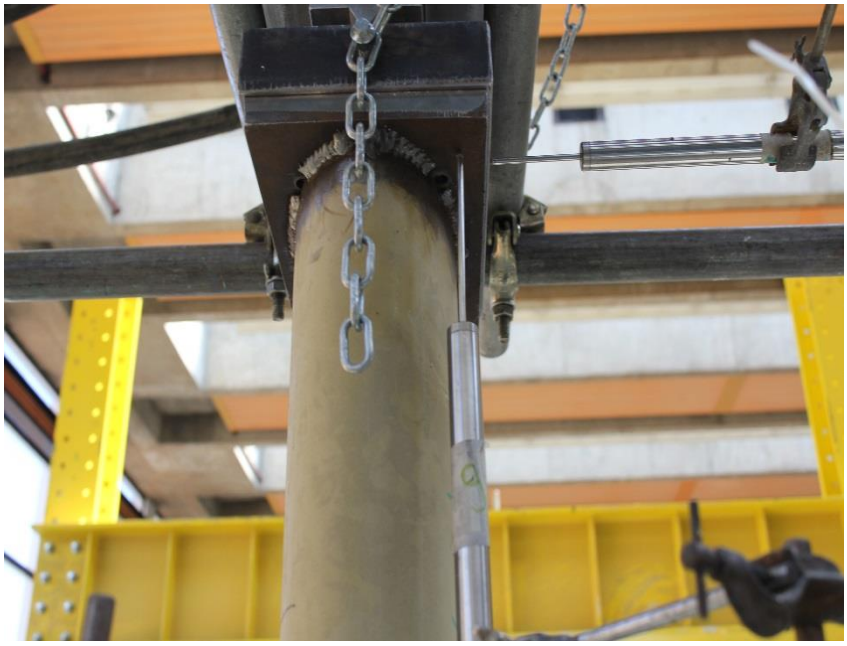

Figure 4.2 Location of LVDTs for axial shortening

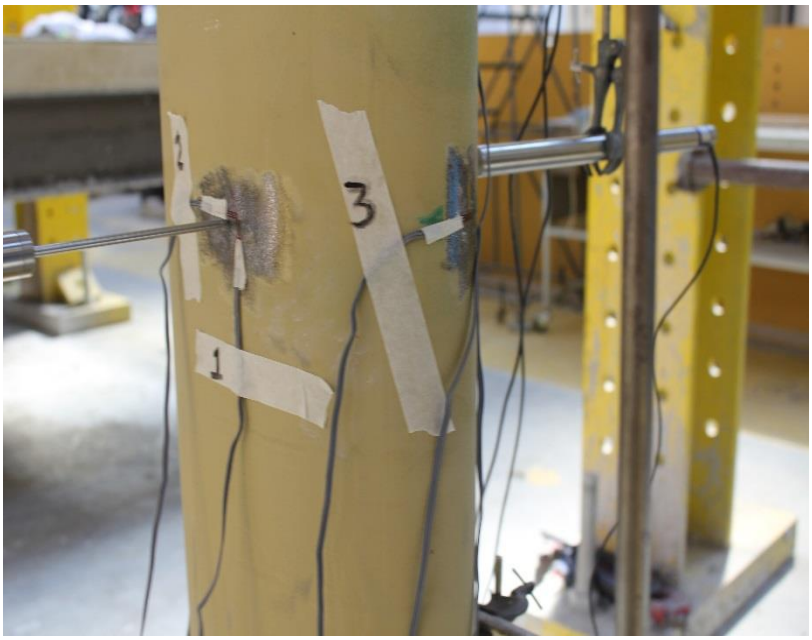

Figure 4.3 Location of strains and LVDTs in the middle of the columns

4.2.3 Column set up and test procedure

A total of eight SCC-filled elliptical columns and two hollow elliptical columns were constructed. All columns were tested in a vertical position subjected to axial compression as shown in Figure 4.4. Pinned end joints were constructed using groove plates and a steel triangle at each column end. This allows free rotation at both ends as shown in Figure 4.4c. The reason for using a steel triangle (or knife edge) is to ensure that the global buckling only occurs around the minor axis of the elliptical column.

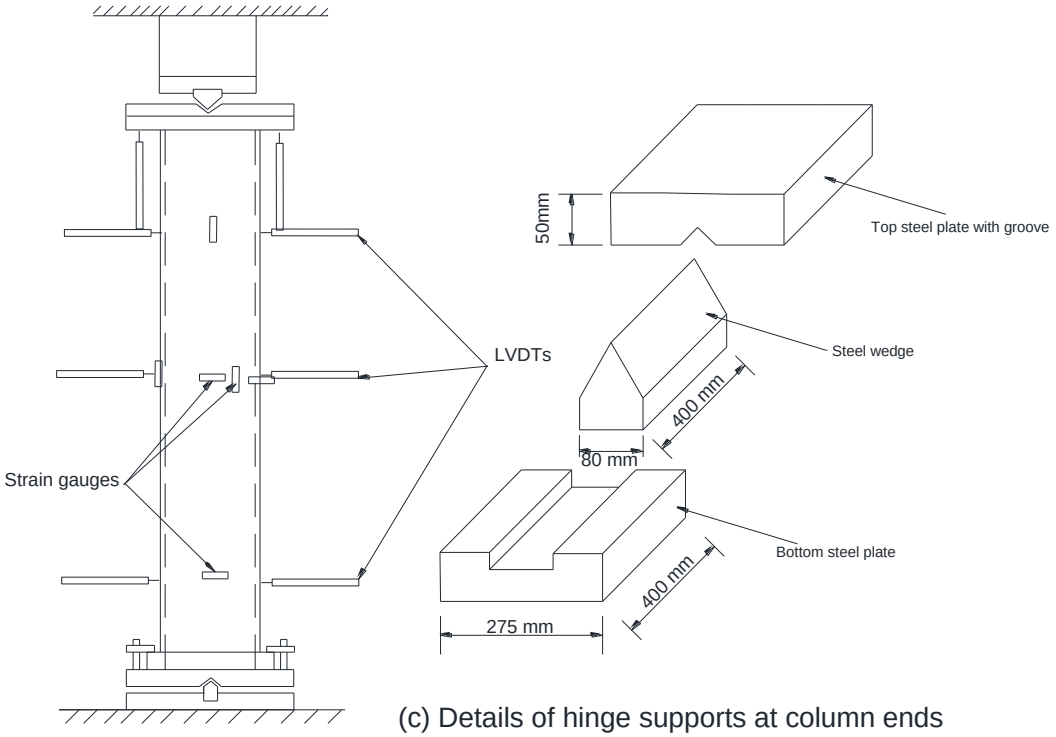

(a) Column in vertical testing position

(c) Details of hinge supports at column ends

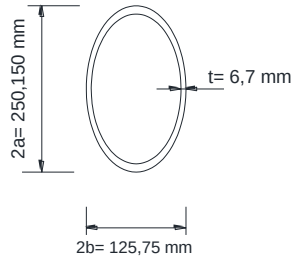

(b) Column cross section

Figure 4.4 Columns set up

For the hollow column specimens, both column ends were capped by the steel plates to ensure full contact between specimens and end plates; for filled column specimens, steel plate was positioned at the bottom of the columns. Three days after casting each specimens, a layer of high strength mortar was capped at the top of the concrete core to fill the gap between the

concrete core and the top of the columns and ensure a uniform distribution for the applied load on the composite section. After that, the top plate was welded to the other end of the specimens.

After a column was placed in the test rig, a small load was applied to hold the specimen upright, and then the specimen was carefully centralised using a plumb bulb and spirit level. Before the test began, pre-loading was conducted to ensure that the loading was applied concentrically. The top plate in contact with the jack was fixed by two bars to avoid horizontal movement as shown in Figure 4.5.

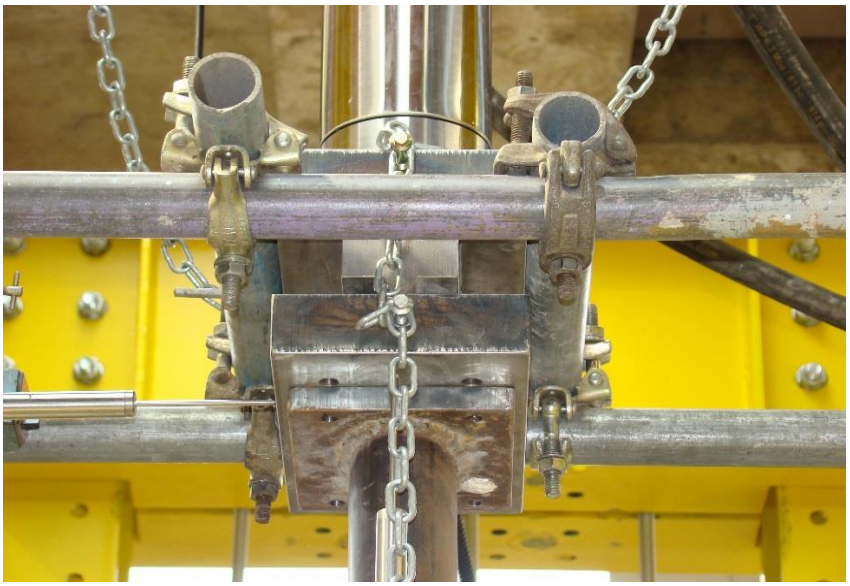

Figure 4.5 Top plate in contact with the Jack

Two test frames were used to perform experiments on all the long columns. A four-legged height-adjustable test frame enabled experimentations on the specimens. A 2500 and 1000 KN hydraulic jack was located at the top of the frame for the big and small section respectively. Finally, tube bars were

located around the whole column to avoid the possibility of columns falling down after failure load was reached, or even during the test.

4.2.4 Columns labelling and dimension

The tested column specimens were divided into three series depending on their length (height) as summarised in Table 4.1. Series I, II, and III have lengths of 1500, 2000 and 2500 mm respectively. The specimen ID in Table 4.1 is specified according to length, section size and nominal concrete strength. For instance, in CII-150-L-2: the first letter and Roman numeral, CII, represents a column from series II (column length 2000 mm); the number 150 in the centre of the ID represents the major outer diameter of the elliptical steel hollow section; the letter L represents the concrete infill grade (low strength); and the number at the end of the ID tells the length of the tested column. Low concrete strength is defined as being between 45 to 55.17 MPa. An H would represent high strength concrete (from 85.5 to 103.75 MPa), while the letter N would indicate that the column was unfilled. The imperfection (out of straightness) of each tested column was measured and presented in Table 4.1. There were two nominal sizes of specimen chosen in this study, 150x75x6.3 mm and 250x125x6.3 mm. The tubes were supplied by the manufacturer in lengths of 6m. The specimens were accordingly cut to the desired lengths, ranging from 1500 mm to 2500 mm. These dimensions were chosen to examine the influence of slenderness ratio on column load capacity. Moreover, no research was found for the slenderness ratios considered in the current study.

To summarise, the experiments were conducted on columns with steel tubes of yield stress of Fy in the range of 388-431 MPa, and were accordingly filled with low and high strength self-compacting concrete. The columns' slenderness ratios ranged from 64 to 133.

Table 4.1 Dimension of the columns

	Specimen ID	2a (mm)	2b (mm)	L (mm)	t (mm)	$\bar{\lambda}$	Imperfection (mm)
Series I	CI-150-L	150	75	1500	6.88	0.9	0.75
	CI-150-H	150	75	1500	6.89	0.95	0.75
Series II	CII-250-N	250	125	2000	5.65	1.08	1
	CII-250-L	250	125	2000	6.3	1.17	1
	CII-250-H	250	125	2000	6.3	1.29	1
	CII-150-N	150	75	2000	7	0.63	1
	CII-150-L	150	75	2000	6.9	0.72	1
	CII-150-H	150	75	2000	7.1	0.82	1
Series III	CIII-150-L	150	75	2500	7.34	1.49	1.25
	CIII-150-H	150	75	2500	6.88	1.57	1.25

$\bar{\lambda}$ is the non-dimensional slenderness which can be calculated from questions (5.1 to 5.9) in the next chapter and more explanation will be presented there as well.

4.2.5 Column supports

Test were performed on pin-ended joints that were constructed by using groove plates and a knife edge at each end of the column. This allowed the free rotation at both ends as shown in Figure 4.6.

Figure 4.6 Groove plate with knife edge

4.2.6 Testing procedure

Figure 4.7 shows the typical test arrangements for all columns. The compression load was applied and monotonically increased. Load, strain and displacement data were recorded during the testing process until the load was observed to be dismissing. The test results concerning failure mode, circumferential strain distribution, load-deformation behaviour, buckling, and evaluation of the strength of the columns were documented during the course of the testing. Load control with a rate of 20 KN/min was used until 80 % of the failure load predicted by Euro code. Displacement was then controlled at the rate of 0.1 mm/min so that the global buckling behaviour of the CFT columns could be carefully observed.

Figure 4.7 Test arrangement for Elliptical composite columns

4.2.7 Casting of composite columns

All CFT columns were filled with concrete in a diagonal position to avoid segregation due to fall down from the top, where the SCC was poured into the tube, 20 mm thick steel plates were welded to the top of the columns after a few days of casting. Six cubes and two cylinders were cast at the

same time as the columns' casting, to obtain the concrete compressive strength after 28 days and on the testing day of the column.

4.2.8 Materials Properties

Self-compacting concrete was chosen for the infill material to avoid the need to compact and to improve the ease of casting, as SCC possesses high workability and can achieve full compaction by self-weight. The materials used in this study are readily available in the UK market.

4.2.8.1 Concrete infill

The following control specimens were prepared during the casting of each column: three 100 mm cubes and two 300 mm high by 150 mm diameter cylinders. After demoulding, all the columns and control specimens were stored in the same place in the lab and covered by polyethylene sheets up to the testing date. The control specimens were tested on the same day as the column test. The results of compressive strength for each test specimen are shown in Table 5.2 in next chapter.

All the materials were checked against the specification in euro code. Fresh properties were achieved in the lab before casting the columns, while hard properties were checked after 28 days of casting. These checks are explained in the following sections.

Portland cement:

Portland cement (PC, class 52.5N), complying with EN 197-1:2011, was used.

Admixtures:

All SCC mixes tested contained a superplasticiser. The superplasticiser used was Glenium C315. The details of this admixture are given in Table 4.2 according to BS EN 934-2:2001.

Table 4.2 Details of chemical admixture

Density	1.1 g/m^3
PH value	5-8
Alkali content %	≤ 2 by mass
Chloride content%	≤ 0.1 by mass

Aggregates:

Mainly local UK gravel and sand were used in the mixes. The maximum nominal size of coarse aggregate and sand was 10 mm and 0-5 mm respectivelly. Seive analysis tests were performed to determine the particale size distrubition, and absorbtion and specific gravity were measured in the laboratory. All the test results complied with Euro code specifications.

Fly ash :

Fly ash 450-S was added into the concrete mixture to improve the fresh concrete proprties.

Mix Design :

Material quantities were predicted by an artificial neural network (ANN) as explained in Chapter three. Different SCC mixes were tested in the laboratory to achieve concrete cubes of nominally low and high strength. Tests of fresh and hard properties were conducted to evaluate the characteristics and quality control process until an acceptable mix specification was found. Table 4.3 shows the summary of the governing parameters adopted for the fresh SCC concrete tests.

Table 4.3 SCC Fresh properties requirements

Tests	Requirement
Slump flow	SF1 class: 550-650 SF2 class: 660-750
T500	Class 1 : ≤ 2
V-funnel	Class 1 : ≤ 8
Segregation	Class 2: ≤ 15%

Trial mixes were assembled in the laboratory to ensure that the predicted mix of ANN was correct. Fresh properties were checked every time before casting the columns. The main tests were known as slump flow, V-funnel and segregation test. All of these tests were conducted by following the European guideline process, and a brief explanation of them will be presented below:

Slump Flow

The slump flow test was used to evaluate the free deformability and flow ability of SCC in the absence of obstructions. A standard slump cone was

used for the test and the concrete was poured into the cone without consolidation. The slump flow value was given by the mean diameter of the concrete (measured in two perpendicular directions by ruler or measurement tape) after lifting the slump cone. Moreover, the time at which the concrete passes a 50 cm dimeter is called T50. This was also measured by using stopwatch. Nagataki and Fujiwara (1995) suggested a slump flow value ranging from 500 to 700 mm for a concrete to be self-compacting. At slump flows greater than 700 mm, the concrete might segregate, and at below 500 mm, the concrete might have insufficient flow to pass through highly congested reinforcement. However, The European guidelines (2005), expand this slump flow limit to 850 mm for some applications. The test results of all the concretes are summarized in Table 5.1 in the next chapter. The results show that all SCC mixes meet the required slump flow value and Figure 4.8 shows the procedure of the slump flow tests.

Figure 4.8 Measurement of slump flow

V-funnel

The deformability through restricted areas can be evaluated using a V-funnel test. In this test, the funnel shown in Figure 4.9 was filled completely with concrete and the bottom outlet was opened, allowing the concrete to flow out. The time of flow from the opening of outlet to the seizure of flow was recorded. Flow time can be associated with a low deformability due to high paste viscosity, high antiparticle friction or blockage of flow. Flow time should be below 6 s for the concrete to be considered as SCC. All mixes performed well with no significant segregation or jamming of aggregate at the contraction. Test results shown in Table 5.1 in next chapter indicate that all SCC mixes meet the requirements of allowable flow time (The European guidelines, 2005).

Figure 4.9 V-funnel Test

Segregation test

Stability is defined as the ability of SCC to resist segregation or to maintain uniform suspension of solid particles. The stability of an SCC mix can be enhanced by reducing the coarse aggregate content and lowering the maximum size of aggregate. It is also important to increase cohesion of the mix to enhance the bond between the mortar and the coarse aggregate. This allows uniform deformation around obstacles. The segregation test method

presented by The European guidelines, (2005) was used. The method includes pouring of 2 Kg of fresh concrete over a 5-mm mesh and measuring the mass of the mortar passing through the screen after 15 mins. The segregation index (SI) is taken as the ratio of the amount of mortar passing through to the amount of mortar contained in the original concrete sample. In the current study, the target SI was below 15, and all mixes satisfied the requirement.

Segregation (or stability) is often associated with static sedimentation. The particles settle in a given sample or in the formwork because their density is higher than the density of the suspending fluid. If the particles' density is lower than the suspending fluid density, the situation is reversed. Test results are shown in Table 5.1 in next chapter, while Figure 4.10 shows the procedure of the segregation test.

Figure 4.10 Segregation test

All the fresh properties of the SCC mix were acceptable and were checked against the European guidelines. The casted columns were then tested after 28 days. Cubes and cylinders were tested after 28 days in order to achieve an accurate representation of their strength, and the CFT column was tested on the same day to gather the actual cubic compressive strength. The results of the compressive concrete cubes are presented in Table 5.2 in next chapter, while Figure 4.11 shows the concrete cubes sits inside the compressive machine.

Figure 4.11 Concrete compressive strength machine

4.2.8.2 Steel

Hot-rolled elliptical hollow section tubes were used, with a steel grade of S355. These tubes were cut into several pieces for the preparation of tensile coupon specimens with an approved shape. The material properties of the steel element were accordingly determined from mechanical testing of the steel coupons. For each section, three coupons were taken from the flatter

side of the elliptical steel hollow section and prepared in accordance with the guidelines (EN 10002-1:1990 Eurocode). The fundamental material stress-strain response of the steel element was obtained by means of tensile tests on each coupon. The yield stress,Fy determined from the tensile strength, is generally accepted as being the same for compression and tension. For columns under axial compression, the stress-strain characteristics of the steel section are approximately the same as those under axial tension up to the plastic range. Linear strain gauges were affixed at the midpoint of each side of the coupons. The behaviour of steel is described through the stress-strain relationship determined from this test. The curves were plotted and the ultimate stress, yield stress and Young's Modulus were obtained. Coupon specimens are shown in Figure 4.12, while a typical load deformation curve for these coupons is presented in next chapter.

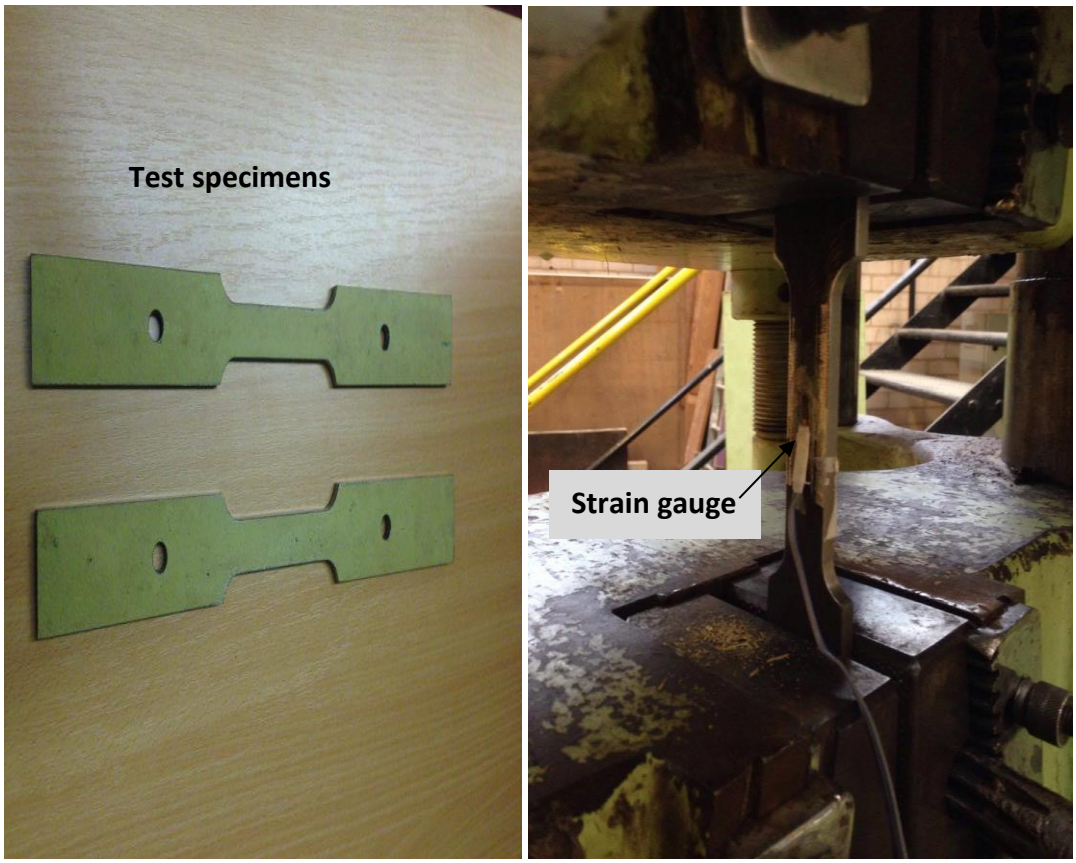

Figure 4.12 Coupon tests

4.2.9 Initial out-of-straightness

The initial tube imperfection of long columns was measured prior to concrete casting taking place. The geometric imperfections were measured for all specimens. The measurement of the imperfection owing to the behaviour of columns was obviously influenced by initial imperfections, particularly for thin-walled steel sections and long columns (Zhang et al., 2007). Furthermore, the overall buckling and strength of the columns were generally affected by the imperfections.

Measurement of the imperfections was obtained using a plumb line from one end to the other end of the steel tubes. A feeler gauge with measurements

ranging from 0.05 to 1.3 mm was used to measure the clearance between the columns along the vertical wire. The tubes were properly positioned on a flat surface and the gauge was moved along the specimen to measure the gap. The measurements were made on both of the wider sides of each tube. The primary aim of this exercise was to record the maximum amplitudes of the imperfections inherent in the tubes. From the measurement, the maximum initial geometric imperfection was found to be at the middle of the columns.

4.3 Summary

In this chapter, the tests to establish material properties were presented the equipment design and the testing of the specimens. The following points are emphasized:

- Material property tests have been conducted. The SCC and steel tube properties were tested, which includes compression for concrete and tensile tests for steel coupons.
- The initial tube imperfection of long columns was measured prior to concrete casting taking place.
- Eight columns were cast; four with law concrete strength and four with high concrete strength.
- For safety, reliability and operability issues, tube bars were located around the whole column to avoid the possibility of columns falling down after failure load was reached, or even during the test.
- Load control with a rate of 20 KN/min was used until 80 % of the failure load predicted by Euro code then displacement was controlled at the rate of 0.1 mm/min.

The results of these tests will form part of the discussion in the following chapter.

CHAPTER FIVE

EXPERIMENTAL RESULT

5.1 Introduction

This chapter presents the results of the tests conducted on the elliptical tube columns filled with SCC. A total of ten column specimens were prepared from two different tube sizes, with the major-to minor outer dimensions of 2:1, and were accordingly categorised into three series. The main aim of the experimental investigation described in this chapter is to study the behaviour of elliptical tube columns filled with SCC. All columns were considered and tested to failure, with the aim of assessing their behaviour. From each test, the behaviour of the axial load displacement and axial load-strain were recorded. The maximum load, point of yielding and post-buckling behaviour for each specimen were measured and identified from the axial load-displacement curve. In this chapter, the test results will be analysed and typical structure responses will be described. Moreover, the experimental study focused on the compressive behaviour of these composite columns to assess the adaptability of current design rules provided in Eurocode 4 for circular and rectangular columns.

5.2 Material properties

5.2.1 Concrete properties

In addition to the overall column tests, a set of materials tests were conducted on the elements used to construct the column specimens. As

explained in the previous chapter, the tests of the fresh and hardened properties of SCC were carried out using the method from euro code. The fresh properties, which included the flow ability, passing ability, filling ability and segregation resistance, were assessed by the slump flow, the T_{50} test, the V-funnel test and sieve stability test, respectively. The fresh properties test results are summarised in table 5.1.

Table 5.1 Fresh properties

Tests	Lab results	
	Mix 1	Mix 2
Slump flow (mm)	575	750
T500 (sec)	1.5	2
V-funnel (sec)	4	6
Segregation %	3.1	2.7

Mix 1 presented low concrete compressive strength, and Mix 2 presented high compressive strength of concrete. All the fresh properties of the SCC mix were acceptable and were checked against the European guidelines.

The tests of the hardened properties of SCC were carried out using the same method as normal concrete. The tests were conducted at test day of tube columns to ascertain the compressive strength of the concrete. Figure 5.1 shows the concrete cubes trail after the tests were complete and the development of compression test results. The compressive cube strength fcu is presented in table 5.2

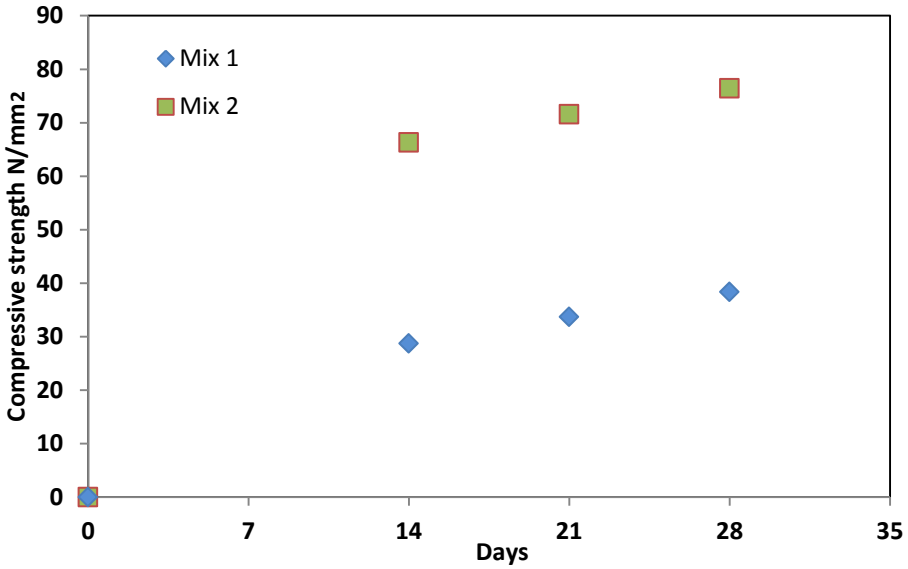

Figure 5.1 Concrete strength development

Table 5.2 Results of cubes compressive strength

Specimen ID	fcu (MPa)
CI-150-L	55.17
CI-150-H	85.5
CII-250-L	47.5
CII-250-H	103.75
CII-150-L	45
CII-150-H	103.2
CIII-150-L	55.17
CIII-150-H	85.5

5.2.2 Steel properties

The material properties of tube steel were determined by the tensile coupon test. Three coupons were taken from the flatter side of the elliptical profile for each steel hollow section, and prepared in accordance with the European

Guidelines (EN 10002-1:1990 Eurocode). Table 5.3 summarises the measured steel properties.

Table 5.3 Properties of the elliptical steel hollow sections

Sample	Section size (mm)	fy (MPa)	fu (MPa)
1	150x75x6.3	431.4	529.4
2		429.5	519.9
3		417.3	504.9
4	250x125x6.3	388.9	523.3
5		392.4	517.2
6		380.7	512.3

In Table 5.3, fy is the steel yield strength and fu is the ultimate strength.

Figure 5.2 shows the stress strain relationship of steel coupons. It can be noticed that there were linear relationship at the beginning with elastic modules equal or greater than 201000 N/mm^2. The measured values represent the ability of the material to resist deformation, which is also known as stiffness. From the tensile tests results the stress-strain steel tube shows an elastic-plastic-strain hardening relationship.

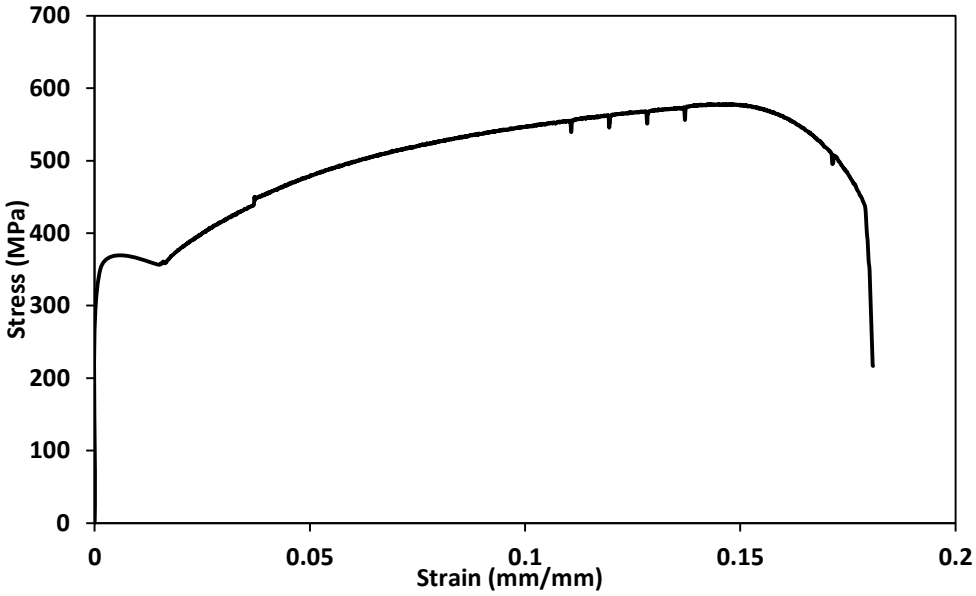

Figure 5.2 Coupon test result

5.3 Experimental results and observations

5.3.1 Axial load capacity

Figure 5.3 shows the axial compressive load with shortening relationships of the column specimens tested. The column behaved in a stiff manner up until the ultimate load was approached, at which point the curves drop quickly. This signifies the crushing of concrete core followed by global buckling of steel columns. It can be observed from the comparison between the filled and unfilled columns that the CFT columns exhibited a superior performance compared with the steel hollow sections, in terms of both the axial compressive strength and initial stiffness.

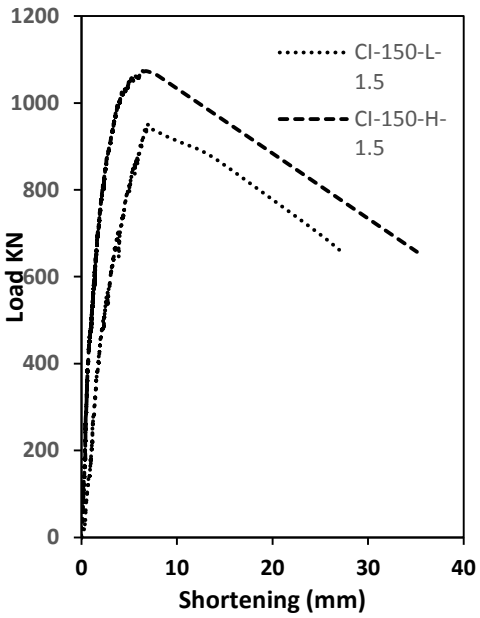

a) L=1.5 m , 150x75

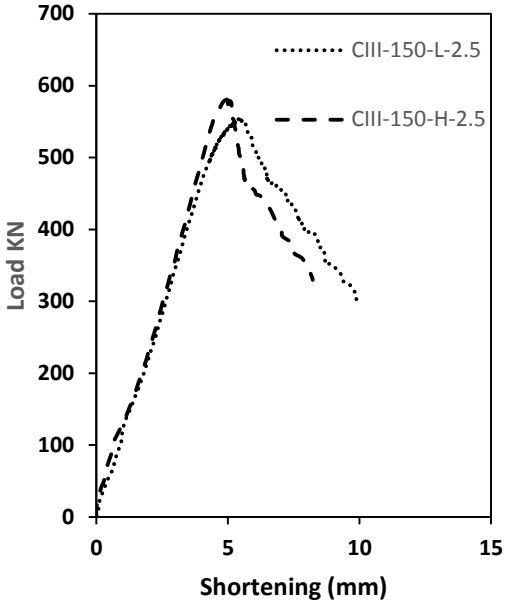

b) L=2.5, 150x75

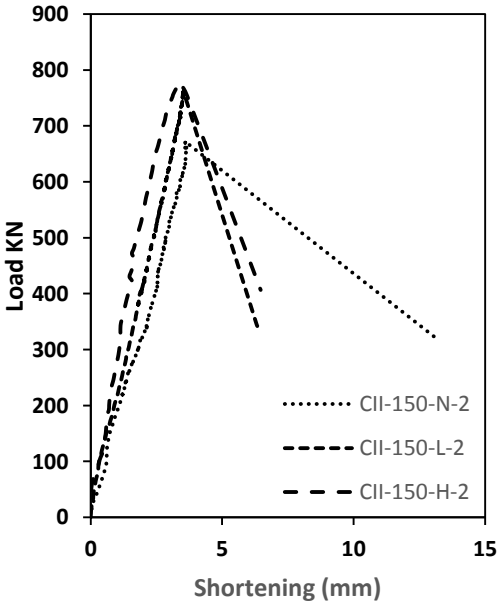

c) L=2m, 150x75 mm

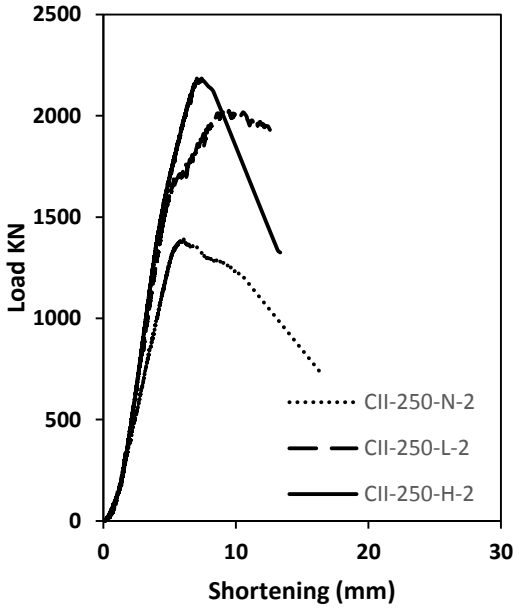

d) L=2m , 250x125

Figure 5.3 Load against axial shortening relation of tube columns

It was noted that for all columns tested, the gradient of the descending branches of the load-shortening curve is very steep after the maximum load is reached. The maximum capacity of the tested columns was governed by the global buckling. It was observed that the global buckling also caused higher stress concentration at the mid-height region, where the lateral deflection and strains increase rapidly as the maximum load was approached. As expected, global buckling deformation was observed in almost all columns tested.

5.3.2 Failure modes

As shown in Figure 5.4, most of the test specimens showed similar failure modes. Most specimens failed due to global buckling apart from the empty hollow section with the larger section size (CII-250-N) which failed due to local buckling. The failure caused by the global buckling modes was found to be consistently concentrated at the centre region for all specimens and the final deflected shape of these columns was symmetrical. This indicates that the SCC infill was homogeneous, or that good consolidation occurred in all columns. However, for the empty hollow section (CII-250-N) having a low slenderness ratio ($\lambda = 64$), the local buckling occurred at the top of the tested column at about 150 mm from the top loading plate as shown in Figure 5.4(i). When comparing the results of the two empty hollow sections (CII-150-N and CII-250-N), it can be concluded that, as the slenderness ratio decreased, the local buckling becomes the prominent mode of failure. On the other hand, when SCC was used to fill the hollow sections, the global buckling was the main mode of failure even for sections having a low slenderness ratio (CII-

250-L and CII-250-H). This can prove that, the use of concrete to fill the hollow sections helps to prevent the local buckling. The failure modes observed from this study were similar to those observed by Jamaluddin et al. (2011) even though the slenderness ratios considered in the current study were different.

In addition, it can be clearly seen that, the final deformation of a typical column after failure load is reached. Inward and outward bulge deformations occurred in the hollow section column. For concrete filled columns, although inward buckling was prevented by the concrete core, outward global buckling was clearly noticed in the deformed specimen as shown in Figure 5.4. The steel tube provided the confining for the concrete core and therefore counteracted the expansion of the concrete, which caused hoop tension in the tube, and subsequently resulted in greatly increased confined concrete. This situation proves that the steel tube in CFT columns shares the carrying of the compressive load with the concrete core. The significant changes in terms of the lateral displacement were only observed after the columns reached failure load. Thus, the load capacity of slender columns was characterised by the initiation of overall buckling. This failure causes higher stress concentration at the middle region of all columns as can be expected from overall buckling analysis. This is the kind of failure mode that the design engineer constantly vigilant against because the buckling is particularly dangerous which can cause a catastrophic failure.

(a) CI-150-L

(b) CI-150-H

(c) CII-150-L

(d) CII-150-H

(e) CII-250-L

(f) CII-250-H

(g) CIII-150-L

(h) CIII-150-H

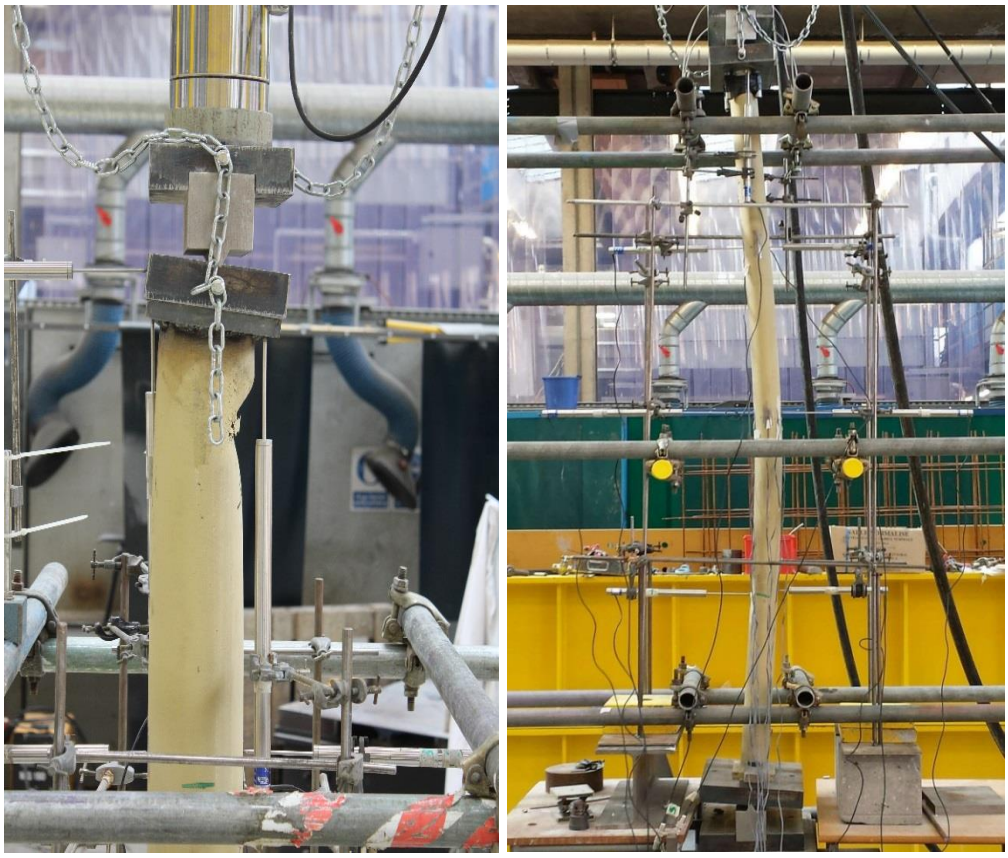

(i) CII-250-N- (j) CII-150-N

Figure 5.4 Typical failure modes

As shown in Figure 5.5, the concrete core after remove the steel, although tensile cracks were developed in the concrete core, it remained intact due to the constraint and confinement of the steel section.

Figure 5.5 Tensile cracks after removing of steel tube steel

5.4 Discussion of the behaviour of SCC filled steel tube columns

5.4.1 Effect of concrete strength

The concrete infill substantially contributes to the load capacity of the concrete filled columns. In comparison to the load capacity of the steel hollow section columns, the load capacity of the filled columns in Series II is nearly 15 % higher for the 150x75 mm columns, and over 45 % higher for 250x125 mm columns as shown in Figure 5.6. The columns filled with high strength concrete, exhibited a smaller confinement effect due to the low dilation of concrete, which prevented the development of the confinement effect. Confinement is only achieved when the micro cracking of concrete core sufficiently increases to enable the concrete infill to expand and exert lateral compressive stress on the steel tube. However, with the increase in concrete strength, the stiffness of concrete also increases, resulting in less

lateral expansion, and therefore the confinement gives little effect to the high strength concrete infill.

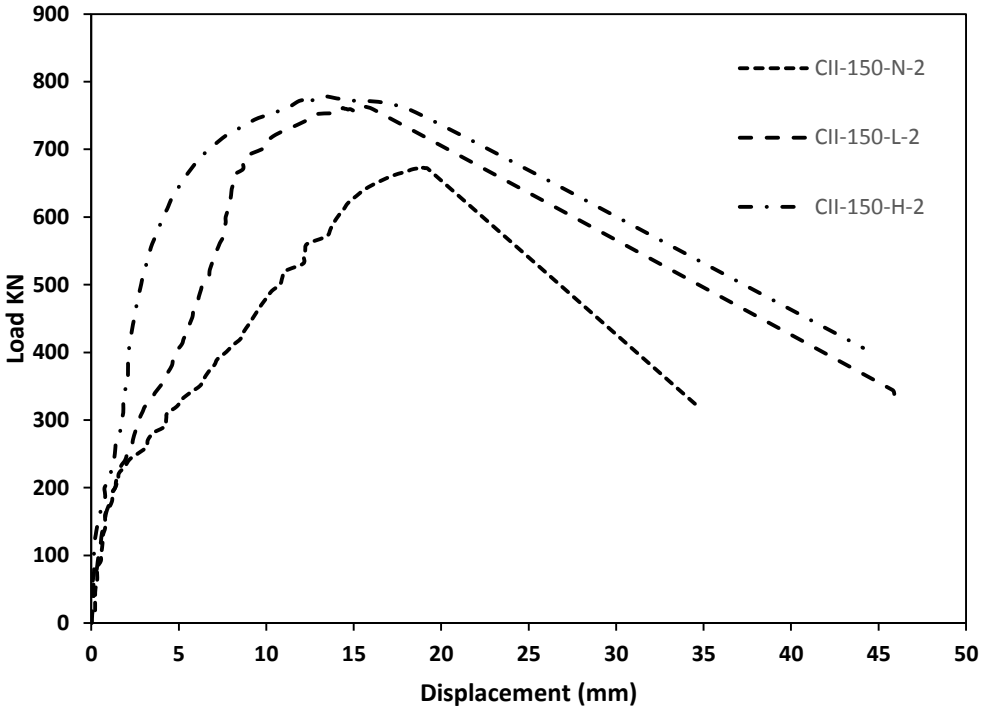

(a) 150 x 75 x 6.3

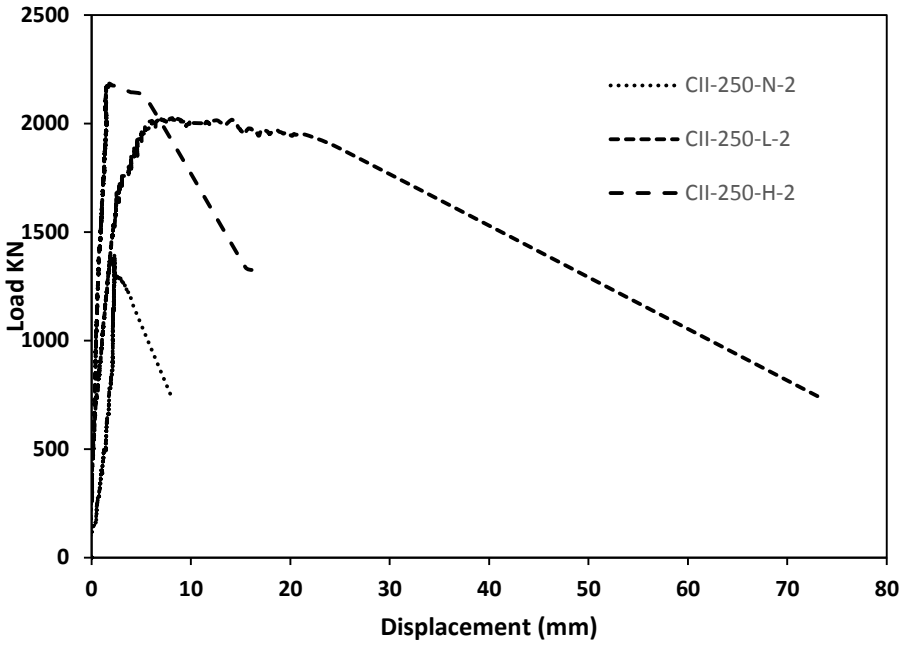

(b) 250 x 125 x 6.3

Figure 5. 6 Comparison between filled and unfilled columns

The influence of concrete strength on the longitudinal strain can be seen from the load curves in Figure 5.7. In general, the strength and stiffness of elliptical columns increase as the concrete strength increases. As expected, specimens with higher strength concrete have larger elastic rigidity in the elastic stage as the initial elastic modulus of concrete increases with the concrete strength. The presence of concrete infill also increases the flexural rigidity as shown by the slope of the curves. It can be seen from Figure 5.7 (a) that change in a column's height can affect the longitudinal strain. Based on the strain readings of steel tubes, the specimens can be divided into two groups. The first one consisted of the steel tubes that failed before reached the yield strain and this was only observed in two columns (CII-250-N and

CIII-150-L). However, the second group included the rest of the columns where the steel tube reached the yield strain before failure. For small sections, the most of the columns failed after yielding except for that having a high slenderness ratio filled with low strength concrete which failed before the yielding of steel. Moreover, empty column with big section size (CII-250-N) failed before yielding of steel.

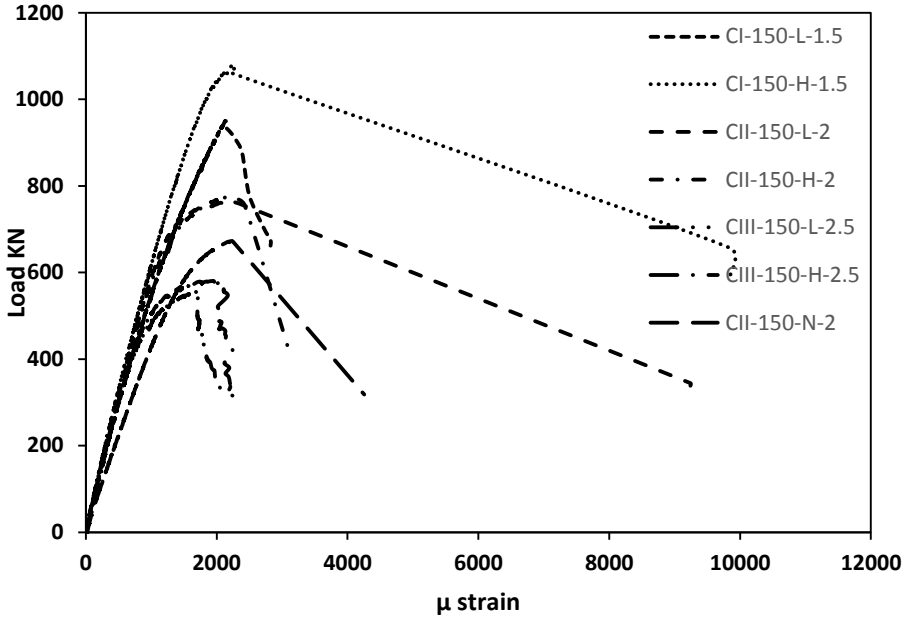

(a) 150 x 75 x 6.3, low and high compressive strength

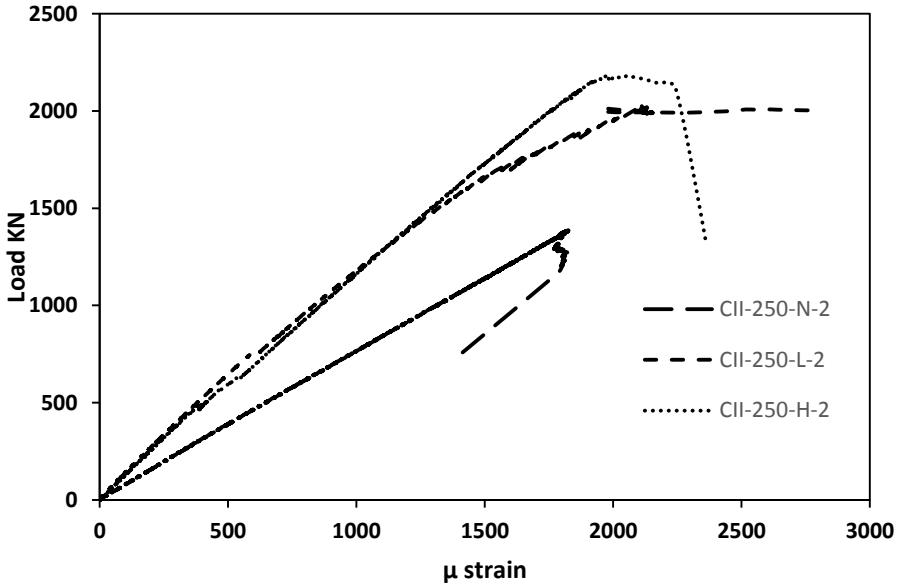

(b) 250 x 125 x 6.3, low and high compressive strength

Figure 5. 7 Load vs longitudinal strain

5.4.2 Effect of column slenderness

Figure 5.8 shows the load vs lateral displacement relationships for columns tested in this study. The tested column with higher slenderness was found to have greater flexibility, which resulted in larger mid-height lateral displacement and lower stiffness. As the height of the column increases, the columns with higher slenderness had a lower maximum load than columns with lower slenderness, and the load reduced quickly once the ultimate load was reached. All tested columns failed with global buckling about the minor axis. The failure mode is consistent with the measured hoop strains at the major axis vertices being larger than those at the minor axis vertices. After maximum load was achieved, significant lateral displacement was observed.

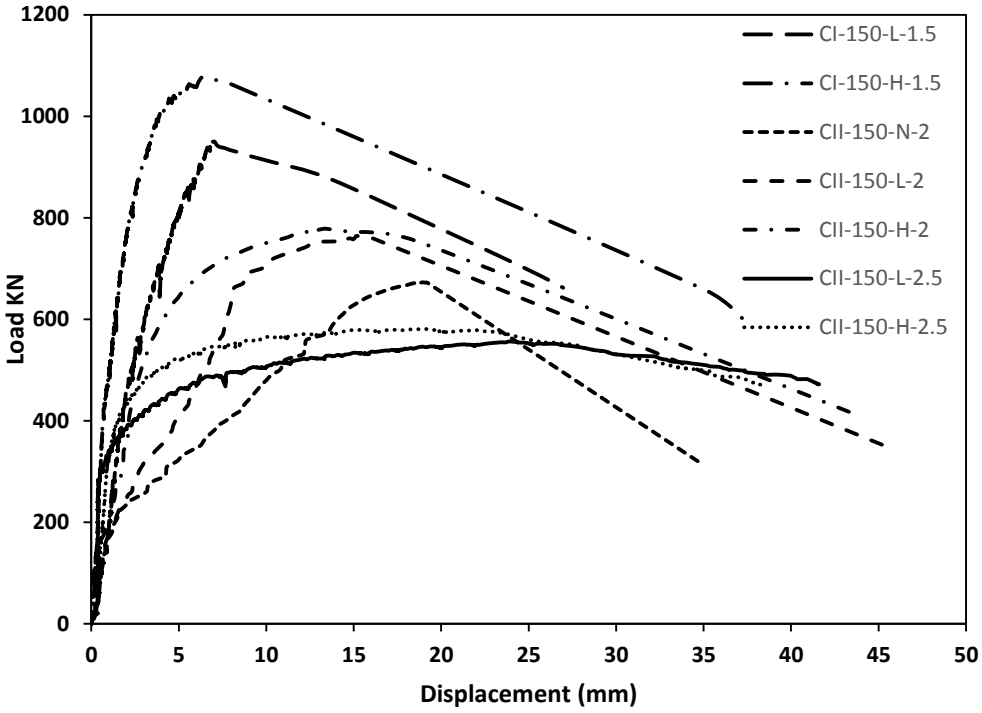

(a) 150 x 75 x 6.3

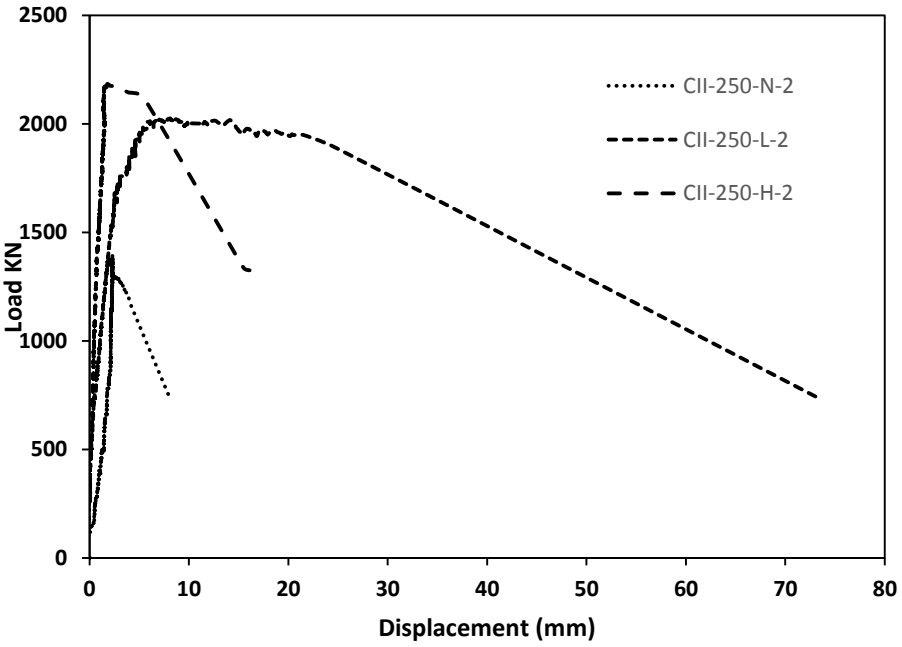

(b) 250 x 125 x 6.3

Figure 5.8 Load vs Lateral displacement (mm)

5.5 Comparison of experimental results with Eurocode 4

Currently, the design calculation of concrete filled elliptical tube columns is not covered by Eurocode 4. The calculation provided in EC 4 covers the design rules for encased, partially encased and concrete-infilled columns with circular, square and rectangular sections.

The simple design and calculation method provided in EC4 is examined in this study to assess its applicability to elliptical CFT composite columns with the buckling curves given in Eurocode 3 (EC3) for steel columns. The resistance of the cross section is calculated by assuming it is fully plastic, and the load is distributed reasonably between the steel and concrete core.

The compressive resistance of concrete filled steel tubes, as stated in EC4, is given by Eq (5.1). This expression is usually applied to circular, square and rectangular tube columns; but in this study, it is used for elliptical tube columns filled with SCC.

$$N_{ed} = \chi \ N_{Pl,Rd} \tag{5.1}$$

where $N_{Pl,Rd}$ is the plastic resistance of the composite section, and χ is the reduction factor for the relevant buckling mode. χ is a function of slenderness, which can be obtained from Eq (5.2),

$$\chi = \frac{1}{(\varphi + \sqrt{(\varphi\text{^}2 + \lambda\text{^}2\ )}} \leq 1 \tag{5.2}$$

where:

$$\varphi = 0.5[1 + \alpha(\lambda - 0.2) + \lambda^2] \quad (5.3)$$

The imperfection factor, α, corresponds to the relevant buckling curve as given by Eurocode 3. The relative slenderness,λ for the plane of bending being considered is given by:

$$\lambda = \sqrt{(N_{pl,Rd}/N_{cr})} \quad (5.4)$$

The reduction factor χ, based on the EC4 method is dependent on the relative slenderness, λ, of columns and on their imperfections. It should be noted that EC3 shows these five buckling curves to reflect the differences in imperfections. These can include geometric imperfection, lack of verticality, straightness, flatness and accidental eccentricity of loading. As most of the experimental failure load points lay above the EC3 buckling curve “a”, using these buckling curves for the slender elliptical CFT composite columns is conservative. Table 5.4 shows the values of χ and λ that are used for Figure 5.8 and $N_{Pl,Rd}$ can be calculated from Eq (5.5). It should be noted that, rectangular form has been used in this study to calculate the buckling resistance of the elliptical tube columns filled with concrete with elliptical properties.

$$N_{Pl,Rd} = 0.85\, A_c\, f_c + A_s\, f_s \quad (5.5)$$

where A_c is the cross-sectional area of concrete, f_c is the compressive concrete cubes strength, A_s is the cross-sectional area of steel tube, and f_s is

the yield strength of steel. A_c and A_s of the elliptical can be calculated from equations (5.6) and (5.7).

$$A_c = \pi\,(a - t) * (b - t) \tag{5.6}$$

$$A_s = \pi\,[(ab) - (a - t) * (b - t)] \tag{5.7}$$

where a and b are the half of larger and smaller outer dimensions of the elliptical section and t is the steel tube thickness.

N_{cr} is the critical elastic normal force for the relevant buckling mode, which may be calculated from the effective flexural stiffness $(EI)_{eff}$ and the actual effective height L:

$$N_{cr} = \frac{(\pi^2\ (EI)_{eff})}{L^2} \tag{5.8}$$

where:

$$(EI)_{eff} = E_{(a)}\,I_a + E_{(s)}\,I_s + 0.6\,E_{(cm)}\,I_c \tag{5.9}$$

I_a, I_c and I_s are the second moments of inertia of the structural steel section and the un-cracked concrete section and the steel reinforcement respectively; while E_a, E_m and E_s are the elastic modulus of the structural steel section and the un-cracked concrete section and steel reinforcement, respectively. I_a, I_c for the elliptical section can be calculated from (5.10) and (5.11) respectively.

$$I_a = \frac{\pi}{4}\,[(a * b^3) - ((a - t) * (b - t)^3] \tag{5.10}$$

$$I_c = \frac{\pi}{4}\left((a - t) * (b - t)^3\right) \quad (5.11)$$

The predicted load-carrying capacities (P_{EC4}) calculated using the method provided in Eurocode, as described above, are compared with test results (P_U) in Table 5.4.

Table 5.4 compares the load capacities of tested column specimens obtained from experimental study against those predicted using the method provided in EC4 for circular and rectangular column sections. It can be seen that the average load ratio is 1.07, with a coefficient of variation COV of 0.069. For all specimens, the load capacities predicted by EC4 are lower than the load capacities obtained from experimental tests, apart from specimen CII-250-H-2 whose measured load capacity is 8 % lower than EC4 prediction. In general, EC4-predicted results are fairly close to those measured in the experiment.

Table 5.4 Comparison of load capacity predicted by EC4 method and obtained from experiments

Specimen ID	$P_{u\ (KN)}$	$\bar{\lambda}$	χ	$P_{EC4\ (KN)}$	$\frac{P_u}{P_{EC4}}$
CI-150-L-1.5	949.8	0.9	0.73	928.6	1.01
CI-150-H-1.5	1076.4	0.95	0.7	988.9	1.06
CII-150-N-2	672.8	1.08	0.6	575.5	1.04
CII-150-L-2	763.9	1.17	0.55	651.6	0.92
CII-150-H-2	778.5	1.29	0.47	725.1	1.17
CII-250-N-2	1392.1	0.63	0.88	1315.9	1.17
CII-250-L-2	2023.1	0.72	0.84	1947.1	1.07
CII-250-H-2	2184.4	0.82	0.79	2382.3	1.02
CIII-150-L-2.5	556.0	1.49	0.37	485.6	1.09
CIII-150-H-2.5	580.5	1.57	0.34	500.3	1.14
				Average	1.07
				COV (%)	6.9

Figure 5.9 compares the experimental results against the non-dimensional slenderness and the buckling curves given in EC3. It can be seen that the EC3 buckling curves generally provide a lower bound to the experimental results. Almost all experimental points lay above the buckling curves, indicating that the buckling curves are deemed safe for elliptical CFT columns, particularly for columns with higher slenderness. For concrete filled tube columns, buckling curve ‘a’ with the imperfection factor α = 0.21 is used. Further analysis shows that the column curve is reliable in determining the influence of

slenderness. Buckling curve ‘a’ agrees reasonably well with the experimental data.

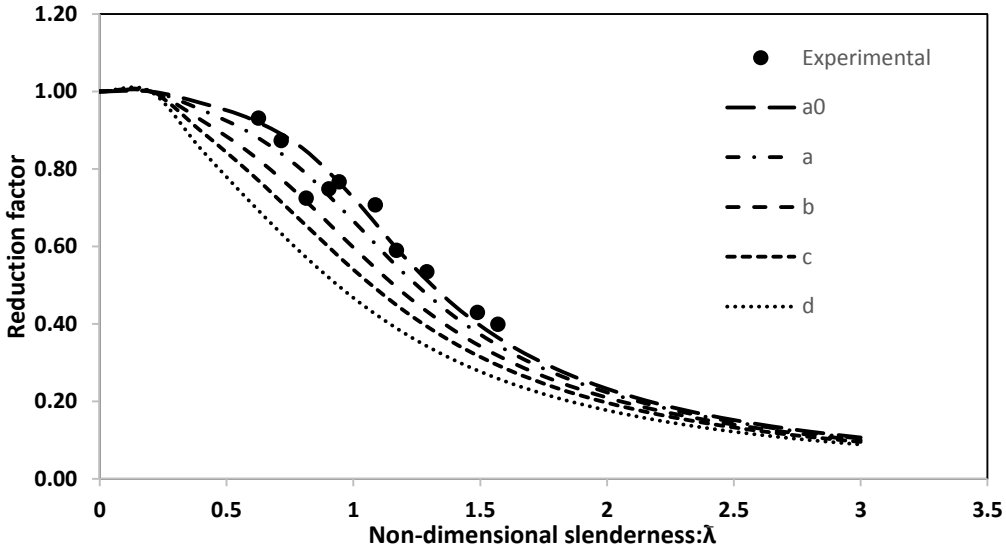

Figure 5.9 Comparison of normalised experimental load to the EC buckling curves

The maximum loads (Pu) obtained from experiments and those predicted by EC4 ($PEC4$) are compared in Figure 5.9, where the solid line represents a gradient of 1.0. The other two dotted lines represent gradients of 1.0 ± 10 %. From Figure 5.10, it can be seen that the ratio of the tested specimens are in the range of 1.0 to 1.0+10 %, indicating a good agreement between EC4 predictions and the experimental load capacities.

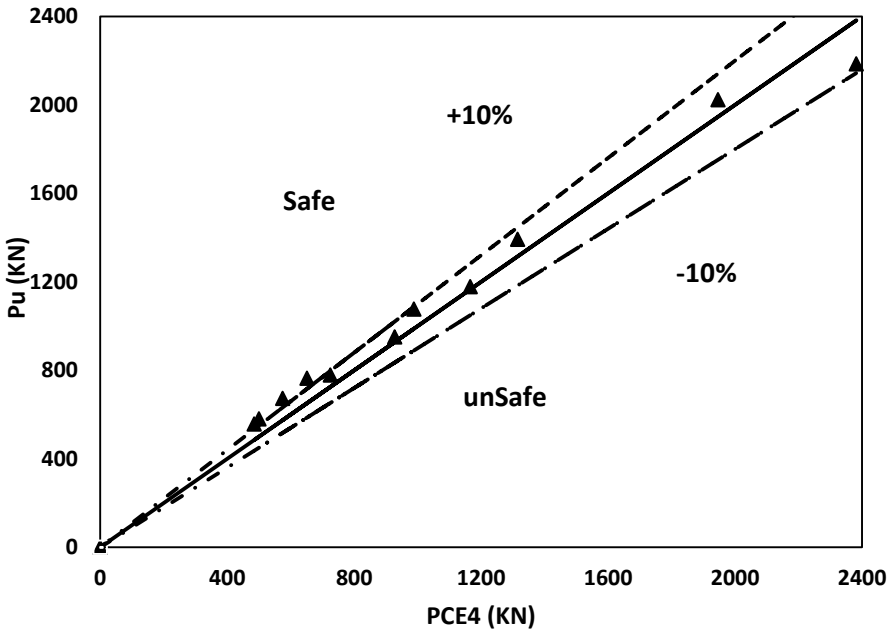

Figure 5.10 Comparison of experimental ultimate load and EC4 predicted loads

5.6 Conclusions

This chapter presented an experimental study on elliptical steel tube columns filled with self-compacting concrete under axial compressive loads. The influence of several parameters on the structural behaviour were investigated, including concrete strength, column section dimensions, and columns height. According to the experimental results, the following conclusions can be drawn:

- All the fresh properties of the SCC mix were achieved the requirements of properties of SCC against the European guidelines.
- The confinement that steel hollow sections provide to the concrete core enhanced the axial compressive capacity of columns and delayed occurrence of global buckling.
- The axial compressive load capacity of composite columns increased with an increase in SCC compressive strength, and reduced with increased slenderness ratio.
- The failure modes were characterised by overall global buckling for most of tested columns.
- For concrete-filled columns, although inward buckling was prevented by the concrete core, outward global buckling was clearly noticed in the deformed specimen, while inward and outward bulge deformations occurred in the hollow section columns.
- The global buckling caused higher stress concentration at the mid-height region, where the lateral deflection and strains increase rapidly as the maximum load was approached.

- The EC4 method displayed reliable results as the confinement effect was considered. The European buckling curves for steel columns can therefore be considered as the basis of elliptical CFT column design.

CHAPTER SIX

FINITE ELEMENT MODEL

6.1 Introduction

Due to the relatively high cost of large scale experimental research, a means of modelling elliptical CFT columns accurately using computer aided methods is needed. This would enable the current knowledge about behaviour of these columns to be broadened, and of the influence of the various components to be will understood. Physical testing has a significant role, but its time consuming and difficult to carry out extensively. Therefore, numerical finite element (FE) analysis has been broadly used as an alternative to provide supplementary information and conduct parametric studies.

The experimental results from chapter five will be used to validate the accuracy of the proposed numerical simulation model. In order to study the behaviour of the elliptical CFT columns, reliable three-dimensional non-linear FE model for elliptical columns subjected to axial load was modelled considering different geometrical and material properties of the concrete core and steel tube. In this chapter, the general purpose nonlinear FE package program, ABAQUS version 6.12, was employed to perform numerical simulation of the elliptical CFT columns subjected to axial compressive loads.

6.2 Finite element model description

There are two different solution strategies in ABAQUS: standard and explicit. The ABAQUS/Standard strategy is used for general purpose analysis. It applies an implicit equation at each user-defined increment to solve a wide range of linear and nonlinear problems involving the static, dynamic, thermal, and electrical responses of components. ABAQUS/Explicit is a special purpose analysis product that uses an explicit dynamic FE formulation. It is appropriate for modelling transient dynamic events, such as impact and blast problems. This analysis solver is efficient in solving highly nonlinear problems involving changing contact conditions, such as forming simulations. The choice between these two approaches of analysis depends on the nature of the problem.

In this study ABAQUS/Standard strategy was used to propose three-dimensional FE model to simulate the behaviour of elliptical CFT columns. The FE model was developed by defining the steel tube, concrete core and plates as individual elements as shown in Figure 6.1. The dimensions of these model sections match those of the columns used in the physical experiments.

The experimentally observed failure mode of elliptical tube columns was symmetric in terms of its major axis. There are two primary means for performing buckling analysis for columns, elastic buckling analysis and non-linear analysis. Initial imperfections were introduced prior to undertaking any non-linear analyses. The imperfections were taken into consideration because they can affect the ultimate load and post-buckling behaviour. To

model the geometric imperfections, the analysis was performed on perfectly straight specimens to establish the probable buckling modes.

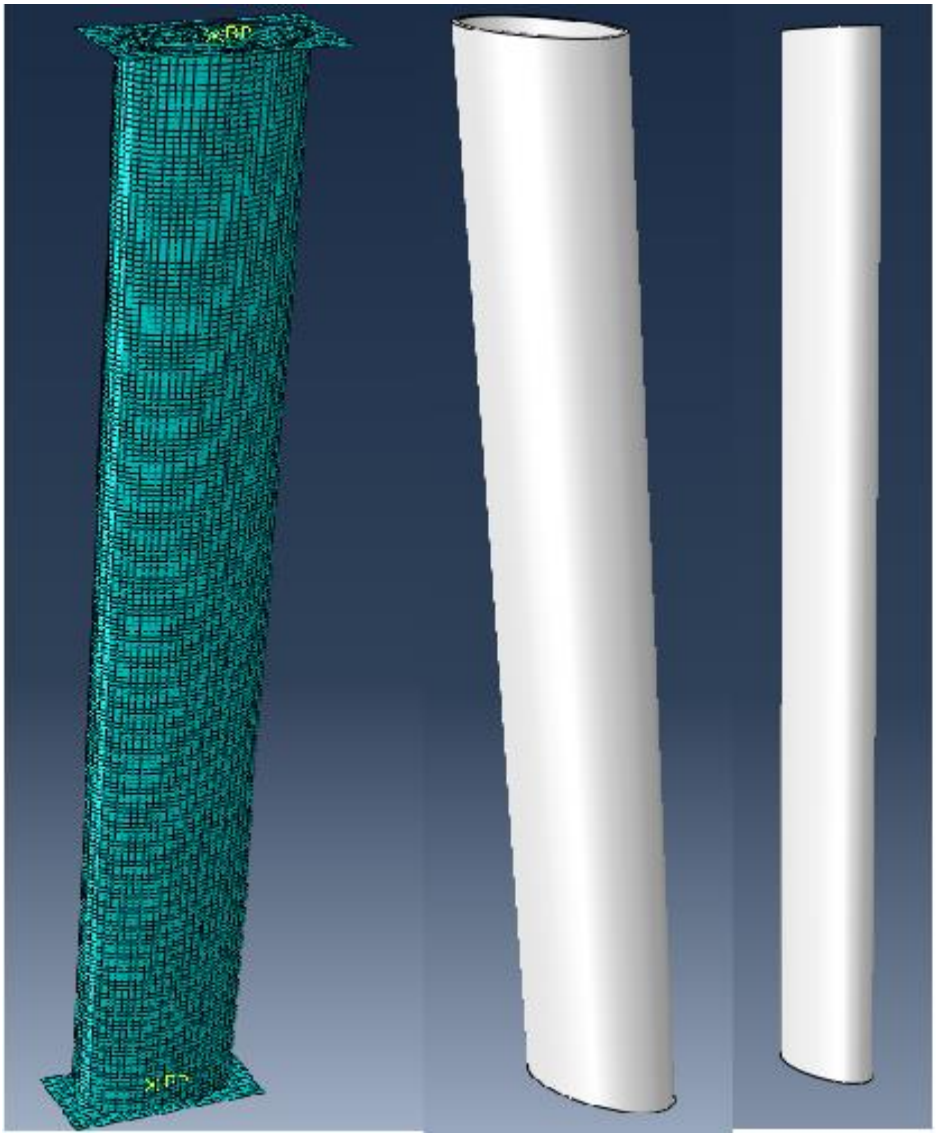

Figure 6.1 Typical FE model of the columns

Imperfections mainly occur during the manufacturing process. For all the columns, the initial imperfection was introduced prior to the nonlinear analysis. It was then acquired through a linear perturbation analysis

of the identical CFT column in which the Aegean mode shape was extracted. The lowest mode shape, combined with the maximum measured column deformation was considered to be the total imperfection in the numerical modelling. The mode shape of the lowest Eigen mode was therefore considered sufficient to adequately characterise the most influential geometric imperfection.

Elastic buckling analysis was followed by non-linear load-displacement analysis. This is a more accurate approach as it incorporates features such as initial imperfection geometry, plastic behaviour and large deflection response. At this stage, the models were loaded to failure to predict the full response and ultimate loads of the columns. In this study, the static general method was used to apply an incremental load for non-linear load-displacement analysis. The displacement control loading method was employed, which simulates the loading method used in the experimental tests.

6.2.1 Boundary conditions and load application

The boundary conditions were applied to the rigid plate as reference points. At both ends, the rigid plate was tied to the tube steel and concrete core. At the lower reference point, the displacement in three directions were fixed and the rotations about three axes were free, in order to prevent convergence problems. This approach was adopted considering that there was no buckling observed about the y-axis during the laboratory experiment. The effect of this approach was investigated and it was found that there was no significant difference in the columns capacities and behaviour if the rotation

of the y-axis was fixed. At the upper plate, rotations about the three axes were also free, and a displacement in the Z direction was applied while displacements in the other directions were fixed. The axial load was applied using displacement technique through the upper rigid body reference point, which was defined as being located at the centre of the column cross section.

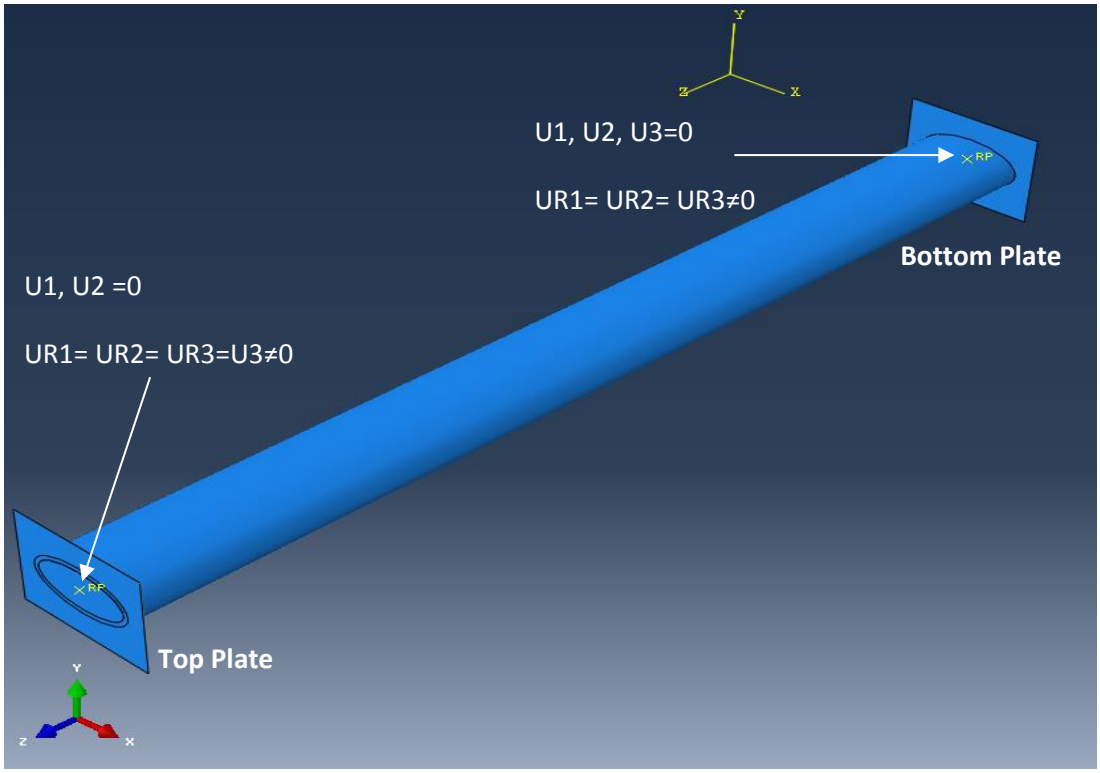

Figure 6.2 Boundary condition of the columns

6.2.2 Members contact

Three components were defined in the numerical model: (i) steel tube; (ii) concrete core; and (iii) steel plates. The 'contact pairs' option was used, with a small sliding parameter, to model the infinitesimal sliding between these

separated deformable bodies. These elements could then interact with each other. For example, the plate transfers the axial load to the steel tube and the concrete core, while the concrete core is confined by the steel tube. The main advantage of using the 'contact pairs' option instead of normal interaction at the interface of the steel tube and the concrete core during the loading course is that, this contact surface allows relative sliding of the elements when the columns experience large deformation. To simulate these interactions, the contact function provided within the ABAQUS software was adopted.

Initially, contact pairs were defined as surface-to-surface contacts to account for the interaction between the steel tube and the concrete core. "Hard contact" was assumed for the normal contact behaviour and reopening was allowed. In the tangential direction, the general bond action between the concrete core and the steel hollow section was simulated through the contact friction. In ABAQUS, different friction coefficients can be used, ranging from 0.1 to 0.5. However, previous studies showed that the friction coefficient had a little effect on the axial resistance while a small friction coefficient is likely to cause a convergent problem at large deformations (Dai and Lam 2010, Dai et al., 2014, Ellobody and Young 2006). Therefore a friction coefficient of 0.3 was adopted in this study for the interaction between the concrete core and the steel hollow section. However, hard contact interaction caused a convergent problem after a few minutes of running the model, so the interaction between the steel tube and concrete was changed to tie to avoid convergent problems.

6.2.3 Element types and mesh density

Element type and mesh size are very important in FE modelling as they strongly affect the accuracy of results and the simulation speed. To select an appropriate element type, several types were selected for analysis in a sensibility study: (i) the 4-noded doubly-curved with reduced integration shell element (S4R) (ii) 8-node solid - reduced integration element (C3D8R). The S4R element type was found to be ineffective, as the simulated failure mode did not replicate the experimental results. Therefore, type C3D8R was selected in the simulation of the concrete core and the steel tube. This is similar to what has been used by other researchers such as Ellobody and Young (2006), Ellobody et al. (2006), Dai and Lam (2010), who found that C3D8R element is more efficient. Although some researchers believe that only shell elements can be used for buckling analysis, it was provide that C3D8R element can be used for displacement, stress/strain analysis as well as for buckling analysis (Dai et al. 2014).

According to Dai and Lam (2010), and Dai et al. (2014), for the steel section, the wall thickness is relatively thin compared to other dimensions, so under an axial compressive load, the hollow section may experience compressive deformation and global buckling; both shell elements and solid elements will be capable to reflect these features. However, if shell elements were used, it is expected that the sizes of the element are much bigger than the shell thickness (wall thickness). The large shell element sizes would reduce the total number of elements of the hollow section, but this may affect the ability of the mesh of the hollow section to follow the curved contact boundary

(contacting surface of a hollow section and the concrete core), which in turn will significantly impair the simulation accuracy of concrete confinement and bond action between two constituent members. Using small three-dimensional 8-node solid elements not only make the hollow section meshes follow the contacting surface reasonably, but also reflect the deformation features of the hollow section, thus a solid element type is adopted for the steel tube. Thus, the reduced integration solid continuum element (C3D8R), was selected to represent both the steel tube and concrete core. The advantage of the reduced integration element is that the strain and stress calculated at the locations provide optimal accuracy. In order to avoid premature steel tube wall buckling, some researchers have used two layers of elements thickness direction of the tube wall (Gardner and Ministro, 2004, Dai and Lam, 2010, Dai et al., 2014). In this study, comparison was made between one and two layer of elements as shown in Figure 6.3. Model with two layers of elements thickness mesh resulted in somewhat better predictions than one layer with regard to load capacity, displacement and shortening. Therefore, two layers of mesh in thickness directions have been used in this study.

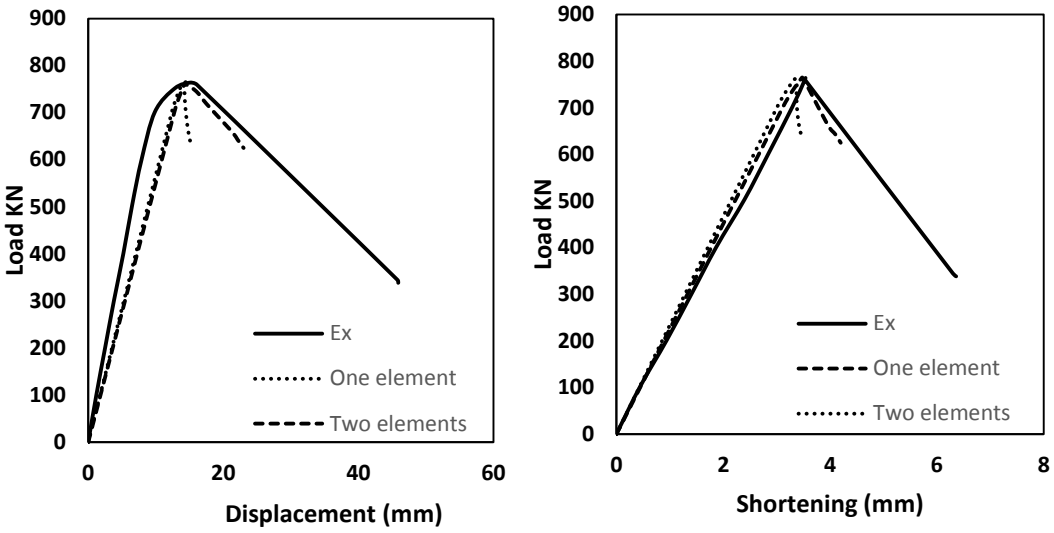

Figure 6. 3 Comparison between different elements of the thickness

Steel plates at the ends of the columns were defined as rigid elements in the numerical model. The rigid plate was assumed in order to eliminate any concern that the top and bottom edges of the columns could be being damaged through the analysis, and to apply axial compressive load uniformly to the column ends. The rigid plates were meshed using four-node three dimensional bilinear rigid quadrilateral elements (R3D4), with an element size of 12 mm. The surfaces of these elements were also defined to connect with the edge of the column. The load was applied as a static uniform displacement through the top of the rigid plate's reference point.

A mesh size sensitivity study was conducted to determine the most suitable finite element mesh size. The mesh size should be fine enough to achieve the desired accuracy. However, mesh refinement leads to an increase in the simulation time and requires more computational resources. Element sizes ranging from 10 mm to 15 mm were compared in the study to obtain the optimum mesh size that would produce accurate results and minimise the

simulation time. These values were chosen in order for the meshing elements to be larger than the aggregate size (10 mm) and also not to too large resulting in a coarse mesh (Genikomsou and Polak 2015). The results were then compared with the experimental results of big and small sections tube columns to establish the best element size instead of choosing the size that provides the closest results to the experimental once. The results of the load-lateral displacement relationship obtained from the model were then compared to those of CII-150-L-2 and CII-250-L-2 as shown in Figure 6.4 a and b.

It can be clearly seen that changing the element size has a clear effect on the load-lateral displacement relation. Moreover, the mesh refinement resulted in significant increase in the load capacity and the computational time. For example, the time taken to run the model with a mesh size of 10 mm is approximately three times that took to run the model with a mesh of 12 mm. Moreover, model with mesh size less than 10 mm could not complete because it takes long time to run then convergent problems appeared. It can be clearly seen from the Figure 6.4 that, 12 mm presented close result of experimental one to compare to other mesh size and computational time was reasonable. The mesh size of 15 and 14 mm seems to be too coarse and did not give close result with regards to load and displacement. The mesh size of 10 mm seems to be too small (close the aggregate size) and for that reason it cannot be considered (Genikomsou and Polak 2015).

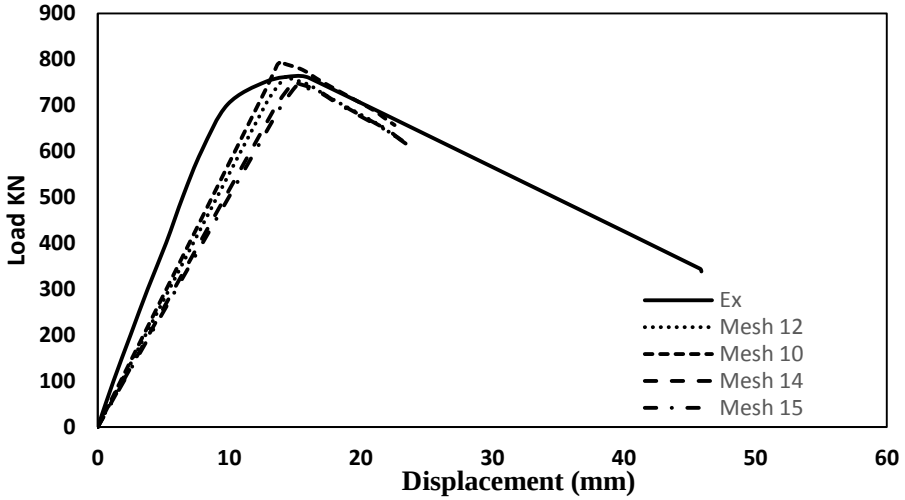

a) CII-150-L-2

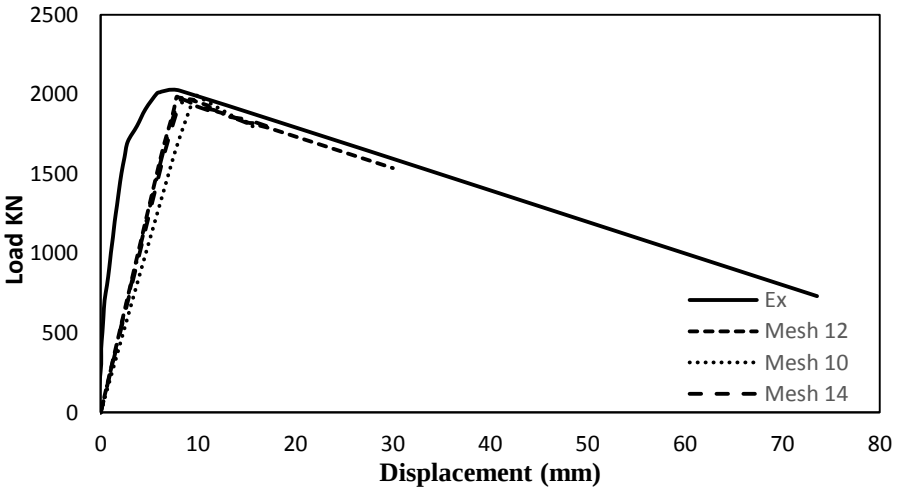

b) CII-250-L-2

Figure 6. 4 Effect of mesh size on the load-displacement response and comparison with experimental results of CII-150-L-2

It can be clearly seen that changing the value of the mesh size affected the load capacity of the columns. For instance, table 6.1 shows the effect of mesh size on the load capacity of CII-150-L-2 and the percentage of reduction for each mesh size. A uniform mesh along the circumferential and longitudinal direction was employed in all models. The sensitivity study compared the numerical prediction with the experimental results and

suggested that a mesh size of 12 mm gives an acceptable degree of accuracy. A uniform mesh along the circumferential and longitudinal direction was employed in all models.

Table 6.1 Computational load capacity of the FE model for different mesh size

Element mesh size (mm)	Prediction Load P_{Abaqus} (KN)	Experimental load P_{Ex} (KN)	$\frac{P_{Ex}}{P_{Abaqus}}$
10	797	763.93	1.04
12	764.2		1.00
14	753.62		1.01
15	747.22		1.02

6.2.4 Imperfection

Initial geometric imperfection can play a significant role in the stability behaviour of columns. In this study, the range of the out of straightness measured from all tested specimens was found to be between 0.75 mm and 1.25 mm, where the global imperfection is about L/2000. Therefore, the amplitude of L/2000 was adopted for the numerical simulation. It was defined by perturbation in nodal coordinates of the perfect column using the "imperfection" option in ABAQUS. During the validation, this imperfect scale provided very good agreement with the experimental results.

6.3 Material properties

6.3.1 Steel

The stress-strain relationship of the steel tube was obtained from a steel coupons test as it was shown in chapter five (see Figure 5.2). Since the model formulation is based on the updated Lagrangian description, the true stress and logarithmic strain are needed to describe the effective stress and

effective strain. The value of Poisson's ratio for steel, used in the numerical analysis, is 0.3.

6.3.2 Concrete Drucker Prager elements

ABAQUS offers several models for the characterisation of concrete behaviour such as the concrete damaged plasticity model and concrete Drucker Prager. Initially, concrete damaged plasticity (C.D.P) was used, this model is designed to model the concrete under arbitrary loading, including cycling loading and assumes an isotropic damaged elasticity in tension and compression to present the inelastic behaviour of concrete. The concepts of stiffness recovery effects under cyclic loading and the elastic stiffness resulting from the plastic strain in tension and compression are also considered in the C.D.P model. The damaged plasticity model can be used for plain concrete as well as for RC structures subjected to monotonic, cycling and dynamic loading under low confining pressure (ABAQUS Inc, 2012). However, this model took long time and caused a convergent problem.

Moreover, the results of the load capacity, lateral displacement and shortening obtained when using C.D.P model were not accurate when compared to the experimental results. For this study, the Drucker-Prager (D.P.) model was selected to obtain the plastic behaviour of confined concrete. It is divided into two parts, with the first part being defined by the angle of friction, the flow stress and the dilation angle and the second part will be explained later. Comparisons between predicted results from the

C.D.P model and D.P model were made to support the choice of the concrete model. The same boundary conditions and stress-strain relationship were used for both concrete models considered. Comparisons between C.D.P model, D.P model and experimental results for section CIII-250-L-2.5 are shown in Figure 6.5. The failure mode shape was similar for all the models compared to the experimental model of failure. However, with regard to the load capacity, lateral displacement and shortening, the results of the D.P model were more accurate than those of the C.D.P model compared to the experimental results. Moreover, the time required for the C.D.P model to predict the results were more than ten times longer than that required for the D.P model. Therefore, the D.P model was selected in the current study.

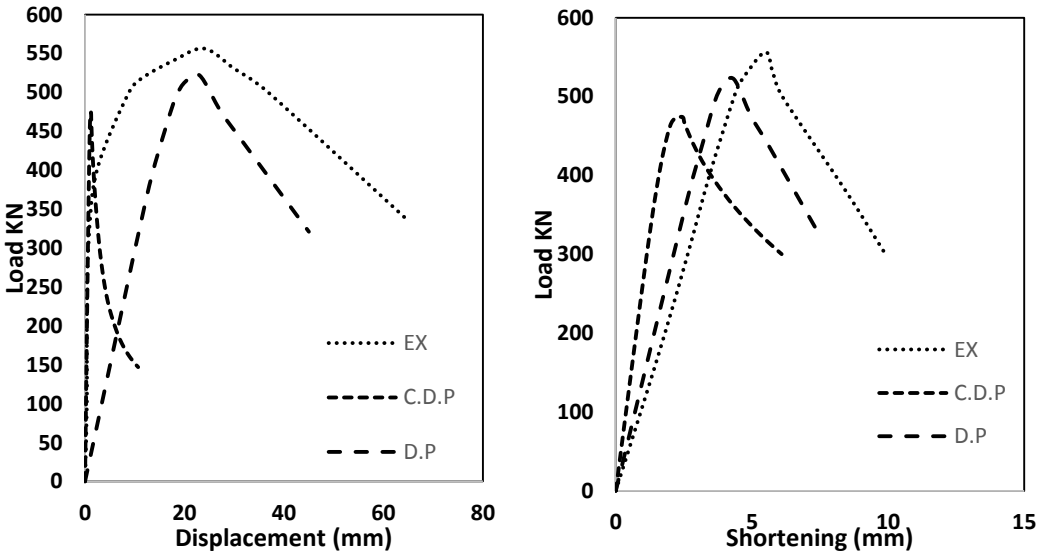

Figure 6. 5 Comparison between Experimental, D.P and C.D.P of CIII-150-L-2.5

6.3.2.1 Friction angle

Different values were adopted in ABAQUS for each element and the selection of the appropriate friction angle value was based on the load-

capacity and lateral displacement response. In order to choose a value for the frication angle, different values were adopted in ABAQUS. The results were then compared to the experimental results of CII-150-L-2 as shown in Figure 6.6. It can be clearly seen that changing the value of the friction angle did not have any effect on the load capacity of the columns. However, it had effect on the lateral deflection and the initial stiffness, as the angle increased, the lateral deflection response decreased and the initial stiffness increased.

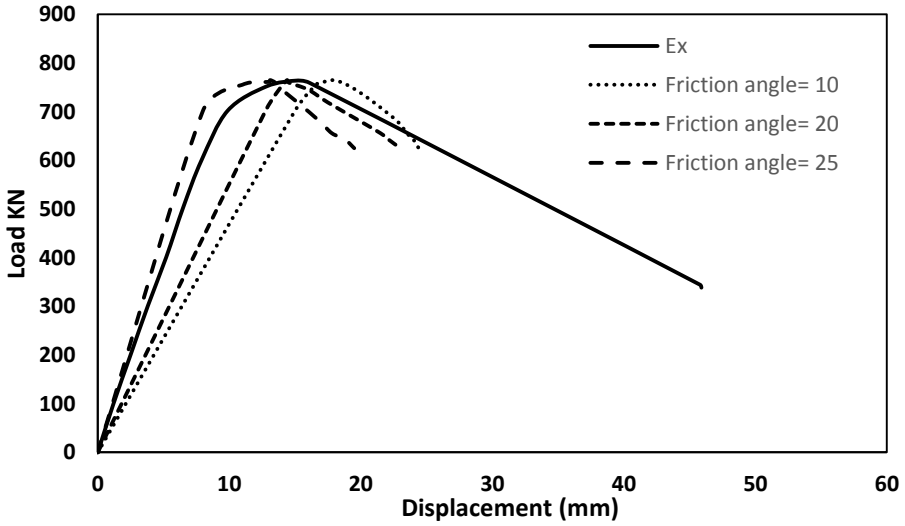

Figure 6.6 Effect of Friction angle on the load-deflection response and comparison with experimental results of CII-150-L-2

6.3.2.2 Flow stress ratio

The ratio of the flow stress in triaxial tension to the flow stress in triaxial compression (K), the value of which must be between 0.778 and 1.0. The default value given in ABAQUS for K is 1.0 which is the value defined for creep behaviour. In this study, 0.8 has been chosen, as no plastic flow was considered, since the confinement effect was directly introduced.

6.3.2.3 Dilation angle

It is defined as a material parameter that controls the plastic strain of concrete. It is also defined as the internal friction angle of concrete or the angle of inclination of the failure surface which evaluates the inclination of the plastic potential under high confining pressure. In order to choose a value for the dilation angle, different values were adopted in ABAQUS: *ψ=20°, ψ=25°* and *ψ=30°.* The selection of the appropriate dilation angle value was based on the load capacity and lateral deflection response. The results were then compared with the experimental results of CII-150-L-2 as shown in Figure 6.7. It can be clearly seen that changing the value of the dilation angle did not have any effect on the load capacity of the columns and lateral deflection.

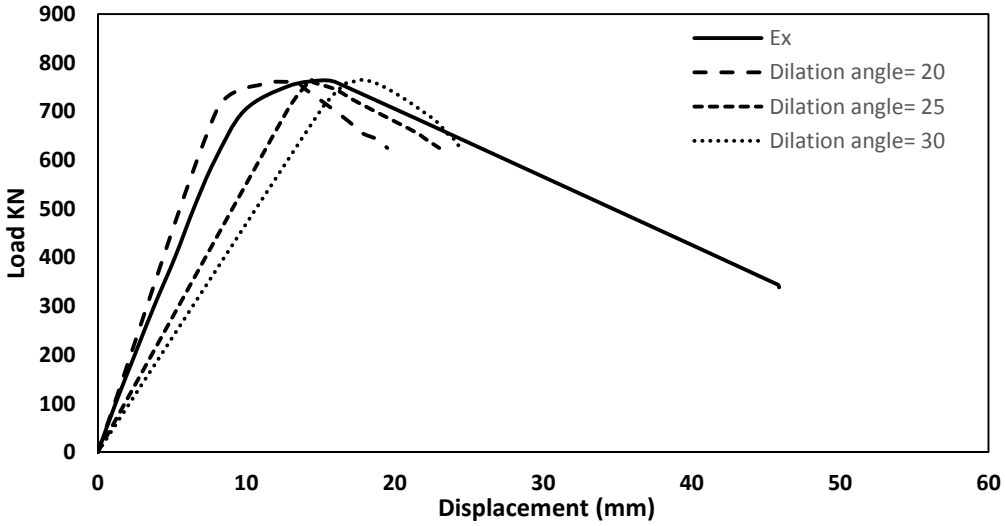

Figure 6.7 Effect of Dilation angle on the load-deflection response and comparison with experimental results of CII-150-L-2

In this study, the values of these variables were selected depending on their prediction accuracy compared to the experimental result and the values

commonly used in previous investigations (Yu et al. 2010; Espinos, 2014; Espinos, 2015). The values assigned to the angle of friction, flow stress and dilation angle were 20°, 0.8 and 25°, respectively. The second part of the D.P model will be explained in the next sub-section.

The elastic-plastic confined concrete properties were considered in three regions by Hu et al. (2003). The uniaxial compressive strength, f_{cc}, and the corresponding strain, ε_{cc}, of concrete subjected to lateral confining pressure were much higher than those of unconfined concrete. Figure 6.8 shows the equivalent uniaxial stress-strain curve.

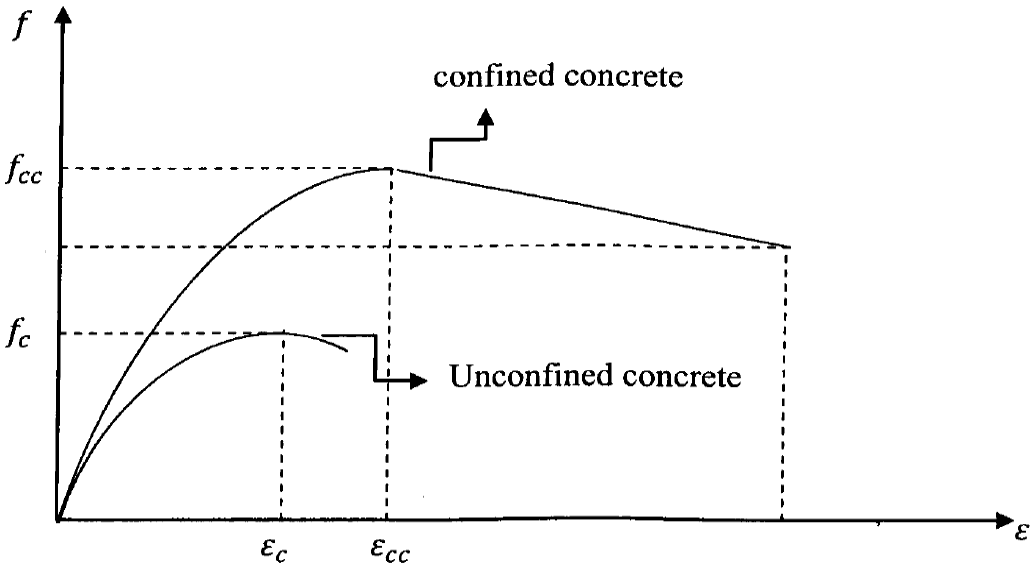

Figure 6.8 The equivalent uniaxial stress-strain curve (Hu et al,2003)

6.3.3 Drucker Prager Hardening

The second part of the D.P. model is D.P. Hardening. The Hardening model requires defining the behaviour of concrete under compression. Specifically, it requires providing the compression stress of concrete as a function of the inelastic strain in a tabular form. The behaviour of concrete under uniaxial

compression is defined by using the stress-strain relationship outside the elastic range. In the proposed model, the stress-strain relationship was defined according to EC2, as shown in Figure 6.9. The relationship between the stress and strain of concrete is assumed to be approximately linear up to about 40 % of the ultimate stress concrete. After this point, the relationship exhibits a steady softening up to the ultimate stress concrete. As compressive strength of concrete is reached, the material stiffness reduces to zero and concrete then exhibits a strain softening up to crushing. Equations (6.1) to (6.3), provided by the EC2, were used to construct the stress-strain relationship of concrete in the current study.

$$\sigma_c = f_c' * \frac{K\eta - \eta^2}{1 + (K-2)\eta} \quad (6.1)$$

$$K = 1.05\, E_c * \varepsilon_{c1}/f_c' \quad (6.2)$$

$$\eta = \varepsilon_c/\varepsilon_{c1} \quad (6.3)$$

where σ_c is the compressive stress of concrete, f_c' is the mean value of concrete cylinder compressive strength, E_c is the elastic modulus of concrete, ε_c is the compressive strain of concrete at any stress σ_c, and ε_{c1} is the strain at peak stress.

It should be noted that these equations can be used for strains from zero up to the ultimate nominal strain ε_{cu1}. The values of ε_{c1} and ε_{cu1} can be obtained from Table 3.1 in the EC2.

After plotting the complete stress-strain relationship, the inelastic strain of concrete ε_c^{in} at any stress, σ_c, can be calculated from equation (6.4) below:

$$\varepsilon_c^{in} = \varepsilon_c - \frac{\sigma_c}{E_c} \quad (6.4)$$

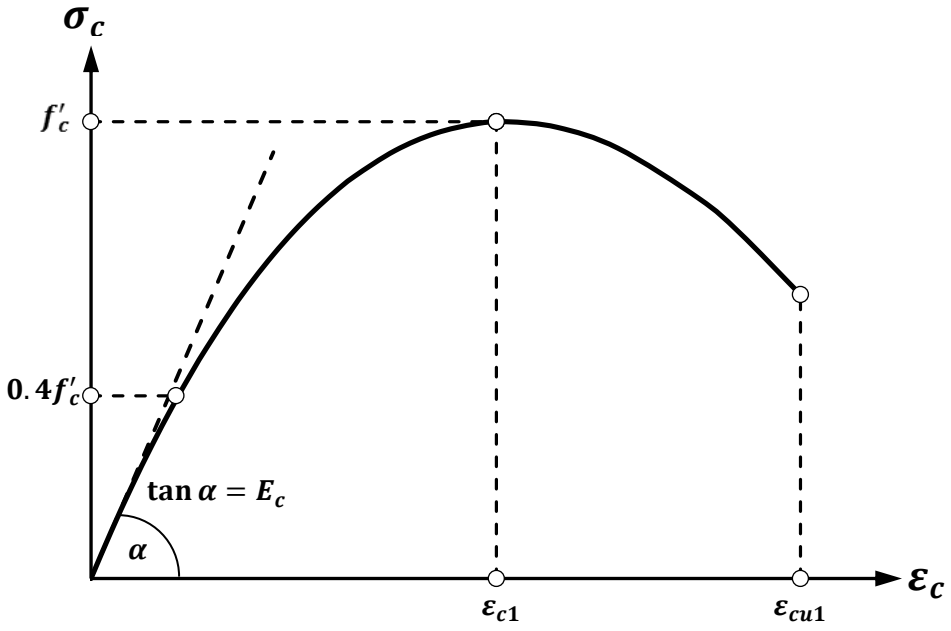

Figure 6.9 Stress-strain relationship of concrete in compression (BS EN 1992-1-1:2004)

6.3.4 Elastic Behaviours

Elastic behaviour of concrete is defined in ABAQUS by two variables, Poisson's ratio (v) and Young's modulus (E_c). In this study, Poisson's ratio was taken to be 0.2, and the value of E_c was obtained from equation (6.5), which is presented elastic modulus of SCC.

$$Ec = 5300\,(f_c')^{0.46} \quad (6.5)$$

where f_c' is the concrete compressive strength of cylinder.

6.4 Validation of FE model

The numerical model was validated by comparing its results with the current experimental results reported in chapter five. The validation include comparing the load capacity, load-axial shortening curve, load lateral displacement curve, and failure modes predicted by proposal model with those collected experimentally.

Table 6.2 shows a comparison between the maximum axial compressive loads of all the specimens, measured in the experiments and those predicted by the proposed FE model. For all columns, the proposed numerical model produced good agreement in term of the axial load capacity estimations. The average ratio of the maximum axial load capacity predicted by FE model to experimental results was found to be 1.01, with a coefficient of variation of 5.41 % and a standard deviation of 5.36%. Only one specimen (CII-250-H-2) exhibited a large variation between the FE model and the test results. The maximum difference in this case was 13 %.

Table 6.2 Comparison of load capacity predicted by ABAQUS and obtained from experiments

Specimen ID	P_{Ex}(KN)	P_{Abaqus} (KN)	$\frac{P_{Ex}}{P_{Abaqus}}$
CI-150-L-1.5	949.8	929.4	1.02
CI-150-H-1.5	1076.4	1076.9	1.00
CII-150-N-2	672.8	665.3	1.01
CII-150-L-2	763.9	764.2	1.00
CII-150-H-2	778.5	772.3	1.00
CII-250-N-2	1392.1	1318	1.05
CII-250-L-2	2023.1	1982.3	1.02
CII-250-H-2	2184.4	2523	0.87
CIII-150-L-2.5	556.0	521.8	1.06
CIII-150-H-2.5	580.5	578.5	1.00
		Average	1.01
		SD (%)	5.41
		COV (%)	5.36

As mentioned earlier, the confined concrete properties were considered in this study. There are many variables that are known to affect the confinement of CFT columns. These include the concrete compressive strength, the shape of the tube cross section and the height of the columns. The compressive cylinder values which were used in the analysis may not represent the true values of the concrete columns due to the size and the different curing environment. All of these factors may cause differences between the numerical predictions and experimental results. Currently, there is no analytical model that is able to take into account all of the variables

such as concrete compressive strength and curing environment. In addition, it is difficult to use FE modelling to analyse columns under large deformation, owing to cracking in the tensile zone of concrete, which has potential to affect the convergence of the solution.

Figure 6.10 shows the global buckling observed experimentally and that predicted by the FE model for the long column CIII-150-H-2.5 under axial compressive load. Generally the deformation predicted by the FE simulation replicated the failure mode observed in the experimental work. In this study, global imperfection was taken into account in the FE model as it was measured in the experiments.

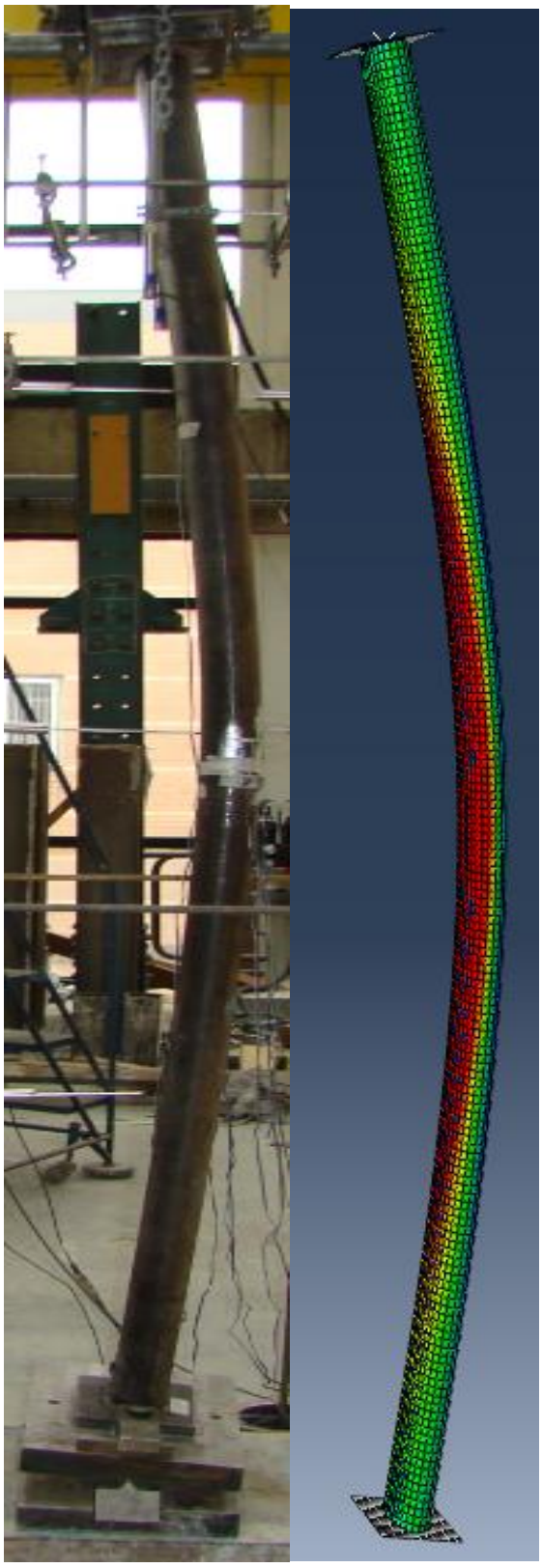

Figure 6.10 the comparison between experimental global buckling of long column and prediction of FE model

Figures 6.11 to 6.14 show comparisons between FE model predictions and experimental results with regard to load capacity, shortening and lateral displacement. Overall, a good agreement is achieved between the test results and those obtained from the numerical model. It can be seen that the FE model is able to accurately predict the load capacity, general load-lateral deformation response, and buckling failure mode observed in the experiment. From these Figures, it is also evident that the increases in infill concrete strength enhanced the load capacity of CFT columns. However, as the columns' slenderness increases, the load-carrying capacity drops significantly. It is also clear that the proposed FE model is able to show the post behaviour once the ultimate load was reached. Following comparisons between the numerical simulations and experimental results, the FE model is deemed to be acceptable as it was able to capture the ultimate load capacity, general load-deformation response and failure pattern as observed in the tests. The interaction between the hollow tube and the confined concrete core has been successfully established by adopting the concrete stress-strain model from Euro code (BS EN 1992-1-1:2004) (Han et al., 2007). For the particular columns examined here, the anticipated sensitivity to imperfections was reflected in the numerical results. The average value of out-of-straightness (approximately L/2000) not only provides the best agreement of results between the FE and the physical tests, but it is also within the specified tolerance of the measured imperfection.

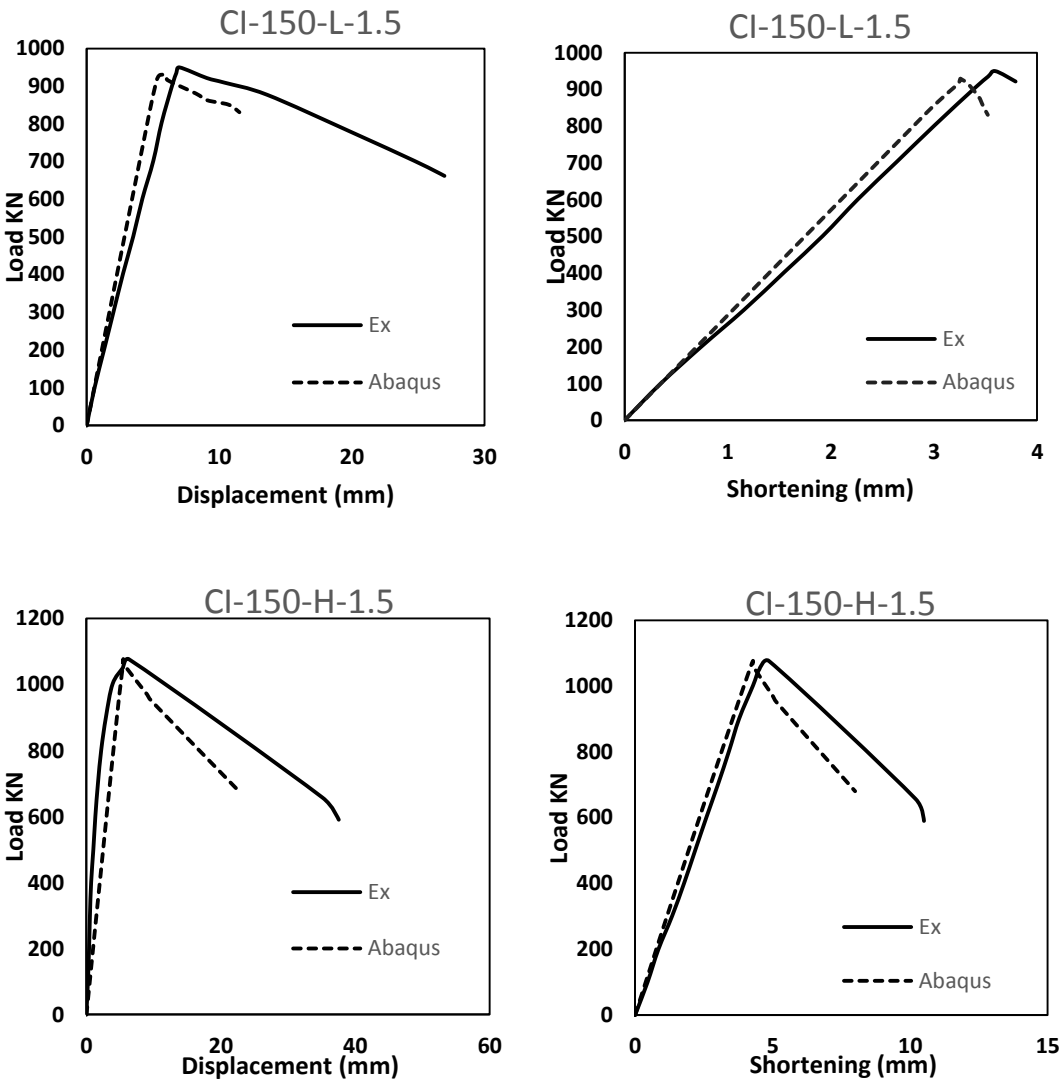

Figure 6.11 Comparisons between FE model and experimental data of column section 150x75x6.3 mm and length 1.5 m

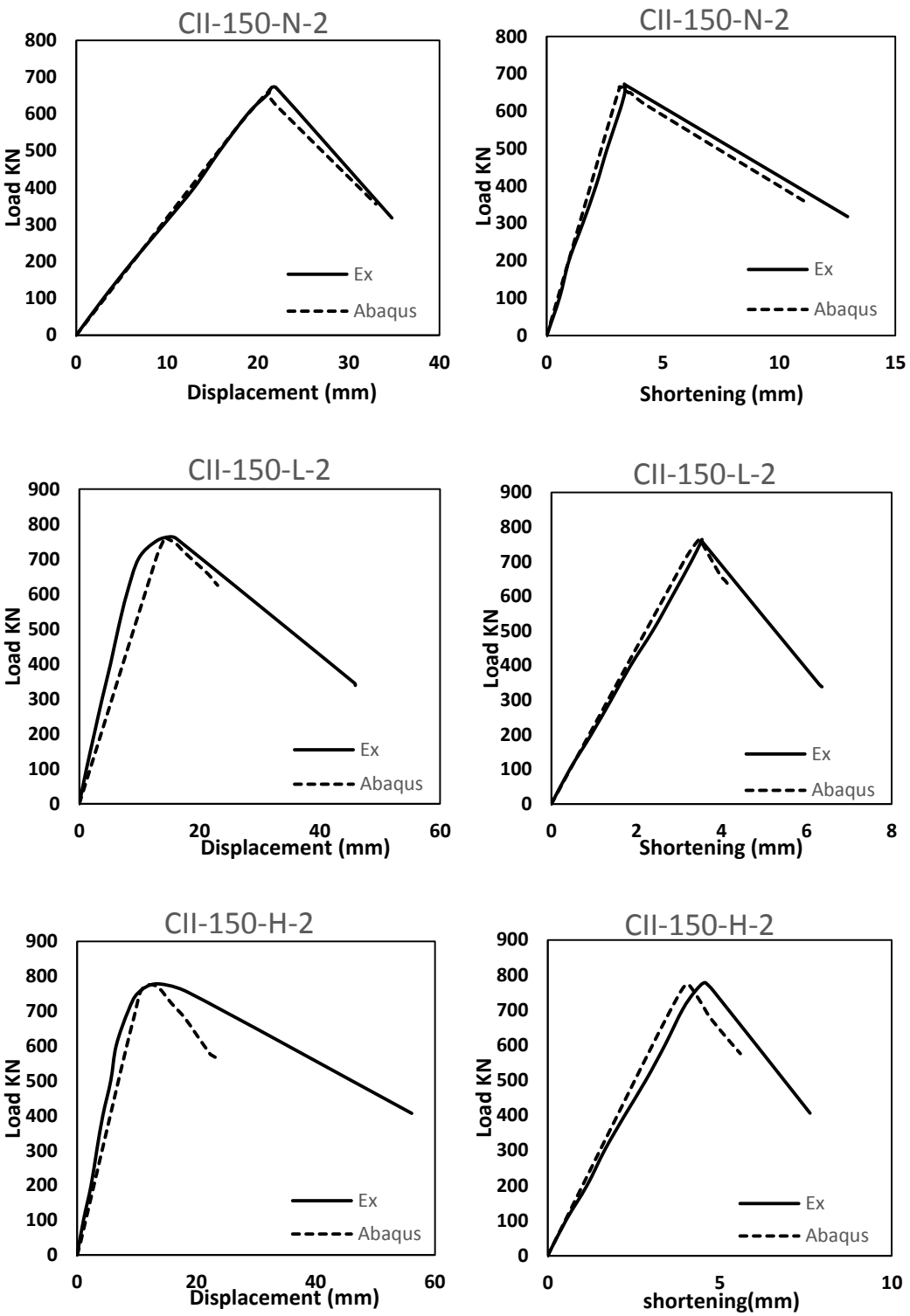

Figure 6.12 Comparisons between FE model and experimental data of column section 150x75x6.3 mm and length 2 m

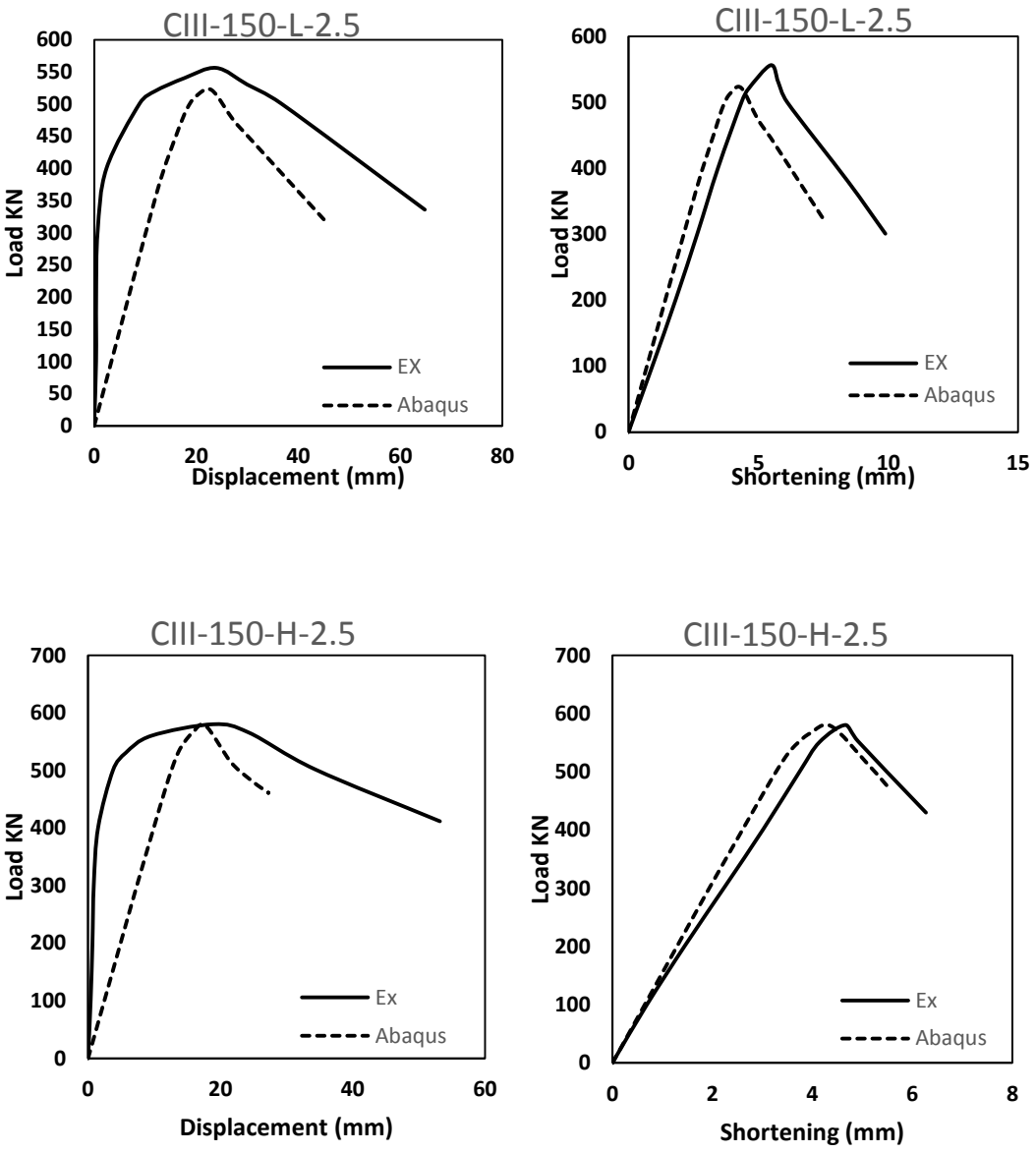

Figure 6.13 Comparisons between FE model and experimental data of column section 150x75x6.3 mm and length 2.5 m

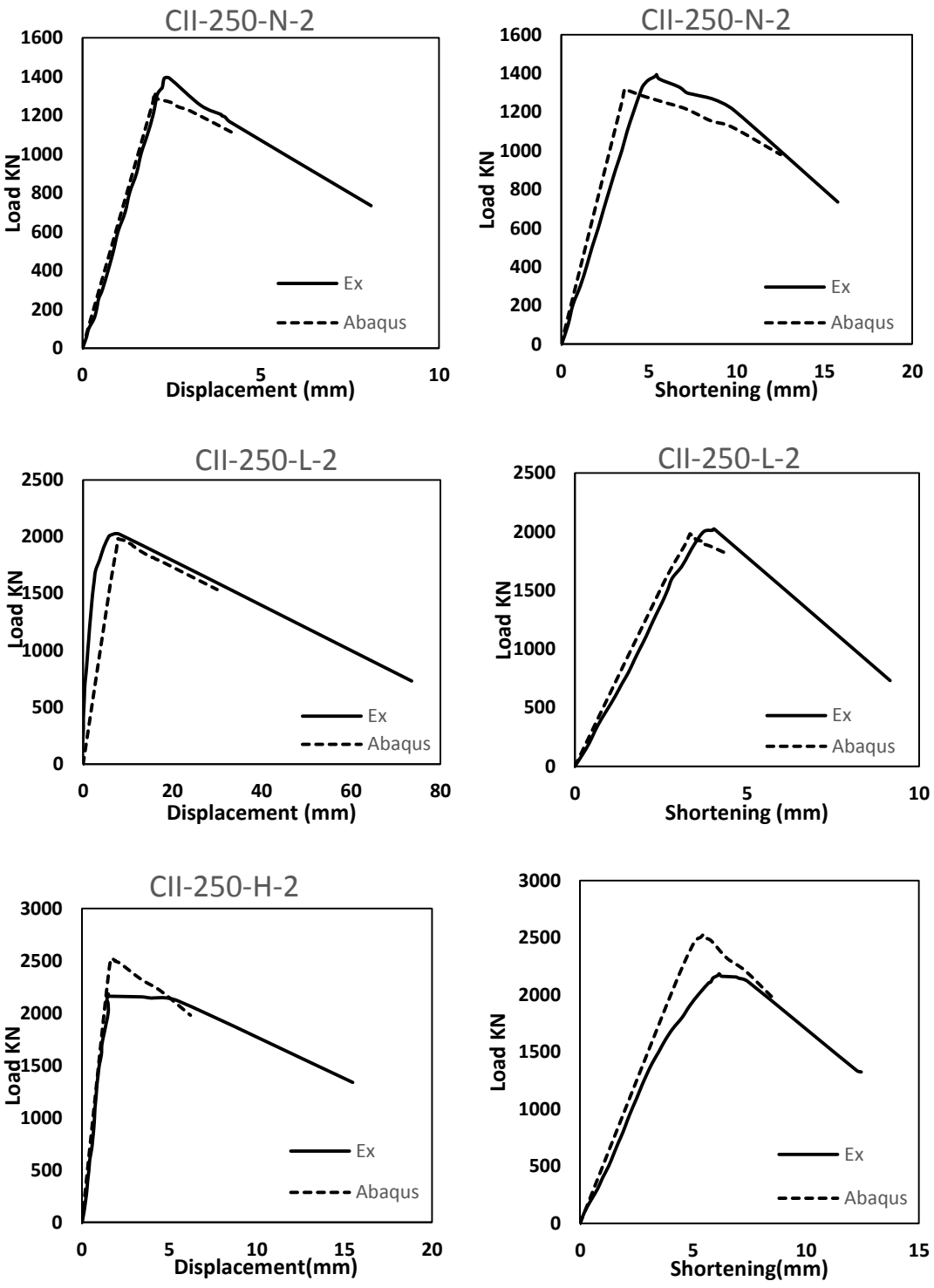

Figure 6.14 Comparisons between FE model and experimental data of column section 250x125x6.3 mm and length 2 m

6.5 Validation against experimental results from literature

In this section, the proposed model is validated against experimental results collected from the literature. The proposed model was used to predict the failure loads of six elliptical tube columns filled with concrete and the results were then compared to the experimental ones. All of these columns were tested by Jamuldine (2011). The details of these columns are given in Table 6.3. All of the selected columns failed under global buckling, similar to the experimental elliptical columns tested in the current study.

Comparisons between the failure loads predicted by the proposed model and experimental results of Jamuldine (2011) are presented in Table 6.3. The failure loads predicted by the current model are very similar to those obtained from the selected studies, achieving a mean of 1.02 and a coefficient of variation of 5.1%. For all specimens, the predictions are reasonable conservative as the load capacities predicted by the model were lower than the load capacities obtained from experimental tests. Figure 6.15 shows a comparison between the load-deflection response predicted by the proposed model and that obtained experimentally for column CII-150-C58 tested by Jamuldine (2011). It is clearly seen that the load-deflection curve predicted by the current model is very similar behaviour to that obtained from the selected studies. In general, the predictions of the proposed ABAQUS model were fairly close to those measured during the experiments.

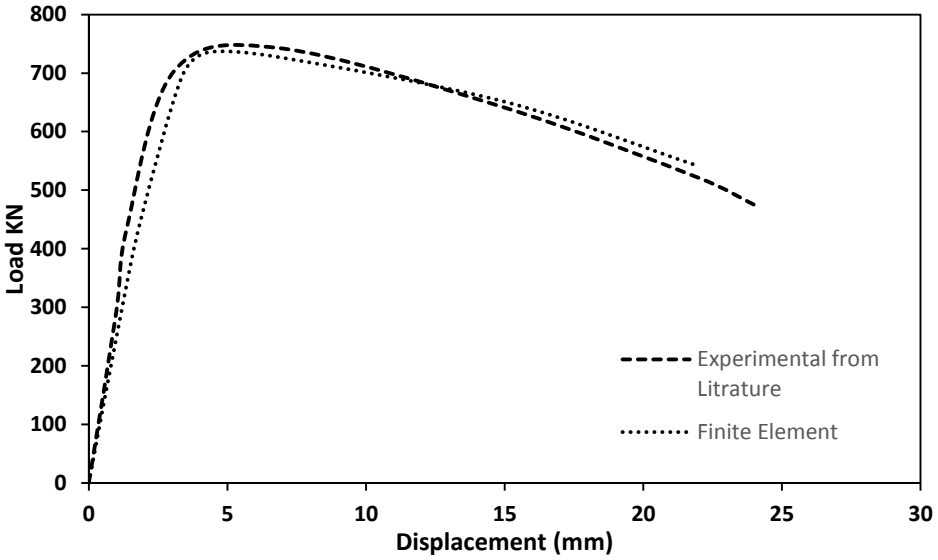

Figure 6.15 Validation of the propose model against previous experimental results (Jamuldine, 2011)

Table 6.3 Details of Elliptical columns collected from literature and analysed by the finite elements model

Columns section	f_{cu} (Mpa)	t (mm)	L (m)	$P_{u\ (KN)}$	$P_{FE\ (KN)}$	$\frac{P_u}{P_{FE}}$
CII150-C58	58	4.2	1.5	742.8	735.7	1.01
CII200-C55	55	5.1	1.5	1064	1056.8	1.01
CIII150C65	65	4.2	1.78	663.2	656.8	1.00
CIII200C63	63	5.1	1.78	1237	1239.2	0.99
CIV150C100	100	4.1	2.5	547.4	519.5	1.05
CIV200C101	101	5.1	2.5	1072	1041.1	1.03
					Average	1.02
					COV (%)	5.1

6.6 Parametric study

There are many factors that might affect the axial compressive behaviour of a slender CFT column. These factors include the member's non-dimensional slenderness, material properties, sectional shape and dimensions and height. In the previous sections, the efficiency of the proposed FE model was validated through comparisons with experimental results obtained from the current research investigation, as well as some examples selected from previous studies. The model was found to be able to accurately predict the load capacity, lateral deflection, shortening and the failure mode, as observed in the experiments. Parametric studies were performed using the measured material properties and geometries to assess the axial compressive behaviour of slender elliptical CFT columns. Physical experiments might be the most reliable research method, but they are expensive, time-consuming and sometimes practically impossible to test in the lab. Therefore, in this case, finite element modelling is more affordable. Numerical analysis allows a study to adopt a virtual combination of the parameters of interest. It is well known that the compressive strength of elliptical CFT columns depends on a number of factors, such as the cross-section dimensions, length of the column, and its constituent material properties. These parameters can easily be included in a parametric study to investigate the influence of these parameters on the failure load of elliptical CFT columns.

To extend the specimen range, a group of elliptical CFT columns with various slenderness ratios (L/D), different thicknesses and concrete

strengths range between 30 and 90 MPa were selected to be used for investigating the buckling behaviour. A total of 54 column specimens were analysed in the parametric study. The studies covered two tube section sizes, three different thicknesses and various column lengths up to 4 m. A global imperfection of L/2000 was assumed for all columns due to their high slenderness. Table 6.4 shows group one for columns having a section size of 200x100 mm while Table 6.5 shows group two for columns having a section size of 300x150mm.

The results of the parametric study are presented and discussed in this section. Due to the similarity in the relationship between the load capacity and the investigated parameters, only sample Figures are presented in this chapter to show the effects of these parameters on the load carrying capacity of elliptical CFT columns.

Table 6. 4 Parametric studies group one

Specimens	sections	F_{cu} (MPa)	Thickness (mm)	Height (mm)	P (KN)
s1	200x100	30	4	3000	875
s2			6		1170
s3			8		1310
s4		60	4		945
s5			6		1332
s6			8		1485
s7		90	4		1182
s8			6		1519
s9			8		1712
s10	200x100	30	4	3500	784
s11			6		1132
s12			8		1284
s13		60	4		848
s14			6		1192
s15			8		1402
s16		90	4		1064
s17			6		1375
s18			8		1592
s19	200x100	30	4	4000	701
s20			6		946
s21			8		1127
s22		60	4		768
s23			6		1089
s24			8		1224
s25		90	4		978
s26			6		1301
s27			8		1393

Table 6.5 Parametric study group two

Specimens	sections	F_{cu} (MPa)	Thickness (mm)	Height (mm)	P (KN)
s28	300x150	30	4	3000	1352
s29			6		1590
s30			8		1772
s31		60	4		1568
s32			6		1847
s33			8		2012
s34		90	4		1860
s35			6		2023
s36			8		2189
s37	300x150	30	4	3500	1213
s38			6		1534
s39			8		1737
s40		60	4		1453
s41			6		1772
s42			8		1881
s43		90	4		1739
s44			6		1871
s45			8		2041
s46	300x150	30	4	4000	788
s47			6		1086
s48			8		1297
s49		60	4		901
s50			6		1239
s51			8		1470
s52		90	4		1138
s53			6		1339
s54			8		1602

6.6.1 Effect of column slenderness

It is well known that the slenderness plays an important role in the buckling resistance of columns subjected to axial compression. In order to illustrate the effect of the column slenderness on the load capacity of elliptical CFT columns, a set of columns having cross sectional dimensions of 200x100 mm and 300x150 mm with a thickness of 4, 6 and 8 mm were chosen. The influence of the relative slenderness was investigated by varying the column length from 3 to 4 m with initial imperfection L/2000.

As expected, from Tables 6.5, 6.6, the load capacity of elliptical CFT columns decreased with an increase in relative slenderness. Moreover, the load capacity of group two are higher than those in group one, since the larger the cross section of the column, the greater the effect of the concrete filling in delaying the buckling. Figures 6.16 and 6.17 show the relation between slenderness ratio L/r and load capacity of section (200X100) and (300X150) with three different thicknesses and different concrete strength grades. From the tables and Figures, it can be concluded that the columns' load capacity decreases with the slenderness ratio increase.

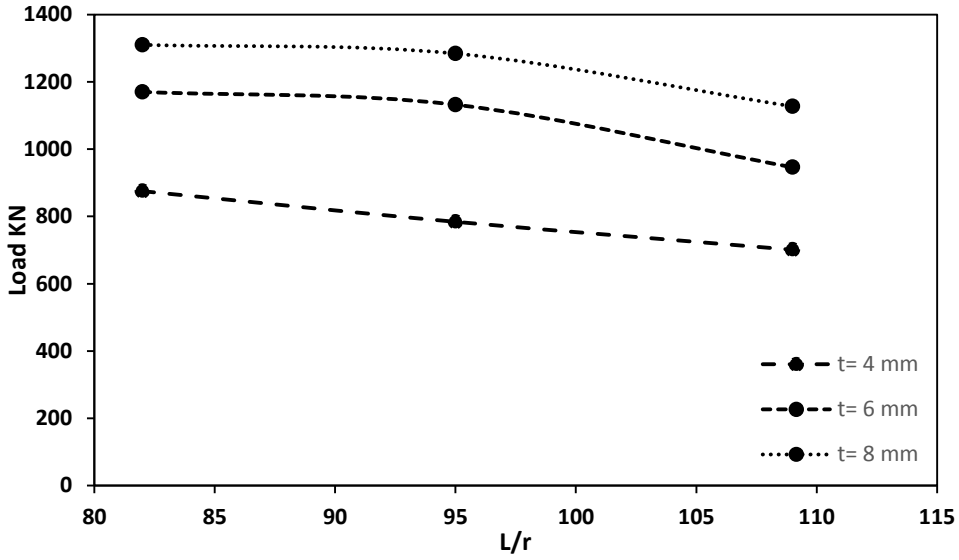

(a) $f_{cu} = 30$ MPa

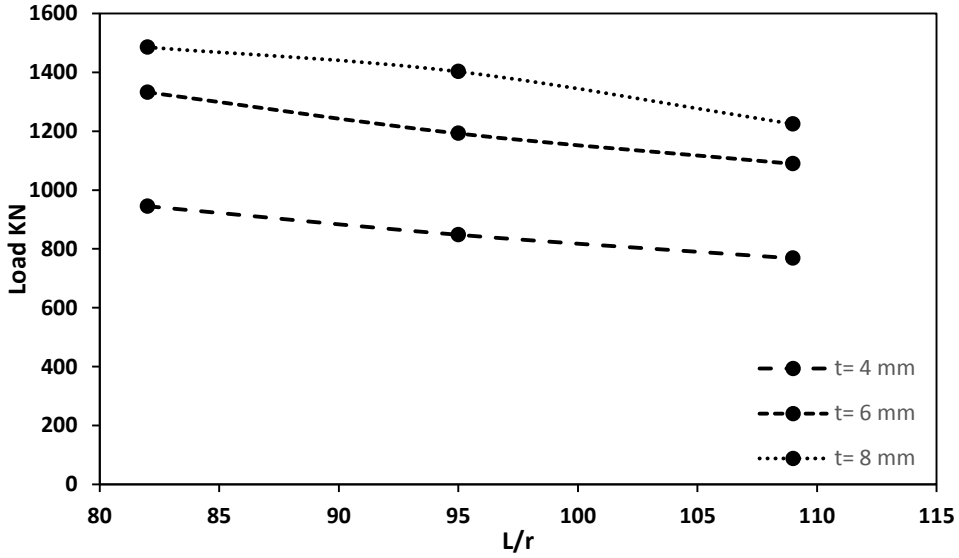

(b) $f_{cu} = 60$ MPa

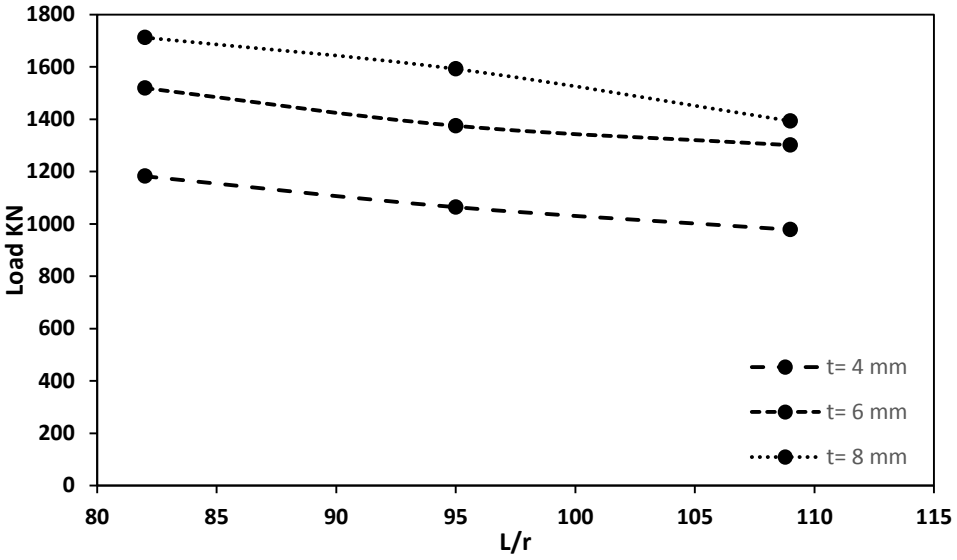

(c) f_{cu} = 90 MPa

Figure 6.16 Slenderness ratio vs load capacity of section 200x100

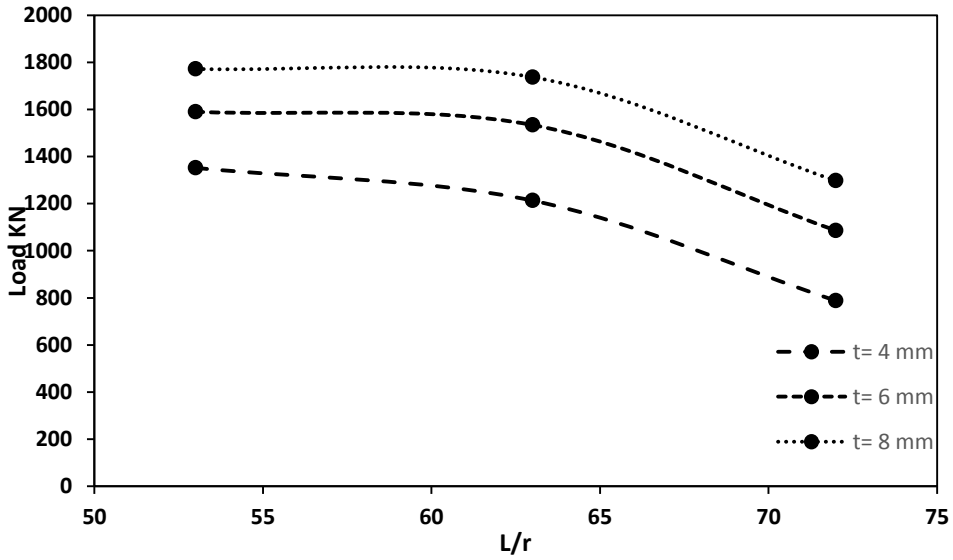

(a) f_{cu} = 30 MPa

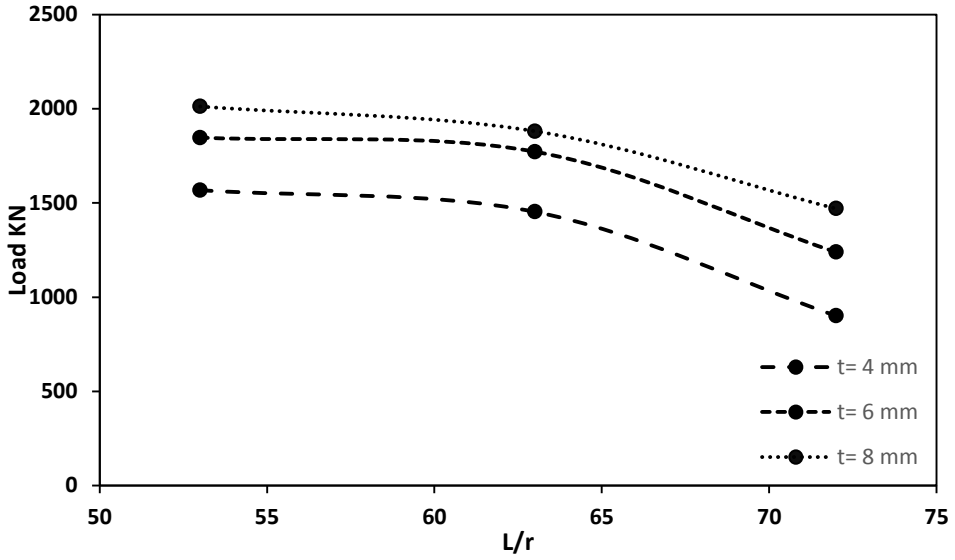

(b) $f_{cu} = 60$ MPa

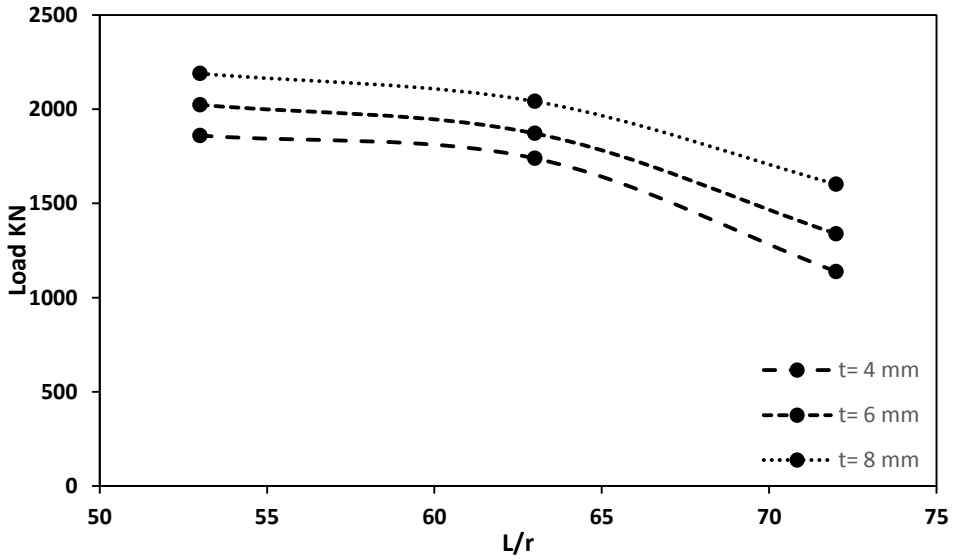

(c) $f_{cu} = 90$ MPa

Figure 6.17 Slenderness ratio vs load capacity of section 300x150

Figure 6.18 shows a comparison between sections (200X100) and (300X150) with different thicknesses and different concrete strength grade

for columns having a length of 3.5 m. From the Figures, it can be concluded that the columns' load capacity increase with increase the cross sections area of tube columns.

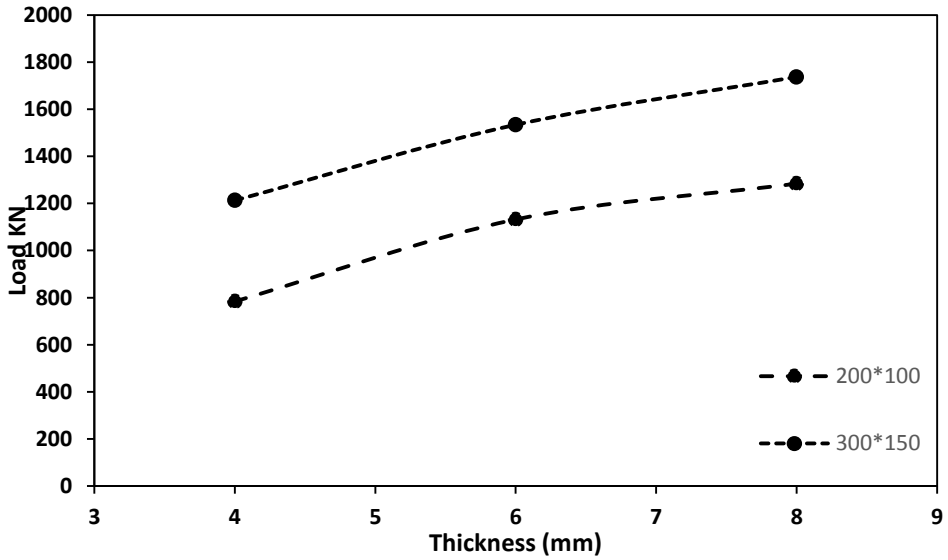

(a) $f_{cu} = 30$ MPa

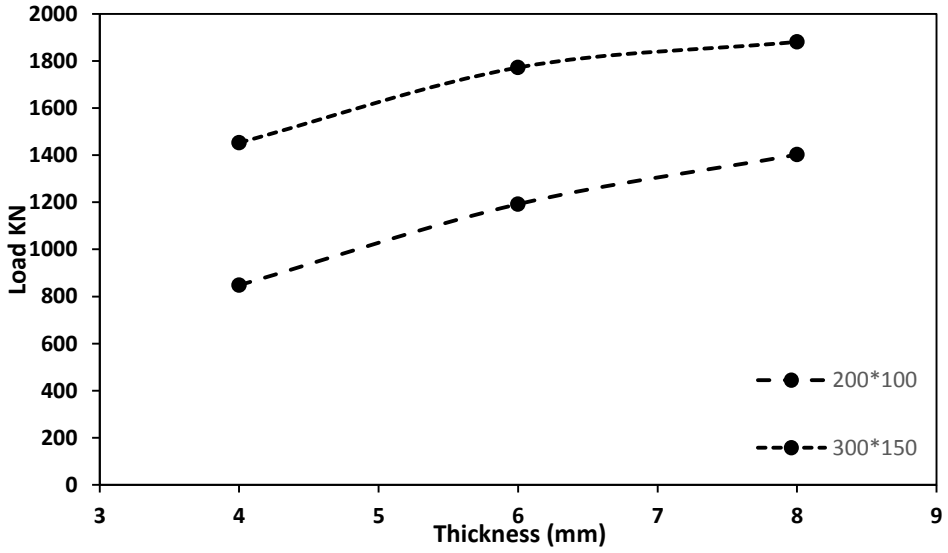

(b) $f_{cu} = 60$ MPa

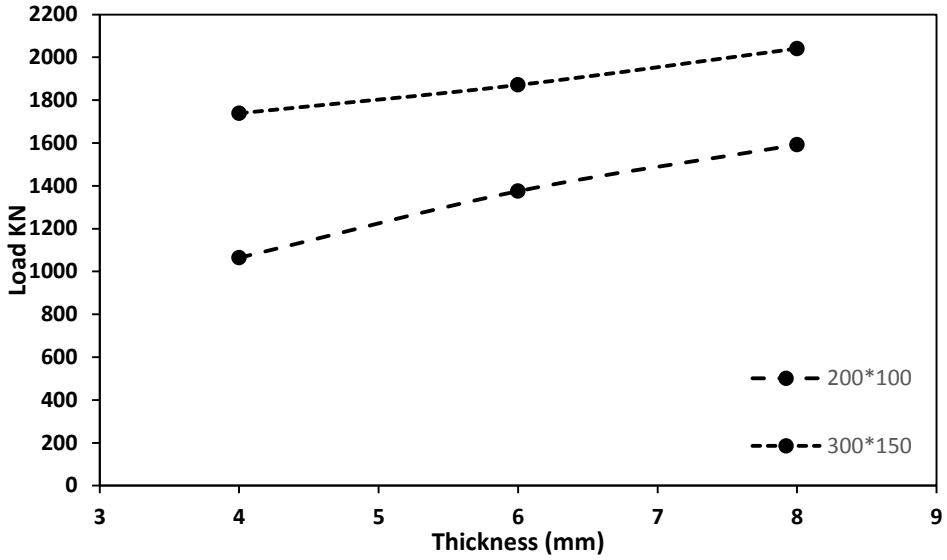

(c) $f_{cu} = 90$ MPa

Figure 6. 18 Cross section area vs load capacity with length 3.5 m

6.6.2 Effect of concrete compressive strength

Concrete compressive strength is one of the most important factors that control the load carrying capacity of elliptical tube columns. In this study, three different concrete compressive strength values were selected: 30, 60 and 90 MPa to represent normal and high strength concrete and cover the range of the concrete strengths used in the experimental investigation. The effect of compressive strength was evaluated for different cross sections, different thicknesses and different height of the columns.

Tables 6.5 and 6.6 show the effects of compressive strength of concrete on the load carrying capacity of elliptical tube columns filled with SCC with some variation in the other selected parameters.For all the considered compressive strength values, increasing the compressive strength of

concrete led to similar behaviour in all columns, irrespective of the values of other parameters. It was observed that increasing the compressive strength leads to a gradual increase in the load carrying capacity as predicted by the proposed ABAQUS model. Similar observations were found by Jamuldine (2011). Figure 6.19 shows the relationship between the failure load of the columns cross section (200x100x4) mm and concrete cylinder strength obtained from the parametric study. From the table and Figure, it can be concluded that the columns' load capacity increases with the concrete compressive strength.

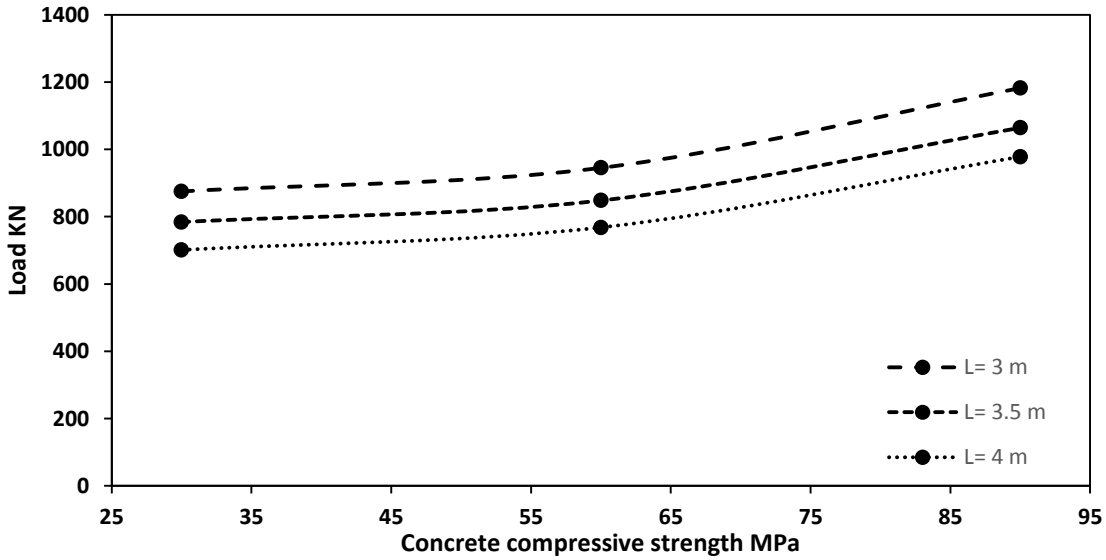

Figure 6.19 Relationship between load failure and concrete strength

6.7 Conclusions

This chapter described a non-linear FE model that was developed through the ABAQUS/Standard solver to investigate the axial compressive behaviour of slender elliptical CFT columns. After the numerical method was verified by comparing the predicted results against the experimental observations, an extensive parametric study was conducted and presented. Based on the comparison and analyses, the following conclusions can be made:

- The simulation methodology is appropriate. This includes the ABAQUS element types used to simulate the different parts of the connection (R3D4 type for rigid plates and C3D8R for steel tubes and concrete core).
- A mesh size sensitivity was conducted to determine the most suitable finite element mesh size and close results to experimental obtained with mesh size 14 mm.
- Drucker Prager concrete model was implemented and the model showed good agreement with experimental results in adequate time of running without convergent problems.
- The FE numerical method developed via the ABAQUS/Standard solver, combined with the Euro code stress–strain model for confined concrete in slender elliptical hollow sections, could be used to predict the axial compressive behaviour of slender elliptical CFT columns.
- The comparison between the finite element results and the experimental results for the columns with different concrete strengths

and different geometric dimensions showed good agreement. Moreover, FE model had good agreement with specimens from literature.

- Both experimental and numerical modelling results demonstrated that the failure mode of a slender CFT column under axial loads was global buckling with the first buckling mode shape.
- Parametric studies were performed to investigate the load capacity response of elliptical CFT columns with different aspect ratios and of varying slenderness. Increasing the compressive strength, cross section and thickness resulted in a gradual increase in the load capacity. However, increasing the height led to a decrease in the load capacity of the columns.

CHAPTER SEVEN

CONCLUSIONS AND RECOMMENDATIONS FOR FUTURE WORK

7.1 Summary

The behaviour of elliptical tube columns filled with self-compacting concrete were investigated in this thesis. The research consisted of three phases: an experimental investigation; evaluation of predictability of the design code (EC4) method against the experimental results of this research; and the development of a numerical modelling program (ABAQUS).

The experimental phase contained the casting and testing of eight elliptical tube columns filled with SCC. In addition, two control elliptical hollow tube section columns were tested. The compressive strength of SCC was predicted by using artificial neural network model (ANN). A comprehensive database has been collected from different sources in the literature and used to train and test the developed ANN then the predictive compressive strength of SCC was used for filling elliptical tube columns.

All columns were tested in a vertical position subjected to axial compression load up until failure. The different section size, length and concrete compressive strength were the main parameters investigated in this study.

The theoretical phase was to assess the adaptability of current design rules provided in Eurocode 4 for circular and rectangular columns. The performance of EC4 was validated against the results obtained from the experimental phase in this project.

The last part of the research included the numerical simulation. As the EC4 can only predict the failure load, a numerical approach is needed to predict the full behaviour of elliptical tube columns filled with SCC. A three dimensional nonlinear finite element model was proposed using ABAQUS 6.12 package. The proposed model was validated against the experimental results of this research, and some examples collected from previous studies as well.

This chapter presents a summary of the main conclusions from this study and recommends a number of further studies.

7.2 Conclusions

The principal findings drawn from the current investigation can be summarised below:

- ANN has been used to predict the compressive strength of SCC using data from different studies, and the experimental results were about 5% higher than prediction results. Different parametric studies have been performed, and the results were reasonable, as expected graphs were obtained. The ANN was more accurate when trained with increasing amount of input data.
- The axial compressive load capacity of composite columns increases with an increase in SCC compressive strength, and reduces with increased slenderness ratio.
- The confinement that steel hollow sections provide to concrete core enhanced the axial compressive capacity of composite columns by

delaying the occurrence of global buckling and eliminating tube wall local buckling.

- The EC4 method displays reliable results as the confinement effect was considered. The European buckling curves for steel columns can therefore be considered as the basis of elliptical CFT column design as was also found by other investigations with different elliptical tube columns section and length.
- The FE numerical method developed via the ABAQUS/Standard solver, combined with the Euro code stress–strain model for confined concrete in slender elliptical hollow sections, could be used to predict the axial compressive behaviour of slender elliptical CFT columns.
- The comparison between the finite element results and experimental results for the columns with different concrete strengths and different geometric dimensions showed good agreement. Moreover, the FE model showed good agreement with specimens from literature.
- Experimental and numerical modelling results demonstrated that the failure mode of a slender CFT column under axial loads was global buckling with the first buckling mode shape due to the larger slenderness ratio adopted.

Overall, although some previous studies showed that columns filled with SCC are similar to those filled with traditional concrete in terms of the load capacity, other studies indicated that the load capacity of tube columns filled with NC can be higher than those filled with SCC if NC has a perfect compaction and no segregation appeared. In contrast, it is impossible to

achieve perfect compaction in columns due to their small sections compared to its height, making it difficult for NC to properly be placed and vibrated. On the other hand, SCC requires no vibration, and therefore, it is easier to construct columns with SCC.

7.3 Recommendation for future work

- More experimental data are needed for concrete-filled tubular columns with a relative slenderness ($\bar{\lambda}$) of higher than 1.5 and a height ranging between 3.0- 4.0 m, which represent a typical storey height in multi-storey buildings. The experiment concerning on the effect of global buckling behaviour and the effects of the width-to-thickness ratio on the confinement behaviour should also be carried out.
- Since this thesis focused on columns loaded in axial compression, the study of eccentrically loaded columns is suggested for future work, because columns is likely to carry eccentric loading, leading to bending moment and, consequently, reducing the load capacity of columns.
- It is important to evaluate the seismic performance of full scale moment resistance frames using CFT columns. To achieve this purpose, efficient and accurate global models should be developed. Therefore, it is essential to establish a realistic hysteresis model for CFT columns and important features of hysteresis response such as primary curve (i.e., stiffness, strength, toughness/ductility, and

hardening), stiffness degradation, and strength decay needs to be evaluated.

- An analytical study such as a moment curvature method to simulate the behaviour of elliptical tube columns filled with concrete with dedicated cross sections are needed.

REFERENCES

Adeli, H. (2001) Neural networks in civil engineering: 1989–2000. Computer-Aided Civil and Infrastructure Engineering 16 (2), 126-142.

Aggarwal, Y. and Aggarwal, P. (2011) Prediction of Compressive Strength of SCC Containing Bottom Ash using Artificial Neural Networks. World Academy of Science, Engineering and Technology 53, 735-740.

Ahmadi, M., Alidoust, O., Sadrinejad, I. and Nayeri, M. (2007) Development of mechanical properties of self compacting concrete contain rice husk ash. International Journal of Computer, Information, and Systems Science, and Engineering 1 (4), 259-262.

Ahmed, S. A. (2013) Properties and mesostructural characteristics of linen fiber reinforced self-compacting concrete in slender columns. Ain Shams Engineering Journal 4 (2), 155-161.

Alatshan, F. and Mashiri, F. R. (2013) Finite Element Modeling of Concrete-Filled Steel Tubes: Review and Recent Developments. Applied Mechanics and Materials. Vol. 330. Trans Tech Publ.

Almeida Filho, F., Barragán, B. E., Casas, J. and El Debs, A. L. H. (2010) Hardened properties of self-compacting concrete—a statistical approach. Construction and Building Materials 24 (9), 1608-1615.

Aoude, H., Cook, W. D. and Mitchell, D. (2009) Behavior of columns constructed with fibers and self-consolidating concrete. ACI Structural Journal 106 (3), 349.

Assaad, J. and Khayat, K. H. (2005) Effect of coarse aggregate characteristics on lateral pressure exerted by self-consolidating concrete. ACI materials journal 102 (3), 145.

Assie, S., Escadeillas, G. and Waller, V. (2007) Estimates of self-compacting concrete 'potential'durability. Construction and Building Materials 21 (10), 1909-1917.

Bai, J., Wild, S., Ware, J. and Sabir, B. (2003) Using neural networks to predict workability of concrete incorporating metakaolin and fly ash. Advances in Engineering Software 34 (11), 663-669.

Bal, L. and Buyle-Bodin, F. (2013) Artificial neural network for predicting drying shrinkage of concrete. Construction and Building Materials 38, 248-254.

Bartos, P. J. and Yu, Z. (2005) Testing-SCC: towards new European standards for fresh SCC. Proceedings of the First International Symposium on Design, Performance and Use of Self-Consolidating Concrete, Changsha, Hunan, Kina.

Basma, A. A., Barakat, S. and Al-Oraimi, S. (1999) Prediction of cement degree of hydration using artificial neural networks. Materials Journal 96 (2), 167-172.

Bignozzi, M. and Sandrolini, F. (2006) Tyre rubber waste recycling in self-compacting concrete. Cement and concrete research 36 (4), 735-739.

Billberg, P. (1999) Self-compacting concrete for civil engineering structures: The Swedish experience. Swedish Cement and Concrete Research Institute.

Bonen, D. and Sarkar, S. L. (1995) The superplasticizer adsorption capacity of cement pastes, pore solution composition, and parameters affecting flow loss. Cement and Concrete Research 25 (7), 1423-1434.

Bonen, D. and Shah, S. P. (2005) Fresh and hardened properties of self-consolidating concrete. Progress in Structural Engineering and Materials 7 (1), 14-26.

Boukendakdji, O., Kenai, S., Kadri, E. and Rouis, F. (2009) Effect of slag on the rheology of fresh self-compacted concrete. Construction and Building Materials 23 (7), 2593-2598.

Bouzoubaa, N. and Lachemi, M. (2001) Self-compacting concrete incorporating high volumes of class F fly ash: Preliminary results. Cement and Concrete Research 31 (3), 413-420.

Campione, G. and Fossetti, M. (2007) Compressive behaviour of concrete elliptical columns confined by single hoops. Engineering structures 29 (3), 408-417.

Chan, T. and Gardner, L. (2008a) Bending strength of hot-rolled elliptical hollow sections. Journal of Constructional Steel Research 64 (9), 971-986.

Chan, T. and Gardner, L. (2008b) Compressive resistance of hot-rolled elliptical hollow sections. Engineering Structures 30 (2), 522-532.

Chan, T. and Gardner, L. (2009) Flexural buckling of elliptical hollow section columns. Journal of structural engineering 135 (5), 546-557.

Chandwani, V., Agrawal, V. and Nagar, R. (2014) Applications of Artificial Neural Networks in Modeling Compressive Strength of Concrete: A State of the Art Review. International Journal of Current Engineering and Technology 4 (4), 2949-2956.

Code, E. (2004) 2, Design of concrete structures-Part 1-1: General rules and rules for buildings, BS EN 1992-1-1: 2004. British Standards (BSi).

Collepardi, M. (1998) Admixtures used to enhance placing characteristics of concrete. Cement and concrete composites 20 (2), 103-112.

Collepardi, M., Borsoi, A., Collepardi, S., Olagot, J. J. O. and Troli, R. (2005) Effects of shrinkage reducing admixture in shrinkage compensating concrete under non-wet curing conditions. Cement and Concrete Composites 27 (6), 704-708.

Concrete, S.-C. (2005) The European Guidelines for Self-Compacting Concrete.

Dai, X. and Lam, D. (2010) Numerical modelling of the axial compressive behaviour of short concrete-filled elliptical steel columns. Journal of Constructional Steel Research 66 (7), 931-942.

Dai, X., Lam, D., Jamaluddin, N. and Ye, J. (2014) Numerical analysis of slender elliptical concrete filled columns under axial compression. Thin-Walled Structures 77, 26-35.

Dayhoff, J. E. and DeLeo, J. M. (2001) Artificial neural networks. Cancer 91 (S8), 1615-1635.

De Nardin, S. and El Debs, A. (2007) Axial load behaviour of concrete-filled steel tubular columns. Proceedings of the Institution of Civil Engineers-Structures and Buildings 160 (1), 13-22.

Dehn, F., Holschemacher, K. and Weiße, D. (2000) Self-compacting concrete (SCC) time development of the material properties and the bond behaviour. Selbstverdichtendem Beton.

Ding, Y., You, Z. and Jalali, S. (2011) The composite effect of steel fibres and stirrups on the shear behaviour of beams using self-consolidating concrete. Engineering Structures 33 (1), 107-117.

Domone, P. (2007) A review of the hardened mechanical properties of self-compacting concrete. Cement and Concrete Composites 29 (1), 1-12.

Domone, P. and Illston, J. (2010) Construction materials: their nature and behaviour. CRC Press.

Ellobody, E. and Young, B. (2006) Nonlinear analysis of concrete-filled steel SHS and RHS columns. Thin-walled structures 44 (8), 919-930.

Ellobody, E., Young, B. and Lam, D. (2006) Behaviour of normal and high strength concrete-filled compact steel tube circular stub columns. Journal of Constructional Steel Research 62 (7), 706-715.

Emborg, M. and Hedin, C. (1999) Production of self-compacting concrete for civil engineering: Case studies. International RILEM symposium on self-compacting concrete.

Eramma. H, B.R. Niranjan. (2012). Experimental behaviour of Self Compacting Concrete Filled Steel Rectangular Fluted Columns for Concentric Load. *IOSR* Journal of Mechanical and Civil Engineering (IOSR-JMCE), 3**,** 41-49.

Felekoğlu, B. and Sarıkahya, H. (2008) Effect of chemical structure of polycarboxylate-based superplasticizers on workability retention of self-compacting concrete. Construction and Building Materials 22 (9), 1972-1980.

Felekoğlu, B., Türkel, S. and Baradan, B. (2007) Effect of water/cement ratio on the fresh and hardened properties of self-compacting concrete. Building and Environment 42 (4), 1795-1802.

Felekoğlu, B., Türkel, S. and Baradan, B. (2007) Effect of water/cement ratio on the fresh and hardened properties of self-compacting concrete. Building and Environment 42 (4), 1795-1802.

Flood, I. and Kartam, N. (1994) Neural networks in civil engineering. I: Principles and understanding. Journal of computing in civil engineering 8 (2), 131-148.

Fujimoto, T., Mukai, A., Nishiyama, I. and Sakino, K. (2004) Behavior of eccentrically loaded concrete-filled steel tubular columns. Journal of Structural Engineering 130 (2), 203-212.

Galano, L. and Vignoli, A. (2008) Strength and ductility of HSC and SCC slender columns subjected to short-term eccentric load. ACI Structural Journal 105 (3), 259.

Gardner, L. and Chan, T. (2006) Cross-section classification of elliptical hollow sections. TUBULAR STRUCTURES-INTERNATIONAL SYMPOSIUM-. Vol. 11.

Gardner, L., Chan, T. and Abela, J. (2011) Structural behaviour of elliptical hollow sections under combined compression and uniaxial bending. Advanced Steel Construction 7 (1), 86-113.

Gardner, L., Chan, T. M. and Wadee, M. A. (2008) Shear response of elliptical hollow sections. Proceedings of the Institution of Civil Engineers-Structures and Buildings 161 (6), 301-309.

Gardner, L. and Ministro, A. (2004) Testing and numerical modelling of structural steel oval hollow sections/cL. Gardner and A. Ministro. Imperial College London.

Geiker, M. (2008) Self-compacting concrete (SCC). Developments in the Formulation and Reinforcement of Concrete. British Welding Research Association.

Genikomsou, A. S. and Polak, M. A. (2015) Finite element analysis of punching shear of concrete slabs using damaged plasticity model in ABAQUS. Engineering Structures 98, 38-48.

Giakoumelis, G. and Lam, D. (2004) Axial capacity of circular concrete-filled tube columns. Journal of Constructional Steel Research 60 (7), 1049-1068.

Gibbs, J. and Zhu, W. (1999) Strength of hardened self-compacting concrete. Proceedings of First international RILEM Symposium on Self-Compacting Concrete (PRO 7), Stockholm, Suede.

Gourley, B. C., Tort, C., Hajjar, J. F. and Schiller, P. H. (2001) A synopsis of studies of the monotonic and cyclic behaviour of concrete-filled steel tube beam-columns. University of Minnesota.

Hajjar, J. F. and Gourley, B. C. (1996) Representation of concrete-filled steel tube cross-section strength. Journal of Structural Engineering 122 (11), 1327-1336.

Hakim, S. J. S., Noorzaei, J., Jaafar, M., Jameel, M. and Mohammadhassani, M. (2011) Application of artificial neural networks to predict compressive strength of high strength concrete. Int. J. Phys. Sci 6 (5), 975-981.

Han, L.-H. (2001) Fire performance of concrete filled steel tubular beam-columns. Journal of Constructional Steel Research 57 (6), 697-711.

Han, L.-H. (2002) Tests on stub columns of concrete-filled RHS sections. Journal of Constructional Steel Research 58 (3), 353-372.

Han, L.-H. and Yao, G.-H. (2004) Experimental behaviour of thin-walled hollow structural steel (HSS) columns filled with self-consolidating concrete (SCC). Thin-Walled Structures 42 (9), 1357-1377.

Han, L.-H., Yao, G.-H. and Tao, Z. (2007) Performance of concrete-filled thin-walled steel tubes under pure torsion. Thin-Walled Structures 45 (1), 24-36.

Hanehara, S. and Yamada, K. (1999) Interaction between cement and chemical admixture from the point of cement hydration, absorption behaviour of admixture, and paste rheology. Cement and Concrete Research 29 (8), 1159-1165.

Hassan, A., Hossain, K. and Lachemi, M. (2010) Strength, cracking and deflection performance of large-scale self-consolidating concrete beams subjected to shear failure. Engineering Structures 32 (5), 1262-1271.

Holschemacher, K. (2004) Hardened material properties of self-compacting concrete. Journal of Civil Engineering and Management 10 (4), 261-266.

Hu, H.-T., Huang, C.-S. and Chen, Z.-L. (2005) Finite element analysis of CFT columns subjected to an axial compressive force and bending moment in combination. Journal of Constructional Steel Research 61 (12), 1692-1712.

Hu, H.-T., Huang, C.-S., Wu, M.-H. and Wu, Y.-M. (2003) Nonlinear analysis of axially loaded concrete-filled tube columns with confinement effect. Journal of Structural Engineering 129 (10), 1322-1329.

Hwang, C., Liu, J., Lee, L. and Lin, F. (1996) Densified mixture design algorithm and early properties of high performance concrete. Journal of the Chinese Institute of Civil and Hydraulic Engineering 8 (2), 217-219.

Jacobs, F. and Hunkeler, F. (1999) Design of self-compacting concrete for durable concrete structures. First international RILEM symposium on self-compacting concrete. Rilem Publications SARL.

Jamaluddin, N., Lam, D., Dai, X. and Ye, J. (2013) An experimental study on elliptical concrete filled columns under axial compression. Journal of Constructional Steel Research 87, 6-16.

Jepsen, M. T. (2002) Predicting concrete durability by using artificial neural network. Published in a special NCR-publication.

Johansson, M. (2002) Composite action and confinement effects in tubular steel-concrete columns. Chalmers University of Technology.

Kasemchaisiri, R. and Tangtermsirikul, S. (2008) Deformability prediction model for self-compacting concrete. Magazine of Concrete Research 60 (2), 93-108.

Khairallah, F. (2013) Mechanical behavior of confined self-compacting reinforced concrete circular columns under concentric axial loading. Ain Shams Engineering Journal 4 (4), 641-649.

Khayat, K. (1999) Workability, testing, and performance of self-consolidating concrete. Materials Journal 96 (3), 346-353.

Khayat, K., Ghezal, A., Wallevik, O. and Nielsson, I. (2003) Effect of viscosity-modifying admixturesuperplasticizer combination on flow properties of SCC equivalent mortar. 3rd International Symposium on Self-Compacting Concrete.

Khayat, K., Hu, C. and Monty, H. (1999) Stability of self-consolidating concrete, advantages, and potential applications. 1st International RILEM Symposium on Self-Compacting Concrete.

Khayat, K. H., Paultre, P. and Tremblay, S. (2001) Structural performance and in-place properties of self-consolidating concrete used for casting highly reinforced columns. Materials Journal 98 (5), 371-378.

Kim, K.-H., Jeon, S.-E., Kim, J.-K. and Yang, S. (2003) An experimental study on thermal conductivity of concrete. Cement and Concrete Research 33 (3), 363-371.

Kou, S. and Poon, C. (2009) Properties of self-compacting concrete prepared with coarse and fine recycled concrete aggregates. Cement and Concrete composites 31 (9), 622-627.

Kovler, K. and Roussel, N. (2011) Properties of fresh and hardened concrete. Cement and Concrete Research 41 (7), 775-792.

Kumar, R., Singh, B. and Bhargava, P. (2011) Flexural capacity predictions of self-compacting concrete beams using stress–strain relationship in axial compression. Magazine of Concrete Research 63 (1), 49-59.

Lachemi, M., Hossain, K., Lambros, V., Nkinamubanzi, P.-C. and Bouzoubaâ, N. (2004) Self-consolidating concrete incorporating new viscosity modifying admixtures. Cement and Concrete Research 34 (6), 917-926.

Lachemi, M., Hossain, K. M. and Lambros, V. B. (2006) Axial load behavior of self-consolidating concrete-filled steel tube columns in construction and service stages. ACI structural journal 103 (1), 38.

Lam, D. and Gardner, L. (2008) Structural design of stainless steel concrete filled columns. Journal of Constructional Steel Research 64 (11), 1275-1282.

Law, K. and Gardner, L. (2012) Lateral instability of elliptical hollow section beams. Engineering Structures 37, 152-166.

Leemann, A., Lura, P. and Loser, R. (2011) Shrinkage and creep of SCC–The influence of paste volume and binder composition. Construction and Building Materials 25 (5), 2283-2289.

Lin, C.-H. and Chen, J.-H. (2012) Shear behavior of self-consolidating concrete beams. ACI Structural Journal 109 (3), 307.

Lin, C.-H., Hwang, C.-L., Lin, S.-P. and Liu, C.-H. (2008) Self-consolidating concrete columns under concentric compression. ACI Structural Journal 105 (4), 425.

Liu, M. (2009) Wider application of additions in self-compacting concrete. UCL (University College London).

Mandal, A. (2010) Concrete Filled Steel Tube under Axial Compression. JADAVPUR UNIVERSITY KOLKATA.

Mata, L. A. (2004) Implementation of self-consolidating concrete (SCC) for prestressed concrete girders.

McCann, F., Gardner, L. and Qiu, W. (2015) Experimental study of slender concrete-filled elliptical hollow section beam-columns. Journal of Constructional Steel Research 113, 185-194.

Mehta, P. K. (1986) Concrete. Structure, properties and materials.

Momeni, E., Armaghani, D. J., Hajihassani, M. and Amin, M. F. M. (2015) Prediction of uniaxial compressive strength of rock samples using hybrid particle swarm optimization-based artificial neural networks. Measurement 60, 50-63.

Morino, S. and Tsuda, K. (2002) Design and construction of concrete-filled steel tube column system in Japan. Earthquake Engineering and Engineering Seismology 4 (1), 51-73.

Naderpour, H., Kheyroddin, A. and Amiri, G. G. (2010) Prediction of FRP-confined compressive strength of concrete using artificial neural networks. Composite Structures 92 (12), 2817-2829.

Nagataki, S. and Fujiwara, H. (1995) Self-compacting property of highly flowable concrete. Special Publication 154, 301-314.

Nawa, T., Izumi, T. and Edamatsu, Y. (1998) State-of-the-art report on materials and design of self-compacting concrete. International workshop on self-compacting concrete.

Ni, H.-G. and Wang, J.-Z. (2000) Prediction of compressive strength of concrete by neural networks. Cement and Concrete Research 30 (8), 1245-1250.

Noguchi, T., Oh, S. and Tomosawa, F. (1999) Rheological approach to passing ability between reinforcing bars of self-compacting concrete. Self-Compacting Concrete: Proceedings of the First International RILEM Symposium.

Noumowé, A., Carré, H., Daoud, A. and Toutanji, H. (2006) High-strength self-compacting concrete exposed to fire test. Journal of materials in civil engineering 18 (6), 754-758.

Oehlers, D. and Bradford, M. Composite steel and concrete structural members: fundamental behaviour, 1995. Oxford: Pergamon Press.

Oh, B. H., Cha, S. W., Jang, B. S. and Jang, S. Y. (2002) Development of high-performance concrete having high resistance to chloride penetration. Nuclear Engineering and Design 212 (1), 221-231.

Okamura, H. and Ouchi, M. (1998) Self-compacting high performance concrete. Progress in structural Engineering and Materials 1 (4), 378-383.

Okamura, H. and Ouchi, M. (2003) Self-compacting concrete. Journal of advanced concrete technology 1 (1), 5-15.

Okamura, H. and Ozawa, K. (1994) Self-Compactable concrete for bridge construction. Technical Report NCEER. US National Center for Earthquake Engineering Research. 265-81

Okamura, H., Ozawa, K. and Ouchi, M. (2000) Self-compacting concrete. structural Concrete 1 (1), 3-17.

Ouchi, M., Nakamura, S.-A., Osterberg, T., Hallberg, S. and Lwin, M. (2003) Applications of self-compacting concrete in Japan, Europe and the United States. International Symposium on High Performance Computing (ISHPC).

Ozawa, K., Maekawa, K. and Okamura, H. (1990) High performance concrete with high filling capacity. Admixtures for Concrete-Improvement of Properties: Proceedings of the International RILEM Symposium. Vol. 5. CRC Press.

Öztaş, A., Pala, M., Özbay, E. a., Kanca, E. a., Çagˇlar, N. and Bhatti, M. A. (2006) Predicting the compressive strength and slump of high strength concrete using neural network. Construction and Building Materials 20 (9), 769-775.

Paultre, P., Khayat, K. H., Cusson, D. and Tremblay, S. (2005) Structural performance of self-consolidating concrete used in confined concrete columns. ACI Structural Journal 102 (4), 560-568.

Pentti, G. H.-E. P. (1999) Properties of SCC-especially early age and long term shrinkage and salt frost resistance. Proceedings of the 1 st International

Rilem Symposium on Self-compacting Concrete, Stockholm, Sweden. Rilem, Bagneux, France.

Persson, B. (1999) Creep, shrinkage and elastic modulus of self-compacting concrete. 1st International RILEM Symposium on Self-Compacting Concrete.

Persson, B. (2001) A comparison between mechanical properties of self-compacting concrete and the corresponding properties of normal concrete. Cement and concrete Research 31 (2), 193-198.

Petersson, O. and Billberg, P. (1999) Investigation on blocking of self-compacting concrete with different maximum aggregate size and use of viscosity agent instead of filler. Proceedings of the First International RILEM Symposium Self-Compacting Concrete, Stockholm, Sweden.

Prasad, B. R., Eskandari, H. and Reddy, B. V. (2009) Prediction of compressive strength of SCC and HPC with high volume fly ash using ANN. Construction and Building Materials 23 (1), 117-128.

Raheman, A. and Modani, P. (2013) Prediction of Properties of Self Compacting Concrete Using Artificial Neural Network. International Journal of Engineering Research and Applications (IJERA) ISSN, 2248-9622.

Rols, S., Ambroise, J. and Pera, J. (1999) Effects of different viscosity agents on the properties of self-leveling concrete. Cement and Concrete Research 29 (2), 261-266.

Rozière, E., Granger, S., Turcry, P. and Loukili, A. (2007) Influence of paste volume on shrinkage cracking and fracture properties of self-compacting concrete. Cement and concrete composites 29 (8), 626-636.

Ruiz-Teran, A. and Gardner, L. (2008) Elastic buckling of elliptical tubes. Thin-Walled Structures 46 (11), 1304-1318.

Sakino, K., Nakahara, H., Morino, S. and Nishiyama, I. (2004) Behavior of centrally loaded concrete-filled steel-tube short columns. Journal of Structural Engineering 130 (2), 180-188.

Sakla, S. S. and Ashour, A. F. (2005) Prediction of tensile capacity of single adhesive anchors using neural networks. Computers & structures 83 (21), 1792-1803.

Schneider, S. P. (1998) Axially loaded concrete-filled steel tubes. Journal of structural Engineering 124 (10), 1125-1138.

Schonlin, K. and Hilsorf, H. (1988) Permeability as a Measure of Potential Durability of Concrete--Development of a Suitable Test Apparatus. Special Publication 108, 99-116.

Sedran, T., De Larrard, F., Hourst, F. and Contamines, C. (1996) Mix design of self-compacting concrete (SCC). RILEM PROCEEDINGS.

Seward, D. (2014) Understanding structures: analysis, materials, design. Palgrave Macmillan.

Shanmugam, N. E. and Lakshmi, B. (2001) State of the art report on steel–concrete composite columns. Journal of constructional steel research 57 (10), 1041-1080.

Sheehan, T., Dai, X., Chan, T. and Lam, D. (2012) Structural response of concrete-filled elliptical steel hollow sections under eccentric compression. Engineering Structures 45, 314-323.

Shi, C. and Yang, X. (2005) Design and application of self-compacting lightweight concrete. SCC'2005-China: 1st International Symposium on Design, Performance and Use of Self-Consolidating Concrete. RILEM Publications SARL.

Siddique, R. (2011) Properties of self-compacting concrete containing class F fly ash. Materials & Design 32 (3), 1501-1507.

Siddique, R., Aggarwal, P. and Aggarwal, Y. (2011) Prediction of compressive strength of self-compacting concrete containing bottom ash using artificial neural networks. Advances in Engineering Software 42 (10), 780-786.

Silvestre, N. (2008) Buckling behaviour of elliptical cylindrical shells and tubes under compression. International Journal of Solids and Structures 45 (16), 4427-4447.

Skarendahl, Å. (2000) First international RILEM symposium on self-compacting concrete. Materials and Structures 33 (2), 143-144.

Skarendahl, Å. and Petersson, Ö. (2000) Report 23: Self-Compacting Concrete–State-of-the-Art report of RILEM Technical Committee 174-SCC. Vol. 23. RILEM publications.

Sonebi, M. and Bartos, P. (2002) Filling ability and plastic settlement of self-compacting concrete. Materials and Structures 35 (8), 462-469.

Su, N., Hsu, K.-C. and Chai, H.-W. (2001) A simple mix design method for self-compacting concrete. Cement and concrete research 31 (12), 1799-1807.

Tao, Z., Han, L.-H. and Wang, Z.-B. (2005) Experimental behaviour of stiffened concrete-filled thin-walled hollow steel structural (HSS) stub columns. Journal of Constructional Steel Research 61 (7), 962-983.

Testo, N. (2007) Axial capacity of elliptical concree-filled steel tube columns. Research Report. School of Civil Engineering, University of Leeds.

Topcu, I. B., Bilir, T. and Uygunoğlu, T. (2009) Effect of waste marble dust content as filler on properties of self-compacting concrete. Construction and Building Materials 23 (5), 1947-1953.

Topçu, İ. B. and Bilir, T. (2009) Experimental investigation of some fresh and hardened properties of rubberized self-compacting concrete. Materials & Design 30 (8), 3056-3065.

Topçu, I. l. B. and Uğurlu, A. (2003) Effect of the use of mineral filler on the properties of concrete. Cement and Concrete Research 33 (7), 1071-1075.

Tragardh, J. (1999) Microstructural features and related properties of self-compacting concrete. Self-Compacting Concrete: Proceedings of the First International RILEM Symposium held in Stockholm, Sweden 13-14 September 1999.

Turatsinze, A. and Garros, M. (2008) On the modulus of elasticity and strain capacity of self-compacting concrete incorporating rubber aggregates. Resources, conservation and recycling 52 (10), 1209-1215.

Uchikawa, H., Sawaki, D. and Hanehara, S. (1995) Influence of kind and added timing of organic admixture on the composition, structure and property of fresh cement paste. Cement and Concrete Research 25 (2), 353-364.

Uysal, M. and Tanyildizi, H. (2011) Predicting the core compressive strength of self-compacting concrete (SCC) mixtures with mineral additives using artificial neural network. Construction and Building Materials 25 (11), 4105-4111.

V Chaudhari, S. and A Chakrabarti, M. (2012) Modeling of concrete for nonlinear analysis Using Finite Element Code ABAQUS. International Journal of Computer Applications 44 (7), 14-18.

Van Khanh, B. and Montgomery, D. (1999) Drying shrinkage of self-compacting concrete containing milled limestone. International RILEM symposium on self-compacting concrete.

Wang, Q., Zhao, D. and Guan, P. (2004) Experimental study on the strength and ductility of steel tubular columns filled with steel-reinforced concrete. Engineering Structures 26 (7), 907-915.

Westerholm, M., Lagerblad, B., Silfwerbrand, J. and Forssberg, E. (2008) Influence of fine aggregate characteristics on the rheological properties of mortars. Cement and Concrete Composites 30 (4), 274-282.

Yamada, K., Takahashi, T., Hanehara, S. and Matsuhisa, M. (2000) Effects of the chemical structure on the properties of polycarboxylate-type superplasticizer. Cement and concrete research 30 (2), 197-207.

Yammamuro, H. and Mizunuma, T. (1997) Study of non-adsorptive viscosity agents applied to self-compacting concrete. Special Publication 173, 427-444.

Yang, H., Lam, D. and Gardner, L. (2008) Testing and analysis of concrete-filled elliptical hollow sections. Engineering Structures 30 (12), 3771-3781.

Yu, Q., Tao, Z. and Wu, Y.-X. (2008) Experimental behaviour of high performance concrete-filled steel tubular columns. Thin-Walled Structures 46 (4), 362-370.

Yu, Z.-w., Ding, F.-x. and Cai, C. (2007) Experimental behavior of circular concrete-filled steel tube stub columns. Journal of Constructional Steel Research 63 (2), 165-174.

Zeghiche, J. and Chaoui, K. (2005) An experimental behaviour of concrete-filled steel tubular columns. Journal of Constructional Steel Research 61 (1), 53-66.

Zhang, W. and Shahrooz, B. M. (1999) Comparison between ACI and AISC for concrete-filled tubular columns. Journal of Structural Engineering 125 (11), 1213-1223.

Zhao, X. and Packer, J. (2009) Tests and design of concrete-filled elliptical hollow section stub columns. Thin-Walled Structures 47 (6), 617-628.

Zhu, M., Liu, J., Wang, Q. and Feng, X. (2010) Experimental research on square steel tubular columns filled with steel-reinforced self-consolidating high-strength concrete under axial load. Engineering Structures 32 (8), 2278-2286.

Zhu, W. and Bartos, P. J. (2003) Permeation properties of self-compacting concrete. Cement and Concrete Research 33 (6), 921-926.

Zhu, W. and Gibbs, J. C. (2005) Use of different limestone and chalk powders in self-compacting concrete. Cement and Concrete Research 35 (8), 1457-1462.

Zhu, W., Gibbs, J. C. and Bartos, P. J. (2001) Uniformity of in situ properties of self-compacting concrete in full-scale structural elements. Cement and Concrete Composites 23 (1), 57-64.

Zhu, W., Sonebi, M. and Bartos, P. (2004) Bond and interfacial properties of reinforcement in self-compacting concrete. Materials and structures 37 (7), 442-448.

APPENDIX (A)

Sr.NO	Researcher	C	FA	ggbs	W/b	SP	S	CA	R	SE	SA	$\frac{SA}{SE}$
1	(Sonebi and Bartos, 2003)	290	100	0	0.45	0.8	913	837	0	42.7	40.21	0.9
2		250	261	0	0.55	0.5	478	837	0	17	16.48	1.0
3		210	100	0	0.65	0.8	910	837	0	19.1	23.09	1.2
4		250	160	0	0.55	0.5	742	837	0	24.1	25.37	1.1
5		210	220	0	0.45	0.8	768	837	0	26.7	30.05	1.1
6		290	100	0	0.65	0.2	709	837	0	26.6	20.31	0.8
7		290	220	0	0.45	0.2	625	837	0	32.9	33.18	1.0
8		250	160	0	0.55	0.5	742	837	0	26	25.37	1.0
9		250	160	0	0.55	0.5	742	837	0	28.5	25.37	0.9
10		250	160	0	0.55	0.5	742	837	0	26.4	25.37	1.0
11		250	160	0	0.55	0	739	837	0	27.3	25.47	0.9
12		317	160	0	0.55	0.5	594	837	0	29.1	24.58	0.8
13		210	220	0	0.65	0.2	562	837	0	10.2	12.69	1.2
14		250	160	0	0.55	0.5	742	837	0	25.3	25.37	1.0
15		250	160	0	0.38	0.5	919	837	0	36.3	41.73	1.1
16		250	160	0	0.55	1	746	837	0	26.7	25.37	1.0
17		250	160	0	0.72	0.5	566	837	0	11	12.08	1.1
18		183	160	0	0.55	0.5	891	837	0	22.1	26.28	1.2
19		210	100	0	0.45	0.2	1006	837	0	54.3	34.58	0.6
20		250	29	0	0.55	0.5	1006	837	0	51.7	30.51	0.6
21		220	180	0	0.39	0.35	916	900	0	49	44.04	0.9

22		220	180	0	0.39	0.35	916	900	0	49	44.04	0.9
23		160	240	0	0.39	0.35	886	900	0	44	41.78	0.9
24	**(Siddique 2011)**	193	158	0	0.39	0.35	1024	900	0	44	44.45	1.0
25		220	180	0	0.45	0.35	850	900	0	38	41.16	1.1
26		198	232	0	0.34	0.2	874	900	0	46	44.07	1.0
27		248	203	0	0.39	0.35	808	900	0	50	43.68	0.9
28		237	133	0	0.36	0.2	1034	900	0	49	45.66	0.9
29		220	180	0	0.39	0.35	916	900	0	49	44.04	0.9
30		237	133	0	0.43	0.5	960	900	0	46	44.01	1.0
31		275	155	0	0.43	0.5	827	900	0	48	43.45	0.9
32		280	120	0	0.39	0.35	946	900	0	45	45.34	1.0
33		170	200	0	0.43	0.2	930	900	0	31	41.70	1.3
34		220	180	0	0.39	0.6	916	900	0	43	43.98	1.0
35		220	180	0	0.39	0.35	916	900	0	47	44.04	0.9
36		220	180	0	0.39	0.1	916	900	0	44	44.10	1.0
37		198	232	0	0.36	0.5	872	900	0	52	43.91	0.8
38		220	180	0	0.39	0.35	916	900	0	45	44.04	1.0
39		220	180	0	0.33	0.35	982	900	0	51	45.52	0.9
40		170	200	0	0.43	0.5	928	900	0	33	41.47	1.3
41		275	155	0	0.43	0.2	830	900	0	36	43.64	1.2
42		247	165	0	0.45	0.12	845	846	0	34.6	37.90	1.1
43		238	159	0	0.4	0.29	844	844	0	37.8	35.12	0.9
44		232	155	0	0.35	0.38	846	847	0	48.3	33.98	0.7
45		207	207	0	0.45	0.4	845	843	0	33.2	36.15	1.1
46	**(Bouzoubaa**	200	200	0	0.4	0.17	842	843	0	34.9	33.73	1.0
47	**and Lachemi**	197	197	0	0.35	0.28	856	856	0	38.9	35.85	0.9
48	**2001)**	169	254	0	0.45	0	853	853	0	30.2	38.11	1.3
49		163	245	0	0.4	0.2	851	851	0	26.2	35.37	1.4
50		161	241	0	0.35	0.3	866	864	0	35.8	37.45	1.0
51		336	0	0	0.5	0	739	1105	0	34.6	45.37	1.3
52		350	162	0	0.59	0.09	768	840	0	51.7	44.16	0.9
53	**(Siddique et**	349	162	0	0.57	0.14	779	852	0	59.9	44.83	0.7
54	**al. 2011)**	350	133	0	0.52	0.16	815	883	0	55.3	45.50	0.8
55		350	111	0	0.51	0.15	831	900	0	61	45.56	0.7
56		250	257	0	0.77	0.11	787	853	0	51.5	43.46	0.8
57		427	115	0	0.45	0.12	779	844	0	59.4	46.02	0.8
58		348	224	0	0.5	0.43	783	848	0	58.6	46.19	0.8
59		350	90	0	0.48	0.14	852	923	0	46.5	45.82	1.0
60		327	173	0	0.53	0.2	902	803	0	61.6	45.34	0.7
61		380	145	0	0.48	0.1	788	854	0	73.5	45.73	0.6
62		350	186	0	0.51	0.11	786	851	0	70.4	45.69	0.6
63		380	145	0	0.48	0.13	988	659	0	65.5	44.20	0.7
64		380	192	0	0.53	0.1	931	621	0	67.8	43.01	0.6
65		275	250	0	0.67	0.09	775	840	0	54.5	43.94	0.8
66		325	60	0	0.55	0.43	899	850	0	30.8	40.87	1.3
67		325	60	0	0.55	0.43	899	850	0	32.6	40.87	1.3
68		325	120	0	0.55	0.43	755	850	0	32.2	37.80	1.2
69		249	60	0	0.55	0.43	1079	850	0	24	41.97	1.7
70		325	60	0	0.72	0.43	722	850	0	13.3	23.71	1.8
71		370	96	0	0.45	0.25	833	850	0	39.5	44.59	1.1
72		400	60	0	0.55	0.43	718	850	0	30.4	39.37	1.3
73		325	60	0	0.55	0.43	899	850	0	35.3	40.87	1.2
74		370	24	0	0.65	0.62	770	850	0	18.7	33.09	1.8
75	**(Khayat et al .2003)**	325	0	0	0.55	0.43	1042	850	0	41.2	44.10	1.1
76		280	24	0	0.45	0.62	1172	850	0	16.9	45.20	2.7
77		325	60	0	0.55	0.75	896	850	0	27.7	40.54	1.5
78		325	60	0	0.55	0.43	898	850	0	35	40.81	1.2
79		325	60	0	0.55	0.12	900	850	0	31.4	41.07	1.3
80		370	96	0	0.45	0.62	830	850	0	38.8	44.44	1.1
81		325	60	0	0.55	0.43	898	850	0	34.3	40.81	1.2
82		280	96	0	0.65	0.62	817	850	0	15.9	30.37	1.9
83		370	24	0	0.65	0.25	772	850	0	26.4	33.51	1.3
84		280	96	0	0.65	0.25	820	850	0	19.6	31.00	1.6
85		363	109	0	0.38	1.3	1109	526	0	47.7	45.48	1.0

86	**(Almeida Filho et al. 2010)**	363	109	0	0.38	1.3	1109	526	0	48.59	45.48	0.9
87		363	109	0	0.38	1.3	1109	526	0	46.56	45.48	1.0
88		363	109	0	0.38	1.3	1109	526	0	42.38	45.48	1.1
89		363	109	0	0.38	1.3	1109	526	0	45.54	45.48	1.0
90		363	109	0	0.38	1.3	1109	526	0	47.39	45.48	1.0
91		363	109	0	0.38	1.3	1109	526	0	47.19	45.48	1.0
92		363	109	0	0.38	1.3	1109	526	0	45.75	45.48	1.0
93		363	109	0	0.38	1.3	1109	526	0	49.1	45.48	0.9
94		363	109	0	0.38	1.3	1109	526	0	47.98	45.48	0.9
95		363	109	0	0.38	1.3	1109	526	0	41.9	45.48	1.1
96		329	99	0	0.39	1.31	947	781	0	50.5	42.04	0.8
97		329	99	0	0.39	1.31	947	781	0	48.23	42.04	0.9
98		329	99	0	0.39	1.31	947	781	0	42.74	42.04	1.0
99		329	99	0	0.39	1.31	947	781	0	50.7	42.04	0.8
100		329	99	0	0.39	1.31	947	781	0	50.62	42.04	0.8
101		329	99	0	0.39	1.31	947	781	0	50.62	42.04	0.8
102		329	99	0	0.39	1.31	947	781	0	49.21	42.04	0.9
103		329	99	0	0.39	1.31	947	781	0	49.48	42.04	0.8
104		329	99	0	0.39	1.31	947	781	0	49.59	42.04	0.8
105		329	99	0	0.39	1.31	947	781	0	40.98	42.04	1.0
106		329	99	0	0.39	1.31	947	781	0	49.85	42.04	0.8
107		329	99	0	0.39	1.31	947	781	0	49.6	42.04	0.8
108		334	100	0	0.38	1.31	940	776	0	44.47	41.96	0.9
109		334	100	0	0.38	1.31	940	776	0	43.34	41.96	1.0
110		334	100	0	0.38	1.31	940	776	0	38.08	41.96	1.1
111		334	100	0	0.38	1.31	940	776	0	43.53	41.96	1.0
112		334	100	0	0.38	1.31	940	776	0	42.82	41.96	1.0
113		334	100	0	0.38	1.31	940	776	0	43.46	41.96	1.0
114		334	100	0	0.38	1.31	940	776	0	45.99	41.96	0.9
115		334	100	0	0.38	1.31	940	776	0	39.72	41.96	1.1
116		334	100	0	0.38	1.31	940	776	0	41.19	41.96	1.0
117		334	100	0	0.38	1.31	940	776	0	43.47	41.96	1.0
118	**(Su et al. 2001)**	200	157	67	0.42	1.8	961	743	0	27.5	32.77	1.2
119		250	154	66	0.4	1.8	945	731	0	34.3	38.68	1.1
120		300	148	63	0.34	1.6	928	718	0	41.2	42.23	1.0
121		350	142	61	0.31	1.6	912	706	0	48	44.40	0.9
122		240	180	0	0.49	0.59	900	830	0	25.6	40.51	1.6
123		280	170	0	0.43	0.81	900	830	0	28	43.67	1.6
124		320	160	0	0.38	1	900	830	0	36	45.33	1.3
125		360	150	0	0.35	1.16	900	830	0	40	46.14	1.2
126		400	140	0	0.33	1.31	900	830	0	44	46.52	1.1
127	**(Prasad et al. 2009)**	440	130	0	0.31	1.44	900	830	0	48	46.70	1.0
128		240	180	0	0.49	0.59	900	830	0	24	40.51	1.7
129		280	170	0	0.43	0.81	900	830	0	32	43.67	1.4
130		320	160	0	0.38	1	900	830	0	33.6	45.33	1.3
131		360	150	0	0.35	1.16	900	830	0	36	46.14	1.3
132		400	140	0	0.33	1.31	900	830	0	40	46.52	1.2
133		440	130	0	0.31	1.44	900	830	0	48	46.70	1.0
134	**(Felekoğlu et al. 2007)**	377	239	0	0.37	0.6	861	562	0	42.4	38.42	0.9
135		376	246	0	0.33	1.05	886	577	0	39.2	41.81	1.1
136		377	247	0	0.29	1.27	898	593	0	37.6	43.45	1.2
137		376	263	0	0.25	1.41	932	609	0	32.8	45.46	1.4
138		377	272	0	0.22	2	963	630	0	28.8	46.25	1.6
139	**(Topcu et al. 2009)**	380	150	0	0.32	2	1120	520	0	39.6	41.69	1.1
140		380	150	0	0.32	2	1120	520	0	38.88	41.69	1.1
141		380	150	0	0.32	2	1120	520	0	40.88	41.69	1.0
142		380	150	0	0.32	2	1120	520	0	37.12	41.69	1.1
143		380	150	0	0.32	2	1120	520	0	41.92	41.69	1.0
144		380	150	0	0.32	2	1120	520	0	40.24	41.69	1.0
145		380	150	0	0.32	2	1080	500	60	30.48	32.43	1.1
146		380	150	0	0.32	2	1080	500	60	27.92	32.43	1.2
147		380	150	0	0.32	2	1080	500	60	31.84	32.43	1.0
148		380	150	0	0.32	2	1080	500	60	29.2	32.43	1.1
149		380	150	0	0.32	2	1080	500	60	29.6	32.43	1.1

150		380	150	0	0.32	2	1080	500	60	30.96	32.43	1.0
151		380	150	0	0.32	2	1030	490	120	21.76	20.71	1.0
152		380	150	0	0.32	2	1030	490	120	21.28	20.71	1.0
153		380	150	0	0.32	2	1030	490	120	23.84	20.71	0.9
154		380	150	0	0.32	2	1030	490	120	20.8	20.71	1.0
155		380	150	0	0.32	2	1030	490	120	22.4	20.71	0.9
156		380	150	0	0.32	2	1030	490	120	24.16	20.71	0.9
157		380	150	0	0.32	2	980	480	180	13.76	13.10	1.0
158		380	150	0	0.32	2	980	480	180	13.36	13.10	1.0
159	**(Sonebi 2004)**	380	150	0	0.32	2	980	480	180	14.64	13.10	0.9
160		380	150	0	0.32	2	980	480	180	12.08	13.10	1.1
161		380	150	0	0.32	2	980	480	180	15.92	13.10	0.8
162		380	150	0	0.32	2	980	480	180	11.52	13.10	1.1
163		290	100	0	0.45	0.8	913	837	0	42.7	40.21	0.9
164		250	261	0	0.55	0.5	478	837	0	17	16.48	1.0
165		210	100	0	0.65	0.8	910	837	0	19.1	23.09	1.2
166		250	160	0	0.55	0.5	742	837	0	24.1	25.37	1.1
167		210	220	0	0.45	0.8	786	837	0	26.7	31.97	1.2
168		290	100	0	0.65	0.2	709	837	0	26.6	20.31	0.8
169		290	220	0	0.45	0.2	625	837	0	32.9	33.18	1.0
170		250	160	0	0.55	0.5	742	837	0	26	25.37	1.0
171		250	160	0	0.55	0.5	742	837	0	28.5	25.37	0.9
172		250	160	0	0.55	0.5	742	837	0	26.4	25.37	1.0
173		250	160	0	0.55	0	739	837	0	27.3	25.47	0.9
174		210	100	0	0.45	0.2	1066	837	0	54.3	39.54	0.7
175		317	160	0	0.55	0.5	594	837	0	29.1	24.58	0.8
176		250	29	0	0.55	0.5	1006	837	0	51.7	30.51	0.6
177		210	220	0	0.65	0.2	562	837	0	10.2	12.69	1.2
178		250	160	0	0.55	0.5	742	837	0	25.3	25.37	1.0
179		250	160	0	0.38	0.5	919	837	0	36.3	41.73	1.1
180		250	160	0	0.55	1	746	837	0	26.7	25.37	1.0
181		250	160	0	0.72	0.5	566	837	0	11	12.08	1.1
182		183	160	0	0.55	0.5	891	837	0	22.1	26.28	1.2
183		270	180	0	0.55	0.6	647	837	0	24.5	23.18	0.9
184		280	190	0	0.55	0.7	599	837	0	24	22.04	0.9
185		260	170	0	0.53	0.7	717	837	0	27.8	26.65	1.0
186		230	140	0	0.52	0.8	864	837	0	32.1	30.35	0.9
187	**(Boukendakdji et al. 2009)**	240	150	0	0.52	0.6	831	837	0	30.9	31.01	1.0
188		465	0	0	0.4	1.6	867	840	0	68	64.76	1.0
189		420	0	10	0.43	1.6	867	840	0	64	61.50	1.0
190		397	0	15	0.45	1.6	867	840	0	61	59.47	1.0
191		340	200	0	0.53	1.98	695	895	0	35.44	45.01	1.3
192		340	200	0	0.53	1.98	674	895	0	35.6	44.53	1.3
193	**(Kou and Poon 2009)**	340	200	0	0.53	1.98	653	895	0	34.72	43.94	1.3
194		340	200	0	0.53	1.98	632	895	0	33.04	43.21	1.3
195		340	200	0	0.53	1.98	610	895	0	30.96	42.29	1.4
196		340	200	0	0.44	1.75	662	850	0	42.96	41.96	1.0
197		340	200	0	0.44	1.75	642	850	0	51.44	40.88	0.8
198		340	200	0	0.44	1.75	622	850	0	49.84	39.62	0.8
199		340	200	0	0.44	1.75	602	850	0	45.04	38.17	0.8
200		340	200	0	0.44	1.75	581	850	0	42.56	36.44	0.9
201		340	200	0	0.44	1.75	581	850	0	42.56	36.44	0.9
202		340	200	0	0.4	1.86	616	850	0	47.28	39.25	0.8
203		340	200	0	0.35	1.96	662	850	0	51.36	42.04	0.8
204	**(Lin and Chen 2012)**	243	64	32	1.45	0	920	900	0	32.8	36.82	1.1
205		243	64	32	1.45	0	920	900	0	38.7	36.82	1.0
206		243	64	32	1.45	0	920	900	0	47.8	36.82	0.8
207		256	75	38	1.86	0	920	900	0	39	39.82	1.0
208		256	75	38	1.86	0	920	900	0	40.2	39.82	1.0
209		256	75	38	1.86	0	920	900	0	42.3	39.82	0.9
210		256	80	40	2.61	0	920	900	0	39	40.26	1.0
211		256	80	40	2.61	0	920	900	0	40.3	40.26	1.0
212		280	50	88	0.52	0	920	770	0	30.4	37.74	1.2
213		280	50	88	0.52	0	920	770	0	42.9	37.74	0.9

214		280	50	88	0.52	0	920	770	0	49.1	37.74	0.8
215		280	60	95	0.51	0	920	770	0	38.4	38.72	1.0
216		280	60	95	0.51	0	920	770	0	39.5	38.72	1.0
217		280	60	95	0.51	0	920	770	0	39.9	38.72	1.0
218		280	79	100	0.48	0	920	770	0	39.5	40.78	1.0
219	**(Hassan et al. 2010)**	280	79	100	0.48	0	920	770	0	38.5	40.78	1.1
220		315	0	135	0.4	0	900	930	0	45	49.32	1.1
221		315	0	135	0.4	0	900	930	0	53	49.32	0.9
222		315	0	135	0.4	0	900	930	0	53	49.32	0.9
223	**(Ding et al. 2011)**	399	171	0	0.35	1.3	742	724	0	31.44	41.08	1.3
224		399	171	0	0.35	1.3	742	724	25	33.44	39.90	1.2
225		399	171	0	0.35	1.3	742	724	50	38.8	38.53	1.0
226	**(Zhu et al. 2001)**	280	245	0	0.36	0	865	750	0	37.6	43.11	1.1
227		330	200	0	0.58	0	870	750	0	57.5	44.05	0.8
228	**(Zhu and Gibbs 2005)**	380	170	0	0.31	1	817	831	0	39.5	46.11	1.2
229		380	170	0	0.31	1	817	831	0	35.8	46.11	1.3
230		380	170	0	0.31	1	817	831	0	36.9	46.11	1.2
231		380	170	0	0.31	1	817	831	0	39.7	46.11	1.2
232		380	170	0	0.31	1	817	831	0	41.1	46.11	1.1
233		380	170	0	0.31	1	817	831	0	38.3	46.11	1.2
234		380	170	0	0.31	1	817	831	0	36.7	46.11	1.3
235		380	170	0	0.31	1	817	831	0	42.1	46.11	1.1
236		380	170	0	0.31	1	817	831	0	40.8	46.11	1.1
237		245	295	0	0.31	1.2	910	750	0	57.6	44.58	0.8
238		300	240	0	0.31	1.2	920	750	0	40	45.30	1.1
239		405	135	0	0.31	1.2	935	750	0	32	46.07	1.4
										average		**1.05**

Note:

C: Cement content kg/m³, **FA**: Flyash kg/m³, **GGBS**: Ground-granulated blast-furnace slag kg/m³, **S**: Sand kg/m³, **CA**: Coarse aggregate kg/m³, **R**: Rubber kg/m³, **SE**: Experimental Compressive Strength MPa, **SA**: ANN compressive strength MPa, **SP**: Superplasticiser, **w/b**: water to binder ratio.